uc3m | Universidad Carlos III de Madrid

Aerospace Engineering

2017-2018

Bachelor Thesis

Statistical Analysis of Taxi Loads

Álvaro Esteban Luengo

Supervisor

Héctor Climent Máñez

EPS Leganés - July 2018

ABSTRACT

The analysis of taxi loads comprises an airworthiness requirement for the appropriate design and certification of an aircraft, especially if the specimen subjected to study represents a new military transport aircraft with the capability to perform tactical operations in unpaved runways, such as the A400M. Once the design is completed, the definition of EBH curves has constituted the usual procedure to define the taxi operational limitations of an aircraft in order to preserve its airframe integrity. However, more demanding requirements in the current state of the art of military air transport have awakened the need among the different A400M customers to explore the aircraft taxi capabilities beyond its operational limitations. Hence, this actual need have led the different Air Forces operating the aircraft to request the quantification of the risk that this kind of operations involve.

As a consequence, such customer demand has motivated Airbus to develop a new statistical approach with the objective to complement the definition of the A400M EBH curves and decrease the conservatism intrinsic in their computation method by introducing the concept of probability in the assessment of the taxi loads problem. Therefore, the main purpose of this Bachelor Thesis concerns the development of a methodology that makes possible the risk quantification by means of the probability calculation of limit load exceedance at any point of the aircraft structure, given a specific runway roughness profile and aircraft configuration. To accomplish such task, the methodology for the statistical analysis of taxi loads comprises the definition of 2D probability maps and the corresponding probability curves for the sizing load magnitudes subjected to study, first at the design EBH curve analyzed for the validation of the probability calculation philosophy implemented, and then, concerning the operation in more severe runways than that for which the aircraft is designed.

Finally, according to the EBH method guidelines for the analysis of taxi loads, the methodology is illustrated with the results obtained from the numerical simulation of A400M landing manoeuvres over 1-cos bumps of different heights. The definition of 2D probability maps and probability curves is particularized for the nose landing gear wheel axle vertical force and the down bending moment at the wing root, since both are the two main magnitudes of interest for which the taxi phase constitutes the sizing scenario.

Key words: taxi loads, statistical analysis, unpaved runways, EBH curves

ACKNOWLEDGEMENTS

Every journey in one's life comes to an end and an awesome four-year period of my life seems to conclude within these lines. Personal effort might have been the key to succeed but I never forget the contribution of those who made reaching this point a reality.

First of all, to my supervisor, Héctor Climent, for the opportunity to collaborate with the Structural Dynamics and Aeroelasticity Department at Airbus Defence and Space. Your trust and confidence has been essential to achieve such important milestone for my future career.

To all the incredible members of the Department who kindly embraced me during the three-month internship. Special mention goes to Guillermo Pastor, Lucía González and Sebastian Claverías, who directly helped me solving any arising issue to succeed in the completion of this project. Your patience and dedication has been a gift.

To the University of Maryland, who taught me how to never give up even when you are far from home. Dani and Laura, you were family at Leonardtown 245-01.

Undoubtedly, to all my family, especially to my parents, Mª Ángeles and Jose Antonio, and my brother, Alejandro, for your continuous support since day one, literally, and for providing me the means to become the person I am nowadays. Also, to my grandparents and my aunt, Silvia, my best examples of self-improvement. Thanks to teach me how to walk on my own, but better together.

And finally, to her, she is daily inspiration to strive for greatness. (52°08'37.6"N 7°09'53.7"W)

CONTENTS

LIST OF FIGURES

LIST OF TABLES

1. INTRODUCTION TO THE ANALYSIS OF TAXI LOADS

1.1. Presentation of the taxi loads problem

1.1.1. General overview

Most of the efforts during the preliminary and detailed design stages of an aircraft are focused on the flight phases in which the vehicle remains airborne, such as the determination of the aerodynamic efficiency of the lifting surfaces or the flight envelope expansion for flutter studies. Nevertheless, when ground operation requirements are specified, especially in those aircraft which are aimed to be manoeuvred in surfaces of high roughness level, the corresponding ground loads that appear acting on the structure constitute the most critical checkstress magnitude criterion at some very specific locations of the airframe. Therefore, taking them into account is of extreme importance when determining the maximum required structural capability, and consequently, the adequate sizing and material selection of several components of the aircraft structure.

In an analogous manner as with flight loads, ground loads can be split into two categories. On the one hand, the mere fact of standing over its undercarriage, as the example of an airliner stationary at the apron during ground handling operations, makes the aircraft structure be exposed to the presence of ground static 1G loads due to the distribution of its own weight along its different elements according to a specific load path. They are characterized by having a very slow rate of change determined by the aircraft rigid body modes, below one or two Hz, and for simplicity, are assumed to be non-varying in magnitude, direction nor point of application. On the other hand, the relative motion of an aircraft over a surface may excite its inherent normal modes at higher frequencies, leading to the appearance of ground dynamic loads. This type of loads are the ones that add a higher degree of complexity in the design process from the structural dynamics point of view, since due to their nature, its vector definition and point of application vary as time evolves. At the same time, in the certification requirements, ground dynamic loads are essentially subdivided into the two scenarios in which they are found, concerning dynamic landing, characterized by the absorption of a sudden impact and corresponding dissipation of kinetic energy during touchdown, and ground handling, the latter covering taxi, take-off (including rejected TO) and landing roll, braked roll, turning, jacking, and towing [1].

Among the broad variety of ground loads cases previously introduced, the present research study is focused on the expansion of the taxi operational capabilities of the Airbus A400M military transport aircraft over unpaved runways. Hence, to put the scope of the work into context, taxiing is defined as the entire phase of ground movement prior to final take off and following landing [2]. Braking and turning may be required to complement

the taxi phase, but these manoeuvres are considered as separate operations. Therefore, taxiing is simply understood as a straight line motion on the ground [1].

As a consequence, stress dynamic taxi loads are defined as those which are originated during taxi operations on paved or unpaved runways in the scenarios of take-off, landing and rejected take-off manoeuvres. Besides, these kind of loads are described as the combination of the dynamic response of the aircraft and landing gear to the excitation created by the unevenness of a runway (incremental loads) in addition to the steady loads appearing in the aircraft when rolling over a theoretical flat surface at constant speed (1G loads) [3].

From the structural dynamics perspective, taxi operations would not constitute a design problem to deal with if runways and taxiways were built totally smooth. However, far from this ideal case, airfield surfaces are in reality 'rough' to some extent, i.e. the variation of elevation along the longitudinal axis of the runway is not linear [1]. Moreover, the capability of operating in unpaved runways comprises a more critical issue in comparison to taxiing in paved surfaces due to the higher severity of the runway profile. The explanation lies on the fact that, generally, the roughness level exhibited by unprepared surfaces is more exacerbated than that of prepared ones. As a consequence, a magnified dynamical behaviour results from the excitation of the aircraft normal modes and leads to the generation of dynamic loads that need consideration for design.

1.1.2. Background

The analysis of taxi loads has been a matter of study in the structural dynamics field for many years, and nowadays it is a very well consolidated engineering procedure carried out in aerospace industry. The first publications in which dynamic taxi loads are addressed can be dated back to the mid 50's [4]. For instance, companies such as Lockheed had already developed industrial methods to tackle this problem in the mid 60's [5]. TAXI code [6] was one of the pioneer software packages of general use developed for the US Air Force in 1973 and made possible the computation of aircraft dynamic response to bomb damage repair [7]. Likewise, the use of this computer program was extended to the study of the dynamic response of commercial aircraft to runway unevenness. Prototypes of Boeing 707-320C, 727-200, 747, McDonnell Douglas DC-8-63, DC-9-40 and DC-10-10 are examples of aircraft whose dynamical behaviour was analyzed by means of TAXI software [8].

A remarkable event that set the basis on the further development of procedures to compute taxi loads was the AGARD conference (April 4^{th} - 9^{th}, Brussels, 1982). This milestone was aimed to the dissemination and homogenization of the industry standards in the analysis of Aircraft Dynamic Response to Damaged and Repaired Runways [9].

In order to be able to perform the direct engineering problem, i.e. designing the aircraft according to the specifications required by the airworthiness authorities, CASA de-

veloped similar in-house software to cover this issue at the end of the 80's [10], which has suffered many refinements over time derived from component and full-scale tests. In a few words, the code extracts the normal modes of the aircraft using any Finite Element Method commercial software, such as MSC.NASTRAN, and performs the taxi simulation combining the non-linear model of the landing gear kinematics and its components (tyres, dampers, etc.) and the linear dynamic model of the aircraft structure over a given surface roughness profile. As part of the direct engineering problem, the taxi loads model has to be validated, comprising a must in order to achieve final certification of the aircraft. The first steps taken in this certification process have a direct relationship to the proper airframe design, since the engineer must determine the maximum loads and accelerations that the aircraft must withstand given a predefined runway profile. As a consequence, in the several loads loops which are accomplished, the load magnitudes at the different monitoring stations specified across the entire structure are calculated. Then, checkstress verifications are performed to verify if limit loads do not surpass the maximum allowable boundaries. In the case that any of those limiting criteria is exceeded, an update of the taxi loads model is mandatory. In the whole process, multiple iterations may be required to fulfill all necessary conditions. Once the detailed design phase is concluded, the validation of the taxi loads model continues by means of several taxi tests with the first prototypes, whose goal is to retrieve experimental data and then, find a good match between this information and the results obtained in the recreation of the scenario through numerical simulation. By the time a suitable data correlation is achieved, clearance is given to proceed with the final certification stages. Eventually, last certification loads loop is carried out with a model already validated in order to double-check that the results obtained in the previous iterations are still within the required limits.

In the case of the A400M, a total of 9 loads loops were required between 2003 and 2012 for the design and certification of the aircraft. The purpose of all of them was the design of a specimen that fulfilled all the certification airworthiness requirements concerning structural loads as a consequence of the operation in unpaved runways, which are summarized in Section 1.3. The design of the aircraft ensures the compromise for which the airframe will be able to perfectly support the limit loads originated under the scenarios established in the certification requirements [11].

Once the design phase is considered to be completed after having achieved certification, the aircraft model is frozen and the airframe structural capability is known, thus, the inverse engineering problem can be addressed. The inverse engineering problem comprises the EBH (Equivalent Bump Height) Curves Calculation process, in which the engineer must calculate the most severe runway roughness profile on which the aircraft is able to operate given its structural capability. In the case of the prototypes, loads clearance for the flight test campaign may be retrieved through this analysis. In the case of the serial aircraft, this method is worked out to provide the customer with the necessary information to know which is the maximum runway roughness level on which the operation of the aircraft is expected to not lead to limit load occurrence.

Theoretically, the direct problem is said to be deterministic, since the operation in each surface roughness profile and for a specific aircraft condition (including mass state, engine thrust, aerodynamics, brakes setting, rolling speed and ISA offset) yields a unique set of aircraft loads. In contrast, regarding the inverse problem, there are infinite runway profiles that lead to a particular set of airframe loads for each aircraft condition [3].

To solve this non-uniqueness problem following the EBH Method, a numerical analysis is performed to each runway, whose goal is to define which is the most severe 1-cos shape bump or trough for each obstacle wavelength. Therefore, with this method, a unique EBH curve is calculated for each runway roughness profile. Finally, this EBH curve is useful to be compared to other runways EBH curves, providing an accurate estimation of the expected loads levels for each runway.

Once the EBH curves of an aircraft are available, any operation over an unprepared airfield is preceeded by the measurement of the runway profile, so the EBH curve can be calculated and compared to the curves provided in the AFM. This comparison establishes a pass-fail criterion when giving clearance for the operation in that particular runway.

Besides, the computation of the EBH curves can be complemented with the definition of a set of Servicing Classes (tyre inflation pressures) in order to determine the actual flotation capability of the aircraft, which must agree with the flotation requirements determined prior to the conceptual design phase.

1.1.3. Motivation of the present work

In the case of the A400M, after the culmination of the design phase with the Type Certificate and the Initial Operational Capability in July 2013, Airbus Defence & Space proceeded with the EBH curves and flotation capability calculation of such aircraft, whose aim was to provide a more extended envelope of taxi conditions through which the company completely guarantees that the structural capability will never be exceeded. Since the certification requirements only specify a reduced set of runway roughness profiles, this provides the customer a tool to determine whether the unevenness of any particular runway is suitable for the A400M operation, and which are the maximum allowable operational weights and tyre inflation pressures as a function of this roughness level.

However, the method employed in the definition of the EBH curves of the A400M is considered to be very conservative. This conservatism lies in the fact the maximum allowable bump height for each wavelength and roughness level is defined just below the minimum obstacle elevation at which any of the cases analyzed, among all the possible aircraft configurations that can be considered, yields load magnitudes at any point of the airframe which are above the limits imposed by certification. This most critical case that sets the threshold for the operation of the aircraft at each bump wavelength may lead to the definition of weight and servicing class limitations at each roughness level.

Nevertheless, many times the aircraft is operated at some conditions which are very

different from the most critical one at a particular wavelength and thus, far from meaning a compromise in the structural limits of the aircraft. As a consequence, the conservatism intrinsic in the definition of the EBH curves has awakened the interest of the different OCCAR Air Forces, which are currently operating the aircraft, to further extend the taxi operational capabilities of the A400M in unpaved runways. This, in addition to the willing of the company to have a deeper understanding of the aircraft taxi limitations, have motivated Airbus Defense and Space to go one step further in the definition of the EBH curves. This actual customer need of exploring the structural behaviour of the specimen beyond the limitations imposed by the EBH curves implies a customer demand that have led the Structural Dynamics Aeroelasticity Department to define a new path to tackle the taxi problem by introducing the concept of probability in the exceedance of limit and ultimate loads.

1.1.4. Aim of the present work

In order to meet this customers need of exploring the aircraft taxi capabilities beyond its operational limits, Airbus Defence & Space is willing to develop a new statistical approach to complement the EBH curves already defined for the analysis of taxi loads. With this statistical analysis the company would be able to asses the risk in which the customers incur when operating in unpaved runways. As a consequence, the customers demand the quantification of that risk as the probability of limit loads occurrence at any point of the airframe when operating in more severe runways that those included in the AFM. Thus, taking advantage of the EBH method, the output of this statistical approach would comprise the probability of exceeding a given percentage of limit load at any point of the aircraft structure for a particular bump height, and then, with this information, clearance for the operation in a runway with a roughness profile beyond the limitations imposed by the EBH curves defined in the AFM would be given under the responsibility of the customer depending on the risk he is willing to take.

As a result of this idea conceived in the Structural Dynamics & Aeroelasticity Department some decades ago, the aim of this project is to develop a first approach to the methodology of this statistical analysis of taxi loads, with the objective of being applied to any current or future aircraft with capability of operation in unpaved runways. For the sake of simplicity, the scope of this project concerns the definition of 2D iso-load maps and a sensitivity analysis of the most relevant aircraft and operational parameters affecting the down bending moment at the left wing root and the vertical force suffered by the nose landing gear wheel axle during the taxi roll following landing maneuvers. Then, the definition of this 2D iso-load maps leads to the study of the probability of limit load exceedance on the two magnitudes of interest previously mentioned to finally provide, as a first cut, approximate probability curves for the quantification of the risk of operation in unprepared runways as a function of the roughness severity.

In order to unveil the development of this new statistical approach and deeply under-

stand the complexity of the taxi loads problem behind it, the present dissertation is broken down into 5 chapters, for which an outline of the different issues covered in each of them is described below:

- Chapter 1. First, the taxi loads problem is briefly introduced along with some related background, pointing out the main aspects in the assessment of this issue that have led to the current state of the art. Within this framework, the motivation and aim of the present project is described. Then, in order for this study to be meaningful, the relevance of the problem is presented. For that, relevant accidents in aviation history and the main airworthiness regulations concerning taxi are included. Finally, the key concepts that allow a better comprehension of taxi operations in unpaved runways are reviewed. This last section is concluded with a description of the different taxi campaign carried out by Airbus to test the performance of their products in this type of airfields.

- Chapter 2. The aircraft that serves as specimen of study for the development of the taxi loads statistical analysis methodology is presented. Apart from a description of the design and performance characteristics of the aircraft, the numerical model used as input for the simulation of the different taxi cases considered in the statistical analysis is also included. Therefore, detailed explanations of the aircraft structural model, landing gear model, mass model, aerodynamic model, damping model and gyroscopic loads model are provided.

- Chapter 3. The dynamic taxi loads numerical simulation process is described. The basic assumptions of the computation philosophy and a detailed explanation of the software tools involved is provided for a better comprehension of the calculation procedure.

- Chapter 4. The main section of the present project, which comprises the development of a methodology for the statistical analysis of taxi loads in the aeronautical industry, is fully developed. First, the topic is introduced with a brief reference of the overall dimensions of the problem to be studied. Then, the analysis is particularized for an approach, feasible in time, that comprises the definition of 2D probability maps and the corresponding probability curves to assess the likelihood of limit load occurrence when operating in unpaved runways. The fist step to accomplish these tasks starts with the definition of the starting point for the analysis, determining the roughness level subjected to study. Then, the most critical cases at the point of the EBH curve chosen for analysis are defined for the magnitudes of interest studied. Once the most critical cases are identified, the most relevant parameters affecting the taxi load magnitudes are selected and the overall casuistry considered for the statistical analysis is determined. Based on the taxi cases simulated, the methodology for the definition of the iso-load curves in the different probability maps is described. Finally, based on the probability maps already depicted, the probability calculation philosophy for the definition of the probability

curves is explained, including all the statistical and mathematical theory involved in the computation process. This statistical analysis is performed first for the operation in the design EBH curve considered as starting point and then repeated for the operation in more severe runways. In order to apply this approach to the A400M, the methodology is supported with the definition of 2D probability maps and probability curves for the down bending moment at the wing root and the nose landing gear wheel axle vertical force.

- Chapter 5. The conclusions concerning the statistical analysis of taxi loads and the methodology developed in this project are presented. In addition, future activities to be considered as guidelines for the completeness of the statistical approach are provided.

1.2. Relevance of the taxi loads problem

1.2.1. A sizing problem

Due to the elasticity of the aircraft structure, the excitation of its normal modes takes place as a result of taxiing over a surface of prominent unevenness [1]. This excitation makes the aircraft dynamic response to be further amplified and give rise to the presence of dynamic loads on the airframe, which is a consequence of the tuning between the runway roughness profile and the normal modes that occurs at a particular set of critical speeds. Therefore, taxi operations, specially those on unpaved surfaces, are usually the sizing cases for some specific parts of the airframe and landing gear structure. Down bending at the wing root, vertical force of the fuselage in the vicinity of the nose landing gear, front fuselage down bending close to the main landing gear and some nose landing gear components are probably the structural elements typically dimensioned by taxi analyses.

Figures 1.1 and 1.2 show a comparison between dynamic taxi loads (in green color) and other dynamic load scenarios for a real Airbus product:

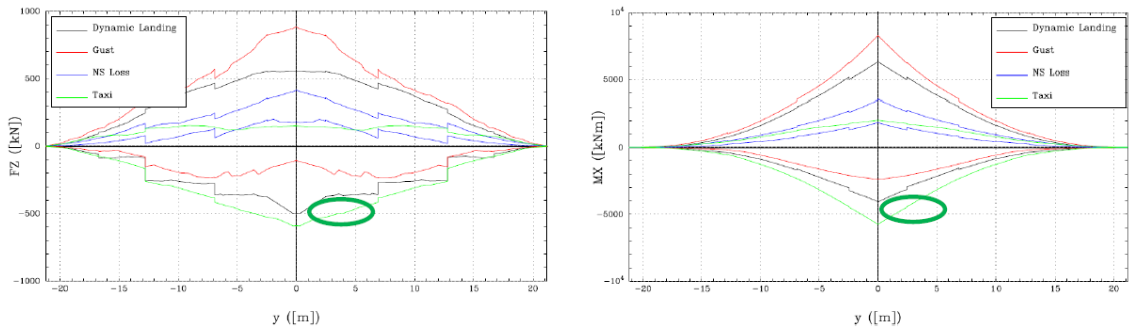

(a) Wing FZ (b) Wing MX

Fig. 1.1. Comparison between dynamic taxi loads and other dynamic load analyses at the wing

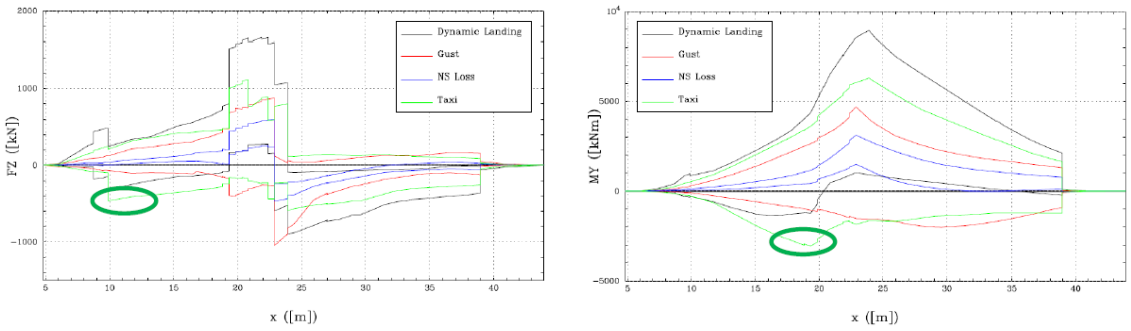

(a) Fuselage FZ

(b) Fuselage MY

Fig. 1.2. Comparison between dynamic taxi loads and other dynamic load analyses at the fuselage

In addition, apart from being a critical issue in the design and checkstress analysis for the certification of an aircraft, the computation of taxi loads may also be required for the determination of fatigue inspection intervals, the definition of maintenance standards or the estimation of the maximum number of allowable taxi operations that can be performed over a particular unpaved surface given the flotation capability of the aircraft.

1.2.2. Relevant accidents

A long list of accidents have occurred in aviation history as a consequence of ground manoeuvres, particularly during taxi roll after landings. The vast majority have involved civil aircraft and none of them was registered during the operation in unpaved runways, but nonetheless, all these accident emphasize the relevance of making an exhaustive assessment of the sizing problem that dynamic taxi loads comprise in the proper design of some specific parts of the aircraft structure, specially the landing gear and its components.

One of the first events of relevant importance happened in 1963, when a commercial Douglas DC-7B landed at Nashville Metropolitan Airport (USA) in foggy and rainy weather conditions. An improper crew operation led to a wrong control of the reverse thrust by the pilot, causing the nose landing gear to collapse as a consequence of asymmetric propulsive conditions [12].

Another more recent incident occurred in October 2015, when a Peruvian Airlines Boeing 737 landed at Cuzco-Velazco Astete Airport (Peru) [13]. During landing rollout, the right main landing gear folded outwards with one of its actuators detached from its mounts. The cause reported by the investigation agency was an improper approach and landing manoeuvre at high altitude airports. This incorrect procedure lead to an increased landing speed, the beginning of the flare manoeuvre at high altitude, and low sinking velocity, what provoked the aircraft to make soft contact with the runway, producing an inefficient operation of the shimmy damper, which could not prevent large oscillations of the shock absorber. In the same year, an Eclipse EA500 jet suffered from landing gear collapse while taxiing for take-off at Sacramento Executive Airport (USA) [14]. The

pilots reported that the left main landing gear strut had penetrated the left wing lower surface skin spilling an abundant amount of fuel onto the taxiway, but the causes are still being investigated.

Concerning military airplanes, one on the few reported accidents took place in 1978 at Reykjavík-Naval Air Station Keflavík (Iceland). A Lockheed EC-121T Super Constellation of the USAF was taxiing out to the runway for a routine training mission when the left main landing gear collapsed due to stress corrosion and the left wing struck the ground [15]. Also, the Air National Guard reported an incident operating a Lockheed C-130 Hercules at Minneapolis-St Paul International Airport in 2004 [16]. The transport aircraft landed with no problem, but as it started taxiing towards the apron, the right main landing gear collapsed.

Moreover, a special remark should be done when referring to the Fokker 100 regional twinjet aircraft series, since it has been involved in several taxi accident during its service lifespan.

The first accident involving this model happened in 1987, at Amsterdam-Schiphol International Airport (Netherlands), when the right main gear of one of the prototypes collapse during landing roll after a high speed (300 km/h) touchdown. The option considered to solve the problem comprised the lengthening of the main gear legs torque-links. Later, accidents originated by the same cause, i.e., main landing gear overload, were reported in 1994 (Netherlands), 1999 (Spain) and 2004 (Turkey).

Fig. 1.3. Fokker 100 prototype accident (1987)

Apart from these events, the most noteworthy incident in which the Fokker 100 was involved took place in 1989 Genève-Cointrin Airport (Switzerland). After the aircraft gently landed, the aircraft experienced unbounded vibrations that cause the left main landing gear to collapse, so the left wing struck the runway. The investigation agency finally determined two causes that instigated the accident: insufficient damping capacity of the main landing gear and its attachment point to the structure, and miscellaneous factors occurred so that the undercarriage experienced a resonant oscillation at 16 Hz [17].

This accident, in addition to other problems concerning strong vibration on the main landing gear during the certification flight test campaign, motivated the definition of several constraints for the operation of this aircraft, which could be skipped by those aircraft incorporating shimmy dumpers. The limitations imposed were the following [17]:

- Landings should not be performed with a flap deflection setting of 25 °or smaller, except if an emergency case enforces this scenario.
- Landings must be performed with spoilers fully deployed.
- Landings are not allowed with the auto-braking system activated.
- Limitations on the maximum allowed tailwind velocity component: 5 knots if the landing weight is equal or above 35000 kg, and 10 knots if the total mass is below that threshold.

Despite of this restrictions, this problem of vibrations appearing at the main landing gear still continued, although it did not involved further structural damage. This is the reason why, at the end, the improvements incorporated after the first accident in 1987 were found to be unsatisfactory, since they did not correct the anomaly causing this issue. In fact, the strengthening of the components damaged in the accidents could be insufficient if the structural damping dropped below a specific limit.

Fig. 1.4. KLM Fokker 100 accident at Genève-Cointrin Airport, March 1989

In addition to the previous ones, the Fokker 100 had also been involved in incidents due to fatigue. The most relevant one occurred at Dallas/Fort Worth International Airport (USA) in 2001, in which the lower part of the right main landing gear assemble separated from the airplane. The investigation agency finally reported that a fatigue crack in the mentioned gear cylinder had been the cause of such failure [18].

As the last example of taxi accidents, an Airbus A340 also suffered the rupture of the right main gear due to a fatigue crack that was developed in a region of high stress

generated by ground manoeuvres. This event took place in 1998 after landing at Brussel-Zaventem Airport (Belgium) [19].

1.3. Airworthiness taxi regulations

Despite the fact that the specimen selected for this study, the A400M, is described as the new generation of military transport aircraft, it is designed to fulfill both civil and military airworthiness regulations. Among all this required specifications, only the ones concerning taxi operations are disclosed in the following paragraphs.

1.3.1. Civil certification requirements

Concerning the compliance with civil regulations, Airbus and OCCAR signed a contract in which a set of certification review items was defined. In this documents, the certification requirements are, in turn, directly extracted from the overall regulations issued and approved by EASA.

The A400M Civil Basis of Certification for Taxi, Take Off and Landing Roll Design Loads is accorded in the CRI C-11 (Loading Conditions for Multi-Leg Landing Gear), which includes SC C-11 and IM C-11.

SC C-11 makes reference for the interest of this study to EASA CS 25.491 Taxi, takeoff and landing roll paragraph. The lines of this paragraph, which is contained in CS-25 Book 1 [20], describe a set of design standard procedures stipulated to comply with the taxi, takeoff and landing roll requirements of turbine powered large aeroplanes.

Likewise, IM C-11 is linked to the guidelines mainly provided in the AMC 25.491 Taxi, take-off and landing roll section. It is presented in CS-25 Book 2 [20] with a composition of seven subsections (see Appendix F for further details) and lays special emphasis on paragraph 4e. In general, AMC outline standard means to show compliance with the certification specifications, but these are considered as guidelines since its application is recommended but not unique nor mandatory. In the particular case of the AMC 25.491, which is specifically referenced in CS 25.491, a special interest is focused on the importance of the runway profile in the study of taxi dynamic loads and describes the required steps to be followed in the assessment of this problem.

Among the different procedures proposed, the approach in which the excitation of the aircraft normal modes is performed with 1-cos bump is preferred over the usage of PSD, practice which is only suggested in the computation of fatigue loads. Besides, for the determination of limit loads produced during taxi, take-off or landing roll phases, a brief documentation about San Francisco Runway 28R, before it was repaired, is included as standard mean of compliance for the study of ground loads. This runway profile has been a referent in taxi since it was known to cause high loads on airplanes and many pilots reported complaints about this issue until resurfaced.

In further detail, subsections 4 (F.2.4), 5 (F.2.5) and 6 (F.2.6) of the aforementioned AMC include more exhaustive information of the specific procedures and casuistry to consider in order to elaborate a complete dynamic taxi loads analysis. Information regarding the paragraphs that shape subsection 4 can be summarized in the following points:

- The analysis model of the airplane studied should reproduce significant airplane rigid body and flexible modes, and the appropriate landing gear and tyre characteristics. In addition, only the symmetric cases must be subjected to study unless the aircraft configuration yields significant asymmetric loads.
- Airplane steady aerodynamics effects should normally be included on dynamic response calculation meanwhile those concerning unsteady aerodynamics may be neglected.
- Conditions should be run at the maximum take-off weight and the maximum landing weight with critical combinations of fuel, and extreme positions within centre of gravity range.
- A series of constant speed runs should be made in both directions of the corresponding runway profile from 20 KTAS up the maximum operating ground speed expected in normal operation (V_R at maximum altitude and temperature for takeoff and 1.25 V_{L2} for landing conditions). The reason behind performing the simulations with constant speed runs lies in the fact that during accelerated runs, the combination of speed and roughness points that leads to peak dynamic loads might not be reproduced. In such a way, every bump defining the runway profile is swept at every possible speed.
- For maximum take-off weight cases, the analysis should include normal take-off flap and control settings and account for both zero and maximum thrust.
- For maximum landing weight cases, the analysis should comprise normal flap and spoiler configurations following landing. Also, steady pitching moments equivalent to those produced by braking with a coefficient of friction of 0.3 with and without reverse thrust should be included. The effects of an automatic braking system that reduces the braking force applied in the presence of reverse thrust may be taken into account.

1.3.2. Military certification requirements

In an analogous way, in the same previous contract agreed by Airbus and OCCAR, several MCRI were elaborated to define the military specifications of the aircraft. Specifically for taxi purposes, two of them were determined: MCRI B-02 Unpaved runways and MCRI C-20 Taxi, take-off and landing roll design loads on semiprepared runways.

Focusing on the latter, MCRI C-20 specifies all the military requirements to be fulfilled, as documents 25.491 specify for civil airworthiness. Also, it makes reference to two additional runway profiles of higher severity than San Francisco 28R, which are included on the British military standars (DEF-STAN). Such roughness profiles are particularly defined on *DEF-STAN 00-970 Leaflet 49: Design of undercarriages - Operation from surfaces other than smooth hard runways. Specification of continuous ground unevenness* [21].

In the end, MCRI C-20 requires optimal aircraft performance on the following runway profiles, each one associated to a take-off, landing or rejected take-off reference weight defined for each mission. This relationship concerning mission weight, manoeuvre and runway profile can be summarized in Table 1.1.

	MANOEUVRE		
MISSION	LND	TO	RTO
Tactical (TLL-1)	DEF-STAN B MLW @ 12 ft/s	DEF-STAN B 80% MTOW	DEF-STAN A 80% MTOW
Logistic Normal (LN-1)	DEF-STAN A MLW @ 10 ft/s	DEF-STAN A MTOW	San Francisco 28R MTOW
Logistic Heavy (LH-1)	San Francisco 28R MLW @ 10 ft/s	San Francisco 28R MTOW	Blagnac MTOW

TABLE 1.1. A400M MILITARY TAXI REQUIREMENTS (MCRI C-20)

Pointing back to the DEF-STAN certification document, its scope particularly focuses the attention on the definition of continuous ground unevenness of a continuous nature, rather than the usage of discrete obstacles for the evaluation of dynamic taxi loads. It determines that the quantitative specification of such magnitude is necessary to establish a level for design that ensures proper aircraft performance in unprepared surfaces. Also, to estimate the roughness profiles used for clearance trials and to establish a correlation between standard design roughness levels and that of a real operating runway.

For the quantification of ground unevenness, the variation of the profile height (h) is determined with respect to the x and y coordinates of the runway reference plane, but this definition is usually concentrated uniquely on the longitudinal coordinate, *h(x)*. Although not in such a great extent, PSD technique is also used with particularization for each runway to model this surface characteristic.

As a consequence of this quantification, runways are grouped into four categories depending on their roughness severity, distinguishing from paved runways regularly maintained to unpaved runways on virgin ground. Thus, the profile mathematical function of a runway, *h(x)*, is the result of multiplying each vertical coordinate of a standard profile shape by the corresponding factor to the class in which it is included. As a result, the more

severe runway for which the A400M is theoretically designed corresponds to the DEF-STAN B, which comprises a rescaling of the DEF-STAN A by a factor of 1.5. Therefore, the higher the severity of the runway roughness profile, the lower the takeoff and landing weights, specified by each mission, the aircraft is capable to operate with.

Likewise, DEF-STAN A is then followed in terms of severity by San Francisco 28R and this, in turn, by Blagnac runway, which is included in this classification due to an internal policy that Airbus follows when evaluating dynamic taxi loads during rejected take-off. Such policy implies that the roughness level employed in this manoeuvres should be that specified for takeoff cases but reducing one degree of severity, as referenced in Table 1.1.

1.3.3. Flotation capability contractual requirements

In addition to the certification requirements that define the runway roughness over which the aircraft must be able to operate, there is an additional requirement in the A400M contract agreed between Airbus and OCCAR regarding the flotation capability.

It stipulates that the aircraft shall be capable of performing the following number of passes for each of the Tactical and Low Weight Tactical MLW specified in Table 1.2. One pass is defined for this purpose as the equivalent of operation of one takeoff or one landing on the operating surface.

	# PASSES	
A/C WEIGHT [T]	CBR4	CBR 6
107	6	73
115	3	34

TABLE 1.2. A400M FLOTATION REQUIREMENTS FOR LANDING MANOEUVRES

Both runway hardness conditions should be fulfilled with a deceleration up to 5 ft/s^2, a tyre deflection not more than 40% and with a centre of gravity excursion from 28% to 32% MAC.

Besides, the aircraft shall also be capable to perform a takeoff at the Tactical MTOW (115 T), with the tyre pressure corresponding to the conditions defined for the previous paragraph.

1.4. Taxi loads model: development and validation

In order to carry out an accurate study of the taxi operational capabilities of an aircraft, a taxi loads model to be used in the numerical simulation of this flight phase must be defined. What apparently seems to be an easy task, may become really complex when

modeling the non-linear behavior of the landing gear. Such non-linearities have their origin in the kinematics and elastic characteristics of some of its components. These nature, in turn, comes from the landing gear requirements, which range from the dissipation of energy during landing to the manoeuvrability of the aircraft on ground, having also the capability of being retracted and stowed in flight [22]. These requirements are thus achieved thanks to the employment of a complex mechanism of shock absorbers and wheel-tyre assemblies. Therefore, the equations of motion of the landing gear preserve all these kinematic and elastic non-linearities [23], considering as rigid the rest of its structural elements. The combination of these two systems leads to a set of equations to model the motion of the landing gear that accounts for its non-linear nature and its coupling with a flexible structure [24]. The equation of motion in matrix form is of the form:

$$\left[TM\right]\left\{\ddot{q}\right\} = \left[\bar{V_r}\right]\left\{F_r\right\} + \left[\bar{V_a}\right]\left\{F_a\right\} + \left\{F_{a/t}\right\} + \left[\bar{F_c}\right] \tag{1.1}$$

where: $\left\{q\right\}$ makes reference to the geometric coordinates of the landing gear, $\left[TM\right]$ corresponds to the generalized mass matrix represented by lumped masses with their associated inertial moments, $\left[V_r\right]$ comprises the geometric transformation matrix of the tyre forces, $\left\{F_r\right\}$ are the forces at the tyres, $\left[V_a\right]$ corresponds to the shock absorber forces geometric transformation matrix, $\left\{F_a\right\}$ are the shock absorber forces, $\left[F_c\right]$ model the non-linear terms in q and $\dot{q}$ and $\left\{F_{a/t}\right\}$ represents the interaction force between the aircraft and the landing gear.

By contrast, the aircraft structure is considered a linear system, whose movement and deformation are formulated in modal coordinates as [24]:

$$\left[GM\right]\left\{\ddot{x}\right\} + \left[GS\right]\left\{x\right\} = \left[\emptyset\right]^T\left\{F_0\right\} + \left[\emptyset\right]^T\left\{F_{t/a}\right\} \tag{1.2}$$

in which $\left\{x\right\}$ constitutes the modal generalized coordinate, $\left[GM\right]$ corresponds to the generalized mass matrix, $\left[GM\right]$ is the generalized stiffness matrix, $\left[\emptyset\right]$ constitutes the modal matrix, $\left\{F_0\right\}$ makes reference to the external forces (the effects of gravity, aerodynamic forces, engine thrust, brakes, etc. can be included among others) and $\left\{F_{t/a}\right\}$ are the forces applied by the landing gear on the aircraft.

With expressions 1.1 and 1.2, this coupled set of equations, through which the displacements of the aircraft-landing gear system is modeled, constitutes a non-linear system whose solution must be obtained by numerical integration in the time domain [24]. As a result, apart from the loads in the landing gear components, including the tyre deformation and shock absorber displacement, the forces at the attachment points of the landing gear to the aircraft structure (pintle points) are obtained.

Unfortunately, the output achieved by combining the two previous mathematical models is not the final solution of the numerical simulation of taxi loads, but an intermediate step of the procedure required to compute the response of the entire aircraft structure.

Such process, which is further elaborated in Chapter 3, has as a starting point the computation of the eigenvalues and eigenvectors, which characteristic to each aircraft. A rigid nonlinear model of the landing gear, in addition to a flexible linear model of the aircraft, are needed to accomplish such computation. Then, to obtain the forces and moments at the aircraft centre of gravity of each taxi case considered, a static balance is carried out. Also, 1G static loads at the wheel axles and pintle points are calculated. Afterwards, the iterative numerical integration of Equations 1.1 and 1.2 comes into play, from which the forces present at the landing gear movable and non-movable parts interface are retrieved. The next step comprises the transformation of these forces to the pintle points previously mentioned, which are then applied to the rest of the airframe to obtain the dynamic response of the aircraft when rolling over a particular surface. This transient response is computed in the frequency domain and the structure deformation expressed in modal coordinates. Eventually, the loads obtained in such response are integrated and defined for different monitoring stations located at particular positions of the airframe.

In order for the results to be considered reliable, the validation of the taxi loads model comprises a must as one of the multiple steps that are required to be achieved in the certification process of the aircraft. So, with the purpose of validating the numerical model, a comparison between the data collected in real runway taxi tests and the the output results computed in the simulation of those trials is performed, as shown in the following flowchart:

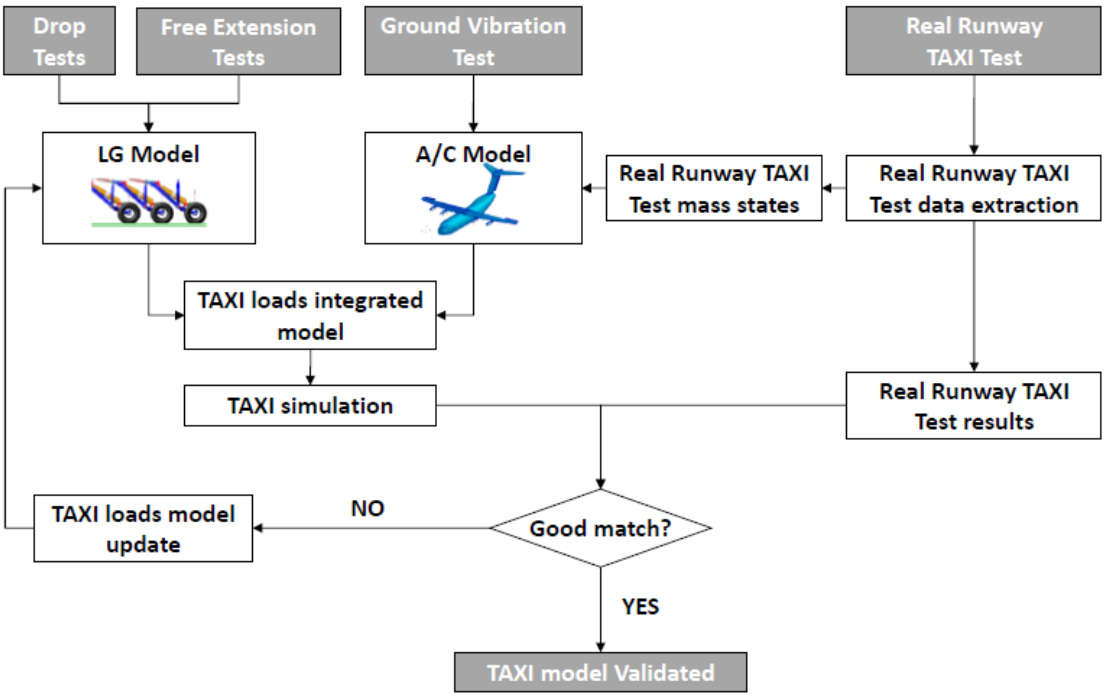

Fig. 1.5. Taxi loads model validation flowchart

According to the procedure illustrated in Figure 1.5, an accurate landing gear model must be first integrated with its corresponding aircraft numerical model, which have been

both previously validated with their corresponding experimental tests [25]. Then, the aircraft parameters and runway operating conditions are reproduced from the test to be incorporated to the numerical simulation, which is finally run following the process explained in previous paragraphs. The transient magnitudes numerically computed can now be compared to the real taxi test aircraft response in order to prove the validity of the taxi loads model.

As a matter of example to illustrate the need of experimental data to validate the taxi loads model, in the case of the specimen studied in the present paper real taxi runs were included in the A400M test campaign performed by Airbus for the required certification of the aircraft. This test was carried out in August 2010 at Francazal airfield, close to Toulouse, making use of the second prototype (A400M MSN2) of the corresponding airplane series [26]. One of its main purposes was to validate the A400M dynamic taxi loads model and perform any update if necessary, so the aircraft was properly instrumented to record all the necessary information about the aircraft response as a consequence of the applied excitation.

Francazal airstrip is characterized to be a paved surface of high evenness. The measurement of its roughness profile was accomplished prior to the tests in which different types of bumps were installed halfway the runway length to test the aircraft taxi capabilities.

Three kind of wooden obstacles were used: a single 1-cos bump of 20 meters long and 14 centimeters high utilized for the validation of the dynamic taxi loads model; a single repair-plate MAT-2 made to examine the aircraft response to a single impact; and a single step used to study the maximum tyre deformation [26].

Fig. 1.6. A400M running over the 1-cos bump during Francazal test

As stipulated in the airworthiness regulations, this taxi test comprised successive trials over each obstacle, sweeping several A/C speeds, centre of gravity positions, thrust and brakes settings and flap and spoilers deflections. Also, during these test trials, the monitoring interest was focused on the vertical forces at the nose landing gear and front right main landing gear leg, along with the wing tip vertical acceleration, front fuselage shear force and wing root bending and torsion moments.

After all the signals of the magnitudes of interest were gathered, the Structural Dy-

namics and Aeroelasticy Department at Airbus Defence & Space performed the data post-processing. The time histories of the experimental data and the ones from the numerical simulations were contrasted and a good correlation was found between them.

In this specific taxi test, a run over the 1-cos obstacle was considered of special importance since severe loads conditions were found to appear for both the wing down bending moment and the vertical force at the nose landing gear, two of the aircraft magnitudes sized by taxi. The parameters that yielded this critical scenario were found to be forward centre of gravity position, pedal braking and reverse thrust setting activated, velocity around 70 knots, 15° for flaps deflection and spoilers out [26].

In addition, several conclusion about the taxi loads model were drawn. One of them stated that dynamic taxi simulations exhibited more similar results to the ones obtained in the test for trials in which the aircraft and landing gear experienced high loads rather that those that originated low ones. Also, the incremental contribution of 1P loads was estimated to be negligible [26]. As a result after the campaign, the pre-test fully coupled dynamic taxi model was said to be enough accurate or conservative for the last loads loop to be the one provided for certification.

1.5. Operation in unpaved runways

The A400M has a special special feature which is only shared with a very few airplane models, mostly military transport aircraft, as it is the capability of operation in unpaved runways. Such feature may imply a higher degree of complexity in the aircraft design process since the aircraft normal modes are excited to a greater extent as a consequence of operating in a surface of a significant roughness profile. These amplification of the aircraft response leads to the manifestation of dynamic loads on the airframe as a result of the coupling between its normal modes frequencies and the excitation produced by a roughness profile at a particular speed [1].

Unpaved runways can be classified into three categories, depending on the degree of prior preparation:

- Prepared runways, in which an exhaustive prior work of levelling and compaction of the airfield has been performed before the operation of the aircraft.
- Semi-prepared runways, which have been simply cleared of possible debris and obstructions.
- Unprepared runways, in which the operation takes place on virgin ground.

Therefore, the analysis of dynamic taxi loads in unpaved surfaces, specially in those of the second and third kinds, requires the assessment of the roughness profile on which the taxi operation is carried out. The severity of the roughness profile of an unpaved surface

will normally be higher that that of a paved one [27], and therefore special attention shall be paid to the structural behavior of specific aircraft components due to the magnification of the consequent dynamic taxi loads, such as the landing gear, the front fuselage where it is attached and the wing root due to the down bending.

In order to evaluate the severity of a specific runway profile or to determine the operational capability of an aircraft in soft soils, concepts such us EBH or flotation capability have been developed to assess this problem.

1.5.1. EBH Method

The Equivalent Bump Height (EBH) method was an approach developed by BAe Systems (former British Aerospace) in 1996 that allows for the quantification of the severity of a particular runway profile [28]. For that, runway profiles are characterized as a function of their similarity to a 1-cos bump over a wide range of bump wavelengths.

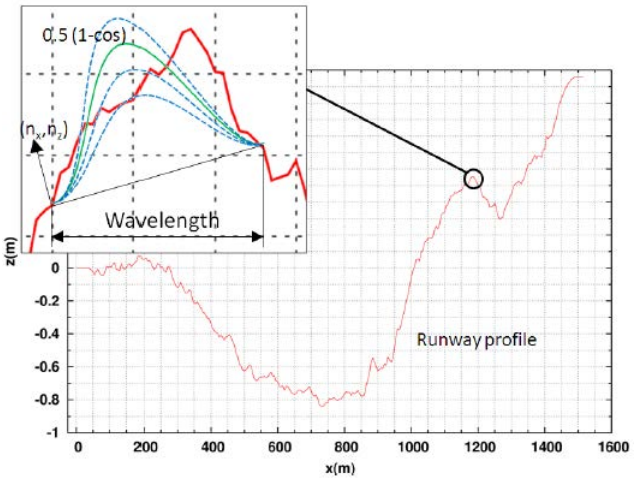

Fig. 1.7. EBH method applied to a particular runway profile

Therefore, for a given wavelength $\lambda = x(i+N) - x(i)$, a least squares fitting with a $0.5(1-cos)$ mask is moved along the whole runway profile to assess how the local roughness profile correlates the 1-cos bump (or through). Hence, for each $x(i)$, the EBH is computed according tho the following mathematical expression [11]:

$$EBH|_{x(i)} = \frac{\sum_{j=1}^{N} \left[n_x \left(x(i+j) - x(i) \right) + n_z \left(z(i+j) - z(i) \right) \right] \frac{1}{2} \left(1 - \cos\left(2\pi j / N \right) \right)}{\sum_{j=1}^{N} \left[\frac{1}{2} \left(1 - \cos\left(2\pi j / N \right) \right) \right]^2} \tag{1.3}$$

where N is the number of steps in which the wavelength λ is divided.

Giving a simpler explanation, the EBH method determines the height of a 1-cos bump shape that better fits a portion of the runway profile of coincident length. The maximum

length that could be used would be that of the whole runway, but computations are usually restricted up to 100 meters.

After considering all the possible or specified sweep of wavelengths at every point of the runway profile, this method outputs the corresponding runway EBH curve. This curves illustrate the greatest height among all the possible fittings of the local profile to a 1-cos mask for each wavelength. In Figure 1.8, the EBH curves of a few runways are presented, including Francazal with the addition of the 1-cos bump used for the validation of the taxi loads model, Blagnac and the three standards previously mentioned, such as San Francisco 28R, for civil aviation, and DEF-STAN A and DEF-STAN B, for military certification. According to the airworthiness regulations described in Section 1.3, it can be appreciated how the DEF-STAN B EBH profile is equal to that of the DEF-STAN A but multiplied by a factor of 1.5.

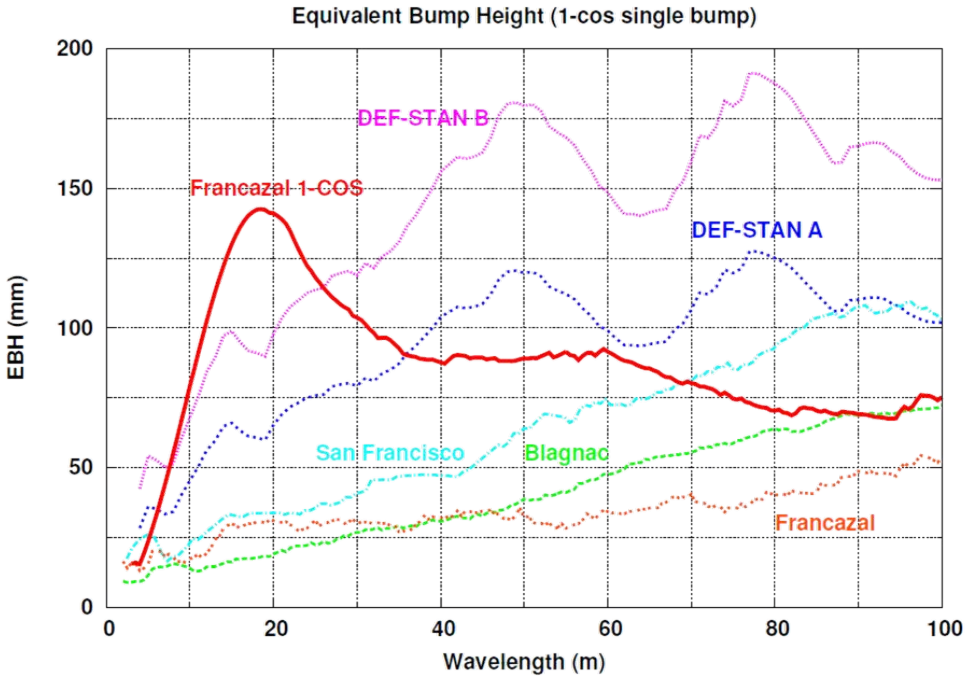

Fig. 1.8. Equivalent Bump Height curves example

Looking also at the previous figure, note that the EBH curves plots do not provide information about the runway position where the maximum EBH value takes place, but only the maximum EBH for each wavelength. Theoretically, this is due to the fact that the excitation produced by a bump of specific length and height will be independent on its position on the runway, but in reality, this is not totally true since not all the points of a runway are crossed at the same velocity. As an example, the greatest EBH that can be found when the wavelength is about 20 meters belongs to Francazal runway with the 1-cos bump previously mentioned. This particular section is the most critical at that specific wavelength range since it is above any of the other EBH curves depicted.

Likewise, once the structural capability of an aircraft is defined, the inverse engineering problem can be assessed in order to specify which is the maximum allowable runway,

in terms of roughness profile, in which the aircraft is able to operate without compromising its structural integrity. In the case of the A400M, 5 EBH curves were computed (refer to Figure 4.1), each one comprising a roughness level in which several limitations concerning maximum operational weights, centre of gravity position and tyre inflation pressures were imposed. Also, the EBH curves of an aircraft allow the capability to compare them with the roughness profile of other runways and asses their severity, since it is not an easy task to perform by looking directly at their profiles.

As a conclusion, the EBH method allows a direct measurement of the level of severity of any runway and an estimation of the load magnitudes that the operation on such roughness profile may involve, since passing through a bump of given wavelength at a particular speed is translated into an excitation of a frequency that may coincide with that of a normal mode of the aircraft in operation.

1.5.2. Flotation capability

Apart from the degree of severity of its roughness profile, the runway surface hardness is also an important parameter to take into count when studying the performance of an aircraft during taxi operations.

The flotation capability of an aircraft specifies its ability to perform operations in an unpaved runway of a given surface hardness. Normally, it is referenced with the number of passes an aircraft is able to carry out before reparation of the runway is required. The scale that allows for the quantification of the surface hardness is established by means of the California Bearing Ratio (CBR). This runway parameter is evaluated with the aid of a cone penetrometer, which is manually handled by an operator to take measurements all along the runway.

Fig. 1.9. Penetrometer application at Pembrey A400M campaign (left) and penetrometer detailed sketch (right)

In addition to the surface hardness, two other parameters should be taken into account when determining the flotation capability of an aircraft, such as the wheel load determined

by the dynamic response of the aircraft, which has a strong dependency on its weight, and the tyre-surface contact area, which varies according to the tyre inflation pressure.

For a given aircraft weight, runway roughness (EBH curve), runway hardness (CBR) and tyre pressure, the aircraft is characterized to have a quantifiable ground flotation capability, which can be improved by diminishing the tyre pressure, so the tyre contact surface is increased. Also, the wheel loads and tyre deflections experienced by the aircraft are determined by this four previous operation characteristics.

Nevertheless, a problem may arise when trying to enhance the flotation capability since there is a limit in the tyre pressure reduction: operation on too rough runways with too deflated tyres can lead to tyre bottoming, with subsequent risk for tyre and LG integrity. Tyre bottoming phenomenon has a high probability of occurrence whenever the tyre pressure is diminished, since the tyre stiffness and its allowable deflection are subsequently reduced. Thus, as a consequence of the deterioration of the deflection capability, the tyre rubber may end up bonded to the wheel rim when operating the aircraft on ground. In general, three scenarios can be summarized as a result of tyre pressure variation:

Tyre Pressures	Tyre Deflection	A/C Loads	Flotation Capability
Higher	Large margin until bottoming	Determined by runway roughness	High runway degradation Risk of sinking
Optimum	Just below bottoming	Determined by runway roughness	Optimum
Lower	Bottoming risk	High A/C loads Tyre degradation	Very high

TABLE 1.3. EFFECT OF TYRE PRESSURES ON AIRCRFT LOADS AND FLOTATION CAPABILITY [11]

Therefore, as a result of the different scenarios that might be encountered, Servicing Classes are established after an iterative process within the EBH curves computation process. They specify the tyre pressure that yields optimum flotation capability depending on the aircraft weight and the roughness profile in which it operates. Regarding the A400M, Structural Dynamics and Aeroelasticity Department of Airbus DS, in collaboration with the Landing Gear Department, defined four Servicing Classes, whose application depends on the aircraft operational weights specified for each mission and the corresponding allowable roughness levels (refer to Table 4.2). These Servicing Classes include:

DESCRIPTION	PRESSURE
A	Extra Low Pressure for maximum flotation
B	Low Pressure
C	Normal Operation
D	Overpressured

TABLE 1.4. A400M SERVICING CLASSES

In addition to the definition of Servicing Classes, another constraint when defining the ground flotation performance of an aircraft might be added as the number of passes that it shall be capable to carry out before the runway in which the manoeuvres take place has to be repaired.

The need for runway reparation to keep guaranteeing optimum operation arises due to the appearance of ruts during taxi rolls over soft surfaces. Taxiing over pre-existing ruts may comprise an additional issue, since the local surface roughness and compactness in these soil strips, as well as its CBR value, will probably differ from the previous characteristics of the overall unpaved airfield. As a consequence, there is a high probability for the landing gear to get partially buried, fact that may lead to the exceedance of limits loads. The most critical case happens when the landing gear gets completely stuck on a deep rut making the aircraft to suddenly stop. Hence, due to the high inertia of the aircraft, this situation may lead to landing gear fracture or even detachment from the fuselage.

Fig. 1.10. Main landing gear partially buried on an unpaved surface

In addition to the certification requirements that define the runway roughness profiles over which the aircraft must be able to operate, there is an additional specification in the A400M contract agreed between Airbus and OCCAR regarding its flotation capability, as explained in Section 1.3.3. The requirements imposed for aircraft flotation capability help perform a good assessment of the two aforementioned problems, such as runway degradation and landing gear burial.

1.5.3. Unpaved Runway Campaigns

The operation in unpaved runways cannot be considered a feature that has been recently implemented on aircraft, since from the very beginning of aviation history, aeroplanes

already performed takeoff and landing manoeuvres in this kind of airstrips. However, note that these were light airplanes and the airfields presented at least partial preparation to make these manoeuvres easier for not so well trained pilots.

But when talking about transport aircraft, only a few military specimens required to operate in very hostile environments are able to deal with these type of operations. Some examples are the Lockheed C-130 Hercules, Boeing C-17 Globemaster III, Antonov An-22 or the former CASA products CN-235 and C295. Regarding civil aviation, only very few airplanes have received certification to operate in unpaved runways, such as the BAe 146/Avro RJ, the Pilatus PC 24 or the Boeing 737 with Gravel Kit, although not as severe as the ones the military products are designed for.

In one case or the other, several campaigns are launched to test the performance of these aircraft on the unpaved airfields in which they are expected to operate.

As a matter of example, one of the first unpaved runway campaigns that Airbus accomplished was the one carried out at Corral de Ayllón. This campaign was later followed by the one devoted to the C295 in 2000, which took place in Agoncillo airfield, near La Rioja (Spain) [24]. After this pionner campaign in real loads monitoring, several conclusion were drawn once the data retrieved was post-processed. The nose landing gear was identified as a key structural component in the analysis of dynamic taxi loads in unprepared surfaces. In addition, sensitivity analysis performed remarked the enormous influence of the aircraft weight and centre of gravity position on the magnitudes of these loads and the irrelevance of the use of reverse thrust when relieving nose landing gear workload, opposite to the idea conceived a priori.

In the case of the A400M, in order to show the customers that the aircraft fulfilled the operation in unpaved runways and flotation capability requirements, four additional taxi campaigns were completed to study the A400M operating performance in several unpaved runways with different characteristics. The first two of them would also complement the one carried out in Francazal for the validation of the taxi loads model.

Ablitas airstrip was the first location in Navarra (Spain) chosen for this operations in 2013. The objective of this trials were to test the specimen in surfaces made of gravel (hard soil). The second campaign was performed in the airfield of Écury sur Coole, near Reims (France), in 2015. Out of the four, it was the most severe runway in terms of roughness profile since it was covered by grass (soft soil).

To reaffirm once again the validity of the dynamic taxi loads model, a numerical simulation of these two campaigns was also performed at the Structural Dynamics and Aeroelasticity Department of Airbus DS (Getafe). Different challenges had to be solved when reproducing the exact conditions of these taxi trials since the aircraft path did not coincide with the runway profile measurement line; the runway profile had to be adapted to match the aircraft variable velocity at each of its longitudinal coordinates; the actual shock absorber volumes differed from the theoretical values due to temperature variations; or a different braking coefficient had to be applied at each leg for the results to show an

accurate correlation.

(a) Ablitas: gravel

(b) Écury sur Coole: grass

(c) Woodbridge: sand

(d) Pembrey: beach sand

Fig. 1.11. A400M Unpaved Runway Campaigns

Later in 2016, the third taxi campaign took place in Woodbridge, Suffolk (England), whose airstrip consisted of sand and bentonite. These trials were aimed to study the aircraft performance in soft unpaved runways without vegetation and allowed the refinement of the servicing classes definition for this type of operations. Finally in 2017, the last campaign was promoted by the Royal Air Force (UK) to specifically prove that the aircraft met the flotation requirements. It was performed in a very soft beach at Pembrey (Wales), whose sand hardness was highly dependant on its water content due to the tides.

2. DESCRIPTION OF THE AIRCRAFT SUBJECT OF STUDY

2.1. General description of the aircraft

As a consequence of the customers need concerning the operation in unpaved runways already discussed in Section 1.1.4, the Airbus A400M was the aircraft chosen as the specimen of study to numerically illustrate the methodology of the taxi loads statistical analysis proposed in the present project.

The A400M is defined as a multirole four-engine turboprop military transport aircraft that was designed by Airbus Military (now Airbus Defence and Space) to replace older transport aircraft, such as the Transall C-160 and the Lockheed C-130 Hercules. Its maiden flight took place by the end of 2009 and the project has received so far 174 orders from eight nations, out of which 62 are in current world-wide operation. Since the very beginning of the design process, the plane was conceived to be capable of operating on many diverse scenarios and thus, receive civil and military certification. As a result, this program would be able to cover many purposes, not only giving rise to one of the most technologically advanced airlifters for a wide range of military operations, but also ready for the completion of any humanitarian mission in which air transport is required.

Accordingly, the A400M program was specially focused to cover the gap in military transport aviation characterized by the lack of aircraft combining both strategic (or logistic) and tactical capabilities. Therefore, the design efforts were concentrated on the design of an aircraft with the ability to cover three missions in one: strategic airlift (transport of strategic assets like outsized and heavy vehicles or equipment), tactical airlift (transport and delivery of personnel and goods directly into theatres of operation) and air-to-air refuelling (certified to be refuelled or to refuel other aircraft by probe and drogue mechanisms or HDU).

As a consequence of all the requirements that the aircraft has to fulfill, the A400M presents particular features to meet each of them [29].

Apart from the three missions previously cited for which the aircraft was developed, the ability to perform aerial delivery, combat offload and large payload transportation, such as tanks or helicopters, is feasible thanks to the large dimensions of the cargo hold, which is accessible by the ramp and door located at the rear fuselage. Some of the main aircraft dimensions are shown in Table 2.1.

Length [m]	45.10
Height [m]	14.70
Wing Span [m]	42.40
Wing Area [m^2]	225.1
Cargo Hold Length [m]	17.70
Cargo Hold Width [m]	4.00
Cargo Hold Height [m]	3.85 - 4.00
Cargo Hold Volume [m^3]	340

TABLE 2.1. MAIN A400M DIMENSIONS

Fig. 2.1. A400M profile, front and floor views

This cargo dimensions also allow the aircraft to accommodate up to 116 fully para-troops or to even accomplish medical evacuations. Main weight definitions are gathered in Table 2.2.

MTOW [kg]	MLW [kg]	MPL [kg]	MFW [kg]
141000	122000	37000	50500

TABLE 2.2. A400M WEIGHT CHARACTERISTICS

High performance STOL characteristics, in addition to reverse thurst setting option, are provided by four EuroProp International (EPI) TP 400 turboprop engines with 8-bladed counter-rotating propellers. Table 2.3 contains the main characteristics of this powerplant.

Propeller Diameter [m]	Max. power [shp]	Propeller RPM
5.34	11000	655/690, 730, 842

TABLE 2.3. A400M POWERPLANT DATA

As a consequence of the large propeller radius, the A400M was designed following a high wing configuration. This feature maximizes the volume of the cargo bay and

makes the loading operations on ground easier due to the wide space around the aircraft. Besides, in order for the propeller flow and the engine exhaust to not interfere directly with the horizontal stabilizer, the aircraft presents a T-tail configuration, which also enables a higher manoeuvrability due to the large elevator surface.

Moreover, thanks to its advanced technological features and engines, the A400M has a maximum range performance of 8,900 km (4,800 nm), cruising at an altitude of 11,300 m (37,000 ft), or even higher, ceiling up to 12,200 m (40,000 ft) during special operations. As a result, this capability translates into a fatigue reduction for crew and transported troops, since it allows to avoid poor weather and turbulence conditions that occur in the lower troposphere. Apart from flying higher, it can also fly faster than other airlifters in its category, reaching speeds up to Mach 0.72, being the efficiency delivered analogous to that of a turbofan powered transport aircraft. All this features give the A400M the suitability to perform a wide range of logistic missions worldwide.

Cruise Mach	0.45 - 0.72
Max. Operating Altitude	37,000 ft (40,000 ft)
Range	4535 - 8700 km

TABLE 2.4. A400M GENERAL PERFORMANCES

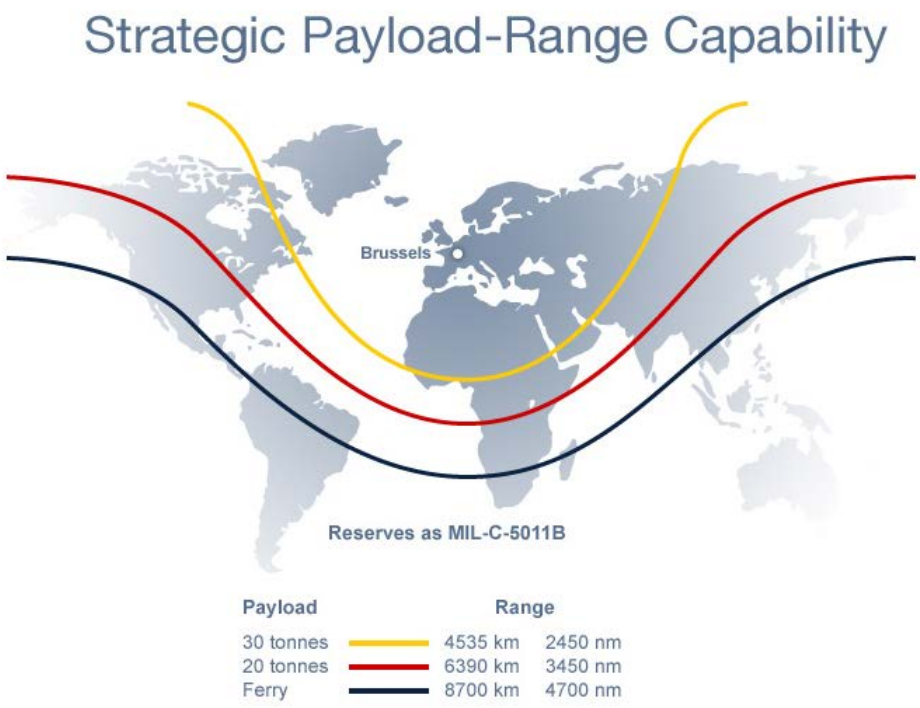

Fig. 2.2. A400M range scheme

In addition, the capability to perform operations in unpaved airfields is limited to the tactical mission characteristics of the aircraft, which were tailored to be able to properly

operate in space-limited hostile facilities with short airstrips thanks to its STOL certification. As matter of fact, the A400M can carry out take-off and landing manoeuvres in quite soft (CBR 6) runway of severe roughness profile with an extension not longer than 750 m (2,500 ft), freighting a payload of 25 tones (55,000 lb) and being loaded with the fuel required for a 930 km (500 nm) return trip.

This capability is in part due to the small landing gear specifically designed for this aircraft, which is stored in the fuselage in order to provide a small ground-fuselage distance to facilitate loading operations. As most of the current airplanes manufactured, the landing gear has a tricycle configuration, which provides the aircraft with high manoeuvrability on ground due to the nose landing gear steerable wheel. Further in detail, the twin-wheel nose gear presents a telescopic configuration, in which the shock absorber mechanism is made up of two chambers: a low pressure chamber, which is the one normally in operation, and a high pressure chamber, which is activated whenever the dissipation of energy in high strength impacts is required.

Regarding the main landing gear, it is composed of 6 independent articulated legs, each one supported by 2 wheels. This main landing gear configuration makes the A400M to have kneeling capability, lowering the rear ramp to ease the access of large vehicles to the cargo hold. Each main gear strut presents a single chamber shock absorber and all the braking action is concentrated on its 12 wheels, which are assisted by an auto-braking system.

(a) Nose landing gear (b) Starboard main landing gear

Fig. 2.3. A400M deployed landing gear on ground

2.2. Aircraft dynamic taxi loads numerical model

In order to simulate the dynamic response of an aircraft when taxiing over a runway of a given roughness profile or to reproduce this excitation according to the EBH method, a numerical model of the specimen studied is required to proceed with the computation process. The main objective of this computer-based and mathematical model is to reproduce in the most accurate possible way all the parameters intrinsic to the design and operation of the aircraft. But time is limited and deadlines must be fulfilled, so a trade-off be-

tween accuracy and computation time must be always considered to match the computer resources available.

The numerical model concerning the A400M is in turn composed by several numerical sub-models, which are explained in detail in the following sections. Each one focuses on one specific field of the design of the aircraft and all of them have been validated with the corresponding experimental tests.

2.2.1. Aircraft structural model

The aircraft structural model is a computational model whose objective is the representation of the aircraft stiffness and its degrees of freedom. It is considered to be linear and flexible and makes use of the Finite Element Method (FEM) technique to be generated (MSC.NASTRAN). In the case of the A400M, the structural model can be considered suitable in the representation of the dynamic behavior of the structure normal modes up to a 50 Hz cutoff frequency, criteria that was proved during its validation in the corresponding Ground Vibration Test.

It addition, this model is developed in such a way to adequately emulate the structure load path among the different aircraft components, including its stiffness characteristics. Accurate models of the lifting surfaces (wing, HTP, VTP), engine and engine mounting system (EMS), control surfaces (ailerons, elevators, rudder) and fuselage are included.

Moreover, the structural model used in the numerical simulations can be considered complete or half symmetric due the characterization of the taxi case in terms of its asymmetry. Asymmetries may arise due to the configuration of the aircraft (application of the ailerons or rudder leading to a roll or yawing moment or asymmetric braking force action) or the taxi manoeuvre itself (asymmetric runway unevenness).

For the purpose of this project, checkstress taxi analysis in which the excitation is carried out with bumps are performed either with full or half symmetric aircraft models depending to a larger extent on the asymmetry induced by the deviation of the aircraft centre of gravity from its symmetry plane. On the other hand, to simulate the runs carried out during taxi campaigns, specially if they are performed on unpaved runways, a complete aircraft model is used to reproduce all the possible asymmetric rolling conditions that may appear during the taxi test.

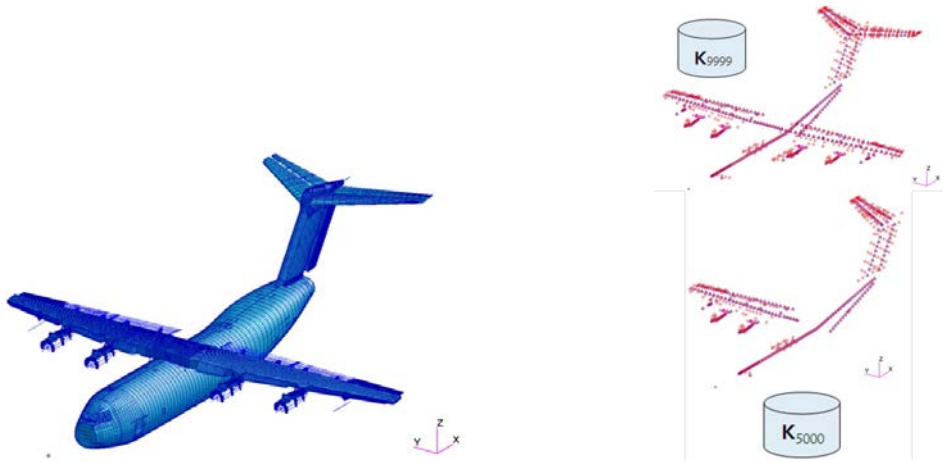

(a) A400M detailed Finite Element Structural Model

(b) Full (top) and half symmetric (bottom) aircraft structural condensed models

Fig. 2.4. A400M FEM structural model

Due to time constraints, in order to reduce the CPU time required to calculate the structure normal modes, both the full and half symmetric models are condensed by using a superelement technique. The datailed FEM model is reduced to a residual structure and a stiffness matrix that relates the grids of the residual structure to each other, representing in such a way the stiffness of the whole airframe. As a result of this condensation process, the combination of all grid points in which inertia and aerodynamic forces are applied is considered the analysis set (A-set), to be used on the solution of the dynamic equations. On the other hand, most of the grid points with no applied forces, included in the omitted set (O-set), are discarded in the normal modes calculation process. The application of this method, known as Guyan reduction theory [30], implies no lack of accuracy and a computation time reduction from 9 hours to 3 minutes in the case of the A400M.

2.2.2. Landing gear model

The landing gear model is the FEM representation of both the nose gear and main gear constituting the undercarriage and mathematically reproduce all the non-linear effects [23] that should be taken into account regarding the dynamic behavior of tyres and damping characteristics of shock absorbers.The flexibility of the two types of legs that model the landing gear, telescopic and articulated, is not represented. In addition to the GVT, drop tests and free extension tests were the two procedures to validate the A400M landing gear model.

Unveiling the mathematical insight of the different landing gear components, nonlinear springs, which are constrained to be perpendicular to the runway profile, are used to model the tyres, for which a single point of contact with the rolling surface is considered at each time step in the computation process. In addition, the force (F_R) felt by the tyres

is correlated to its deformation (δ_r) according to the following equation:

$$F_R = K_{r1}\delta_r^N \tag{2.1}$$

where K_{r1} and N are parameters that depend on the tyre pressure. If bottoming occurs, an extra term directly proportional to K_{r2} is added to Equation 2.1, where this constant is a value that on the rubber plasticity characteristics of the tyre.

Regarding the mathematics of the shock absorber, the force associated to this component is the result of the simultaneous action of other three forces: the liquid force, gas force and friction force. As in any general shock absorber model, the reaction force generated by the hydraulic fluid depends on the piston velocity, being positive or negative depending on whether it expands or compresses, i.e., depending on the direction of the flow rate through the piston orifice.

On the other hand, the reaction force of the gas varies according to the piston position since the gas pressure depends on the available volume of the chamber where it is contained. Every time the gas chamber is compressed up to a deflection within a specified range, out of which the force is linearly dependant, the gas reaction can be estimated with a polytropic reaction that is considered to occur fast enough to be nearly adiabatic. Therefore, in order to simulate a dynamic scenario, the heat capacity ratio of the gas is considered to be within the range from 1.3 to 1.5, because note that $\gamma = 1$ is reserved for quasi-static reactions considered to be nearly isothermal. In the case of the aircraft studied, the shock struts of the nose landing gear legs are composed by a double-stage gas chamber (low and high pressure chambers accordingly), whereas those of the main landing gear present only a single low pressure gas chamber. Hence, in general, the deflection of the shock absorbers is modeled according to the equation shown below, which is solved iteratively due to its dependency with the gas force (F_g):

$$\delta_a = \frac{V_0}{S}\left[1 - \left(\frac{P_0 S}{F_g}\right)^{\frac{1}{\gamma}}\right] + \frac{V_1}{BS}\left[\frac{F_g}{S} - P_0\right] \tag{2.2}$$

where V_0 and P_0 are the initial gas volume and pressure, respectively, although the reference values of the latter may be different between the nose and main undercarriage legs. Similarly, S corresponds to the piston area, γ and B make reference to the polytropic gas constant and bulk modulus, and V_1 determines the initial liquid volume.

The first term of Equation 2.2 models the polytropic reaction that takes places in the first stage chamber of both types of landing gear legs present in the aircraft. On the other hand, the second additive term is exclusive for the second chamber present only in the telescopic NLG leg, implemented as a reinforcement due to the severity of the loads suffered. Moreover, in an actual taxi test, the values of P_0 and V_1 may change from operation to operation, so they must be adjusted when trying to numerically simulate those trials. However, for the aim of this project, as in the EBH curves computation process,

these parameters are held constant to an average value.

Finally, the friction force depends in turn on the gas and liquid forces as well as the dynamic friction coefficient existing among the piston walls.

To conclude, appart from the tyre and shock absorber forces mathematical models, one of the most relevant features of a landing gear FE model is the definition of the landing gear to fuselage attachment points, or commonly known as pintle points, through which the external ground loads are transmitted from the landing gear to the rest of the airframe.

In the case of the A400M computation software, the loads are obtained not directly in the pintle points but in the interface points between movable and non-movable parts of both types of landing gears, corresponding to points designated with letters A and B in Figures 2.5 and 2.6. As a consequence, a rigid landing gear FE model reproducing all the elements with no kinematics in extended position is needed to transmit the landing gear dynamic loads from A and B points to the pintle points through a transformation matrix. Non-movable parts of the nose landing gear are modelled with CBEAM and CELAS elements, whereas those of the main one are represented with very high stiffness CBAR, CROD and CELAS elements.

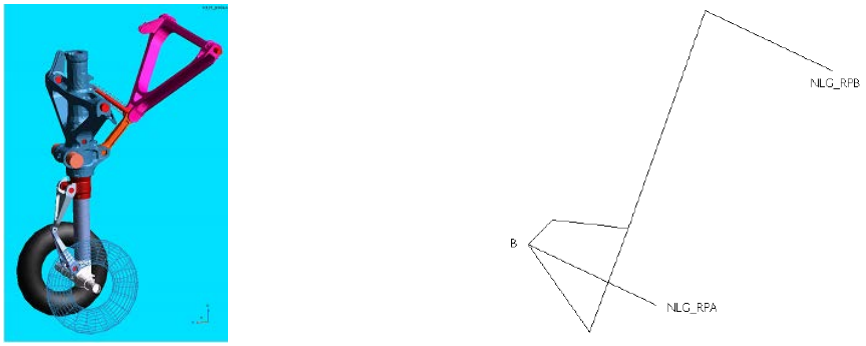

(a) Detailed FEM Model (b) Rigid stick FEM model

Fig. 2.5. A400M Nose Landing Gear FEM Model

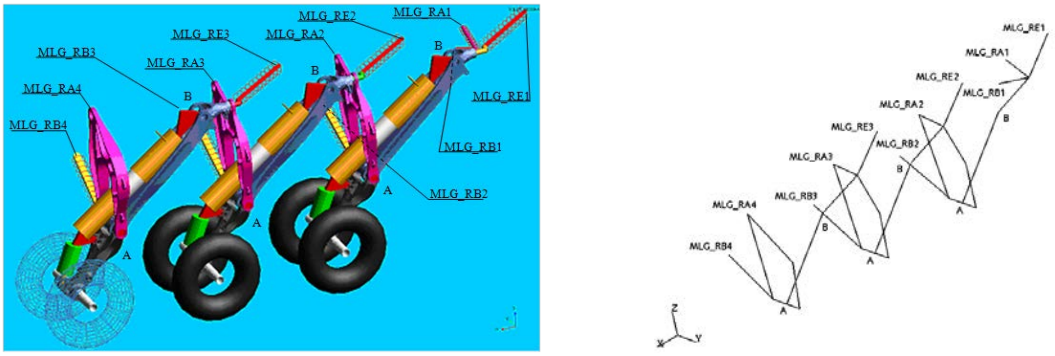

(a) Detailed FE Model (b) Rigid stick FE model

Fig. 2.6. A400M Main Landing Gear FE Model

In the case of the A400M, the landing gear supplier corresponds to Messier-Dowty,

who provides the model in MSC.ADAMS format from which the characteristics of the system are read to specify the inputs for the numerical simulation.

Particularly, in the case of the MLG model, the load path for the longitudinal and lateral links, in addition to the upper and lower ones, is defined in the model. Following the corresponding nomenclature from Figure 2.6, the upper and lower links are designated by A1 and B1 respectively; panel attachments correspond to A2, A3 and A4; lateral links are referenced with a B letter; and letter E is used to name the longitudinal links.

2.2.3. Mass model

Apart from the stiffness matrix defined by the aircraft and landing gear structural models, the normal modes computation process requires an suitable definition of the mass distribution along the aircraft. Every aircraft mass state is composed by a specific set of lumped masses, by which the representation of the overall structural mass is carried out. In this particular cases, the discretization of the different lumped masses is done parallel to the airflow in lifting and control surfaces and by longitudinal strips for the fuselage. In addition to the mass of the airframe, lumped masses are also included to represent the mass of the wide variety of systems and avionics, fuel, payload, landing gear (in extended position for taxi cases) and other extra components, such as armouring or under-wing AAR pods.

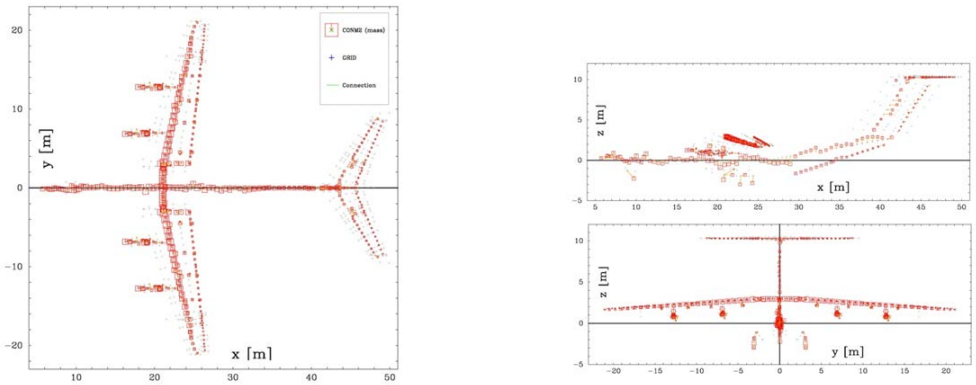

(a) Floor view

(b) Front and port view

Fig. 2.7. A400M mass model

Moreover, the mass data of the A400M model is supplied in MSC.NASTRAN CONM2 format. Each CONM2 entry includes information about the lumped mass value, moments of inertia, centre of gravity position, i.e., coordinates of the point mass where it is located, and also, the identification of the grid point to which the mass item is connected.

Concerning fuel CONM2, they are connected to specific fuel grids by means of appropriate RBE3 elements and its placement should be coherent with the fuel filling sequence specified for each mission. Likewise, payload CONM2 should be connected to specific payload using RBE3 elements connected to the cargo floor. Besides, its arrangement

must fulfill the load density limitations imposed for the different regions of the cargo compartment and the rear ramp. Finally, structural CONM2 should be connected to specific structural grids and each aircraft component (wings, engines and propellers, control surfaces, empennage, etc.) should be identified separately for the correct behavior of the model during the simulation.

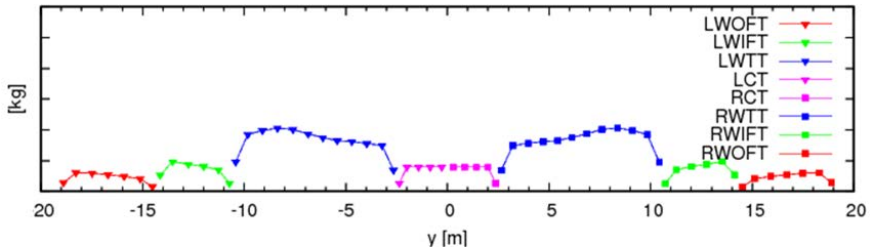

(a) Fuel

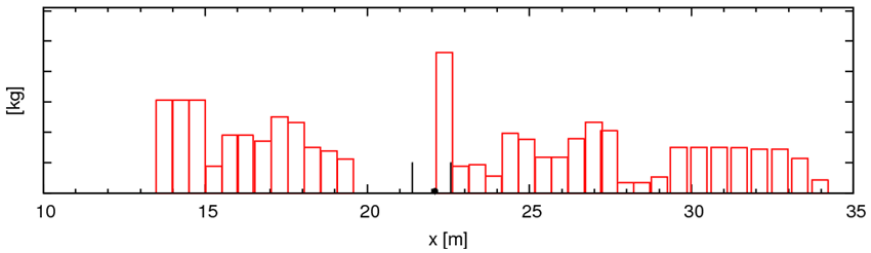

(b) Payload

Fig. 2.8. Fuel and payload CONM2 lumped masses representation

2.2.4. Aerodynamic model

For taxi numerical simulations, a good definition of the aerodynamic characteristics of the aircraft is of crucial importance to perform the static balance of all the forces acting on the aircraft prior to the computation of the dynamic loads resulting from the runway excitation.

In the case of the A400M, the aerodynamic properties of the lifting surfaces are modelled by the corresponding equations defined within the context of finite wings of moderate to high aspect ratio in compressible regime, since the aircraft maximum speed nearly reaches the beginning of the transonic Mach regime. Besides, for time-saving and simplicity purposes in the numerical simulation, unsteady aerodynamic effects are not included in this model (refer to damping model in Section 2.2.5), so the aerodynamic coefficients are treated as constants at each time step of the computation process.

In addition, since the aircraft studied is propulsed by rotating propellers, 1P loads should be considered when defining the aerodynamic model. This type of loads are defined as in-plane static loads appearing on the propeller shaft whenever the propeller is at a given incidence to the incoming flow, or in other words, its angle of atack is different from zero, creating, as a main consequence, a yawing moment. This problem is usually solved by using counter-rotating propellers, being the rotation sense in the A400M

down between engines. Taking into account this effect is necessary since, depending on its magnitude, the different aerodynamic coefficients vary accordingly. Therefore, a 1P correction factor should be added to the final aerodynamic equations. However, when reverse thrust is applied during landing manoeuvres, 1P loads vanish and the preceding correction do not have to be considered.

Considering all the previous assumptions from linear steady aerodynamics, the resulting total lift coefficient and pitching moment coefficient equations implemented in the dynamic taxi loads model are the following:

$$C_L = C_{L_{wing}} + C_{L_{tail}} + \Delta C_L = C_{L_0} + C_{L\alpha}\alpha + C_{L\delta_e}\delta_e + C_{Lih}ih + \Delta C_L \tag{2.3}$$

$$C_M = C_{M_{wing}} + C_{M_{tail}} + \Delta C_M = C_{M_0} + C_{M\alpha}\alpha + C_{M\delta_e}\delta_e + C_{Mih}ih + \Delta C_M \tag{2.4}$$

According to the nomenclature, α corresponds to the wing angle of attack in rad, δ_e to the elevator deflection in rad, and ih is the HTP setting, also in rad. Besides, ΔC_L and ΔC_M accound for the increment induced by the effect of lateral stability derivatives, such as antisymmetric aileron deflection.

Furthermore, apart from the 1P loads, the aerodynamic coefficients depend on the flap and spoiler setting, thrust coefficient and Mach number. Confidential aerodynamic data for the diferent scenarios was requested to perform the taxi simulations.

2.2.5. Damping model

Damping is the property of a system by which it is capable of dissipating kinetic energy into other type of energy, usually thermal energy. In the particular case of the aircraft studied, the sort of damping used in this model correspond to viscous damping, and is mathematically modelled as a force synchronous and proportional with the velocity of the finite element but opposite in direction to it, according to the equation of a simple mechanical viscous damper: $\vec{F} = -c\vec{v}$, where c corresponds to the viscous damping coefficient.

Therefore, the A400M viscous damping model is defined in terms of critical damping, being the critical damping coefficient equivalent to $c = 2m\omega_0$, and it is also considered a tabular function of frequency. Besides, the velocity comprises a very important factor when determining the damping magnitude of the system, so depending on the speed, a different fraction of critical damping is used for the model. Thus, at speeds below 100 KEAS, only the structural damping is modelled. Beyond that threshold, a higher critical damping fraction is used to account also for the alleviation induce by unsteady aerodynamic effects.

In addition, the damping contribution of the Engine Soft Mounts, i.e., elastomers used in the attachment between wing and engines, is modelled by introducing a local loss factor

at a particular frequency. For this, MSC.NASTRAN CDAMP2 entries are used.

2.2.6. Gyroscopic loads model

Gyroscopic loads are those appearing at the engines as a result of the propeller rotation movement. Since the A400M is equipped with turboprop engines, they should be taken into account when computing total checkstress and fatigue loads during taxi operations.

This type of loads vary according to the propeller ration speed, which is in turn a function of the thrust setting, the aircraft speed, altitude and ISA, resulting in a different value for each taxi case considered.

3. NUMERICAL SIMULATION OF DYNAMIC TAXI LOADS

3.1. Introduction

The development of statistical analysis involves collecting data from a large amount of taxi cases varying the aircraft and operational scenario characteristics to be able to come up with a reliable probability of limit load exceedance. Since obtaining all this results by performing a real taxi test trial for each case considered would imply an unaffordable time and money investment, numerical simulation techniques should be used to assess the problem in question.

During the whole of this present chapter, the stress taxi loads calculation philosophy is explained in depth, including the overall assumptions and the computational procedure involved in the numerical simulation. But prior to get into much detail, a brief general guidelines of the numerical simulation process and the corresponding software tools implemented is provided with the purpose of familiarizing the reader within this context.

The first step of the numerical simulation process comprises the computation of the aircraft normal modes, including both the eigenvalues and eigenvectors. Such task is accomplished by means of a commercial software, such as MSC.NASTRAN, for which the aircraft FEM model is required. Then, in-house private software is required to continue with the calculation process up to the acquisition of the final response of the aircraft in its entire structure. This software tools were developed by Airbus Defence and Space (former Airbus Military) and comprise the following programs:

- DYNTAXI, required to compute the initial static balance of the aircraft and the loads at the interface points between the movable and non-movable landing gear parts.
- DATLOAD, by which such forces and moments are translated to the pintle points (landing gear-fuselage attachment points) through a trasformation matrix.
- DYNRESP, necessary to calculate the modal transient response of the aircraft to the previous pintle loads in the frequency domain.
- DYNLOAD, which carries out the transformation of the transient response in modal coordinates to be expressed at specified aircraft structural points (monitoring stations).

In order to perform their corresponding task, several are the inputs required by each program to achieve its final output, which in turn serves as the necessary variables for the next step. Therefore, in order to control all this flow of data and manage the particular

way in which it is implemented on each program, an in-house UNIX shell script already coded was used. However, a full detailed description of the list of inputs and outputs required and delivered by each program, as well as the intermediate steps to transform ones into the others, is later included in Section 3.3.

3.2. Basic assumptions and methodology

In order to find the equilibrium point in the trade-off between the accuracy of the taxi loads model and the computation time required, several considerations are taken into account regarding the taxi loads numerical model and simulation process. Although, this assumptions imply a simplification of the model, this is still complete and accurate enough to help understand the overall problem up to the point it is required.

Continuing with the previous chapter, the definition of the several numerical models that define the behaviour of the aircraft constitutes just a introductory step in the taxi loads computation methodology. In fact, this methodology is aimed to obtain the dynamic response of the aircraft, which is characterized by the appearance of loads on the airframe. The output of such corresponding loads can be provided throughout the numerical simulation process in three formats: incremental loads, 1G static loads or total loads. On the one hand, 1G loads involve gravity and steady aerodynamic effects in combination to 1P steady loads and are the result of rolling the aircraft over an hypothetical perfectly flat runway at constant velocity. On the other hand, incremental loads are those appearing on the aircraft as a consequence of the dynamic behaviour of the structure when the model is subjected to taxi runs on and uneven surface. Finally, the addition of both gives rise to total loads.

Following the basic assumptions that determine the calculation philosophy, among the three load types mentioned in the preceding paragraph, incremental dynamic loads are computed through a full-coupled solution of the non-linear rigid landing gear equations combined with those of the linear flexible aircraft model. This coupling technique utilizes only the free-free modes of the aircraft, which are obtained from a model of the structure that makes use of the FEM technique.

Moreover, for the simulation of the dynamic response by means of DYNTAXI, taxi runs are performed at constant horizontal velocity, inducing the excitation of the aircraft through the roughness profile of a specific runway or a bump of given wavelength and height, according to the EBH method. After sensitivity studies performed, previous taxi loads loops concluded that 40 Hz are a suitable cutoff frequency for this type of ground excitations.

Besides, gyroscopic forces are not taken into account in the coupled solution to obtain the loads calculated with DYNTAXI. Instead, they are included in the calculation of the aircraft transient response performed with DYNRESP. Additionally, neither 1P loads nor Flight Control System laws need to be included in the simulation process.

Finally, the data recovery method is given by the Summation of Forces procedure. The basic assumption underlying this approach states that the dynamics of a system can be represented by simply a reduced set of modes. This is totally opposite to the Displacement Method, by which the magnitudes in question are computed by linear combination of the modal coordinates.

As a consequence, low frequency excitations induce a response of the higher modes which is almost purely static. Therefore, inertia and damping forces present a very small contribution from this higher modes in such a way that they can be accurately estimated using only low frequency modes. Finally, a more accurate response can be retrieved if the loads applied to the structure are combined with the two aforementioned types of forces.

3.3. Stress taxi analysis process

Having the different aircraft numerical models and the corresponding calculation philosophy assumptions already defined, the numerical simulation procedure can be initiated for the final loads computation to take place.

This overall process comprises 6 different steps, each one of them requiring a particular set of inputs to transform them into a specific output, until the final loads at the monitoring stations requested are retrieved.

Figure 3.1 displays graphically a summary of the numerical simulation process in the form of a flowchart.

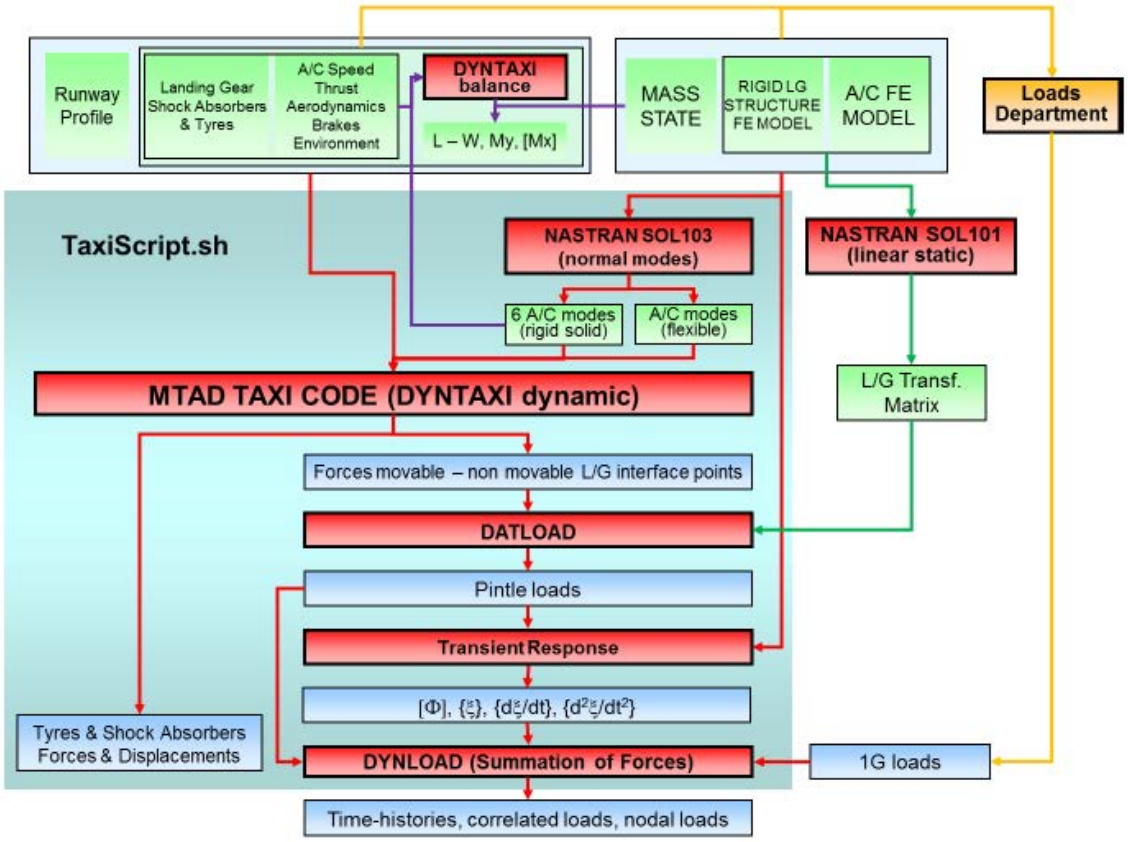

Fig. 3.1. Flowchart of one stress taxi run

3.3.1. MSC.NASTRAN SOL 103

The first step in the numerical simulation procedure involves a commercial software (MSC.NASTRAN in the case of Airbus DS) to compute the aircraft normal modes.

For that, three inputs are required, including a linear flexible aircraft FEM model, a non-linear rigid FEM model of the non-movable parts of the landing gear structure and the complete aircraft mass state in CONM2 format. It is important to remark that the aircraft mass model must include also the mass of the landing gear, since it is not part of its own model.

With all these inputs, SOL 103 builds the corresponding stiffness and mass matrices and yields the aircraft associated eigenvalues and eigenvectors, from which the 6 rigid body and flexible modes can be differentiated.

3.3.2. DYNTAXI

The task developed by this software tool comprises two different subroutines, which are in chronological order: DYNTAXI static balance and DYNTAXI dynamic taxi simulation.

1. **DYNTAXI static balance**

The initial condition ($t = 0$) for each dynamic taxi case consists on the aircraft taxiing over a hypothetically perfect flat runway. In this static condition, the aircraft is balanced, so the sum of all the forces and moments acting on it equals zero. The result of the aircraft static balance includes the overall resultant forces and moments ($F_{z_{CG}}$, $M_{y_{CG}}$, $M_{x_{CG}}$) applied at the centre of gravity, as well as the fuselage to landing gear interface points loads (pintle loads) and wheel axle loads.

To accomplish this task, the required inputs are the 6 aircraft rigid body modes computed in the previous step, the landing gear shock absorbers and tyres properties and the aircraft and runway environmental parameters defining each taxi case.

The resultant vertical force constitutes the apparent weight of the aircraft considered to be applied at the centre of gravity. It accounts for combination of the total mass of the aircraft, aerodynamic forces and propulsion effects if the overall thrust is not strictly parallel to the horizontal plane, as considered in Equation 3.1.

$$F_{z_{CG}} = L - W - T\sin\epsilon = \frac{1}{2}\rho V^2 S\, C_L - W - T\sin\epsilon \tag{3.1}$$

According to the nomenclature, L corresponds to the total lift force, W makes reference to the aircraft weight, T to the total engine thrust and ϵ represents the angle of the thrust with respect to the aircraft horizontal reference line. The lift coefficient (C_L) is computed in the same manner as in Equation 2.3.

On the other hand, the resultant associated pitching moment calculated with respect to the aircraft centre of gravity is estimated according to the following formula:

$$\begin{aligned} M_{y_{CG}} = \frac{1}{2}\rho V^2 S\,\bar{c} C_M + L\,(x_{CG} - x_{CP}) + D\,(z_{CP} - z_{CG}) + T\sin\epsilon\,(x_{CG} - x_T) \\ + T\cos\epsilon\,(z_{CG} - z_T) - (\mu N)_{NLG}\, z_{CG} - (\mu N)_{MLG}\, z_{CG} \end{aligned} \tag{3.2}$$

where C_M corresponds to Equation 2.4, D makes reference to the drag force and $\bar{c}$ to the mean aerodynamic chord (MAC). Besides, μN is the product between the the braking friction coefficient and the normal force acting on either the nose or main landing gear. Subscripts CG, CP and T denote the coordinates of the centre of gravity, centre of pressure of the wing and the engine respectively, to determine the different moment arms.

Although in none of the cases of the statistical analysis was considered, if asymmetric taxi conditions are present in the analysis, as in the case of asymmetric deflection of the ailerons or wings not at level, a rolling moment is induced about the centre of gravity and its magnitude is approximated by the expression shown below:

$$M_{x_{CG}} = \frac{1}{2}\rho V^2 S\,\bar{c} C_l + L\,(y_{CP} - y_{CG}) + T\sin\epsilon\,(y_{CG} - y_T) \tag{3.3}$$

in which $C_l = C_{l\delta_a}\delta_a + C_{l\phi}\phi$, being $C_{l\delta_a}$ and $C_{l\phi}$ the aileron and bank angle contributions to the rolling moment coefficient respectively.

Hence, according to the previous three equations, the input parameters necessary to compute the forces and moments in the static valance comprise the aircraft mass; x, y (if required) and z centre of gravity coordinates; braking coefficient; total engine thrust (C_T) and propeller RPM; aircraft speed; auto-braking deceleration (if activated); flap and spoilers setting; corresponding aerodynamic coefficients and air density value at the studied operational ambient conditions.

Moreover, for the determination of the pintle points and wheel axles 1G loads, the different parameters that define the landing gear are required in addition to the previous inputs, including the undercarriage leg type and reference coordinates, shock absorber properties defined in Equation 2.2, characteristics of the tyres, wheel axles coordinates and location of the interface point between movable and non-movable parts.

2. **DYNTAXI dynamic module**

   This part of the code solves in the time domain the coupled system of non-linear equations of the aircraft and the landing gear constituted by expressions 1.2 and 1.1 respectively. To accomplish this task, the different loads about the centre of gravity obtained during the static balance computation and the landing gear, shock absorbers and tyres characteristics are required. Also, the runway profile and constant aircraft taxiing speed, as well as the eigenvalues, modal matrix, and generalized mass and stiffness matrices of the aircraft must be included as inputs for the dynamic simulation.

   As a result, time histories of the forces taking place at the interface points between movable and non-movable parts of the landing gear, tyres and shock absorbers, as well as the displacements in the last two, are retrieved as outputs of this process. It should be highlighted that all these forces are total forces (1G + incremental) since remind that all external loads acting on the aircraft, excluding the ones coming from the the landing gear, are taken into account through the total vertical force ($F_{z_{CG}}$) and corresponding pitching moment ($M_{y_{CG}}$) applied at the centre of gravity.

   As a final remark, this computation method is in fact an iterative procedure, in which the aim at each time step is to perform a dynamic balance, with inertial terms and time derivatives also included in the differential equations, by slightly modifying the variables of state of the aircraft obtained in the preceding instant, being the initial conditions those given by the static balance at $t = 0$.

3.3.3. DATLOAD

Forces at the interface points between movable and non-movable parts of the landing gear are translated to the pintle points, since such technique constitutes the only manner to implement the landing gear reaction, resulting from the runway profile excitation, to obtain the airframe dynamic response. This process is performed through a transformation

matrix, which is calculated from a linear static solution (MSC.NASTRAN SOL 101) to the rigid landing gear structure FE model.

However, the output loads given by DYNTAXI corresponds to total forces. So, in order to compute the incremental dynamic response of the aircraft in the next step, the resultant forces applied at the pintle points must be incremental. Therefore, the initial 1G load value from the static balance should be substracted to the pintle forces time histories.

3.3.4. DYNRESP

The dynamic transient response of the aircraft to incremental pintle forces is solved in the frequency domain and expressed in modal coordinates. The reason to solve the dynamic problem twice is that integrated loads in monitoring stations cannot be obtained directly from DYNTAXI.

The inputs required for this task include the incremental pintle loads calculated in the previous step and the solution from MSC.NASTRAN SOL 103. Besides, the aircraft mass state and FEM model, the rigid landing gear structure FEM model, the airframe damping model and the gyroscopic contribution from the propellers are also necessary.

3.3.5. DYNLOAD

Using the Summation of Forces method explained by the end of Section 3.2, the output request of total loads time histories is computed by addition of the static 1G loads and the incremental loads. Therefore, the previous modal transient response is necessary to calculate the total loads at the list of monitoring stations desired, which constitutes the input required by this software tool, along with the 1G loads from the Loads Department and the pintle loads previously obtained with DATLOAD.

In order to provide a general overview of the numerical simulation process, a recap of the different inputs and output managed by each program is gathered in Table 3.1 [31].

INPUT	PROGRAM	OUTPUT
A/C FE model Rigid LG structure FE model Mass state (CONM2 format) (Mass & Stiffness matrices)	NASTRAN SOL 103	Eigenvalues Eigenvectors Rigid body modes Flexible modes
A/C total mass x_{CG}, y_{CG}, z_{CG} A/C speed (KTAS, KEAS) Total thrust (C_T) & Prop. RPM μ_{brk} (ABrake. ON/OFF) (μ_{roll} if brakes OFF) C_{L_0}, $C_{L\alpha}$, $C_{L\delta_e}$, C_{Lih}, C_{D_0} C_{M_0}, $C_{M\alpha}$, $C_{M\delta_e}$, C_{Mih} HTP (ih), flaps & spoilers setting h, ρ, ISA offset LG leg type & coordinates Shock absorbers & tyre properties Wheel axles coordinates Interface points coordinates between movable & non-movable parts	DYNTAXI (static balance)	$F_{z_{CG}}$ $M_{y_{CG}}$ $M_{x_{CG}}$ Pintle points 1G loads Wheel axles 1G loads
A/C normal modes Runway profile Taxi case description $F_{z_{CG}}$,$M_{y_{CG}}$,$[M_{x_{CG}}]$ A/C speed (KTAS, KEAS) Propeller RPM Products of inertia	DYNTAXI (dynamic module)	Total forces @ interface points between movable & non-movable LG components Total forces and displacements @ shock absorbers & tyres
Total forces @ interface points between movable & non-movable LG components	DATLOAD	Incremetal loads @ pintle points
A/C & LG FEM models Damping & gyroscopic models Incremental loads @ pintle points	DYNRESP	Incremental loads in modal coordinates
Incremental loads in modal coordinates 1G loads Monitoring stations requested	DATLOAD	Time histories of total loads @ monitoring stations

TABLE 3.1. NUMERICAL SIMULATION INPUTS AND OUTPUTS

4. STATISTICAL ANALYSIS

4.1. Introduction

Resuming the motivational ideas previously presented in Section 1.1.3 that have promoted the completion of the present project, the current A400M customers desire to enhance the tactical capabilities of this aircraft when taxiing over unpaved runways has been translated to the development of a methodology to evaluate the risk that this type of ground operations involve. As a consequence, the probability that may lead to the exceedance of limit loads on the aircraft structure has been the requirement demanded by the different Air Forces to measure the risk of manoeuvring the aircraft at a runway of a given severity.

In order to illustrate the magnitude of complexity to which this problem can extend, the probability of limit load exceedance when rolling over a specific uneven airstrip would be completely determined, as a first approximation, by applying the rule of succession or Laplace's rule. Under the assumption of equiprobability, by which all the sample cases studied are considered to be equally probable, Laplace's rule states that the probability of an event A is equal to quotient of the number of cases that fulfill such event divided by the total number of possible outcomes [32].

$$P(A) = \frac{favourable\ outcomes\ to\ A}{possible\ outcomes} \tag{4.1}$$

As a consequence, in order to determine the favorable cases to limit load exceedance, this statistical approach would comprise performing the numerical simulation of all taxi runs that arise when considering all the possible combinations of aircraft configurations and operational parameters that define a taxi case. In general terms, since the height of the runway is given and considering only normal taxi operations (no RTO), the casuistry involved in a typical loads loop of this kind would be described in the following table:

PARAMETER	# OF CASES	DESCRIPTION
Mass state	156	MLW, MTOW, MZFW, OWE+Fuel...
A/C Speed [KTAS]	9	20, 50, 75, 100, 120, 140, 152, 165, 178
Manoeuvre	2	LND, TO
Thrust setting	4	Max. Reverse, Ground Idle, Flight Idle, MTOP
Brakes	2	ON, OFF
Flaps [°]	5	15, 20, 30, 40, 47
ISA offset [°C]	6	-60, -40, -20, 0, 20, 40
RWY direction	2	forward, backward

TABLE 4.1. CASUISTRY OF A COMPLETE RUNWAY STATISTICAL ANALYSIS

Once the simulations of all this possible scenarios were performed, the probability of limit load exceedance would be determined by the ratio of the number of cases in which at least one of the monitoring stations has reached any of the 6 possible associated limit loads divided by the total number of simulated cases.

From the mathematical point of view, this direct methodology seems fairly simple but the unfeasibility of this statistical approach arises when considering the limitations of the computer resources available nowadays. The total number of cases that the combination of all the parameters gathered in Table 4.1 yields would be about $1.4 \cdot 10^6$ and from the experience acquired in previous loads loops, the required computation time for such long casuistry would last up to several years. However, there are restrictions regarding the association of the different parameters that define a taxi case, since, for instance, a takeoff cannot be performed with brakes on or reverse thrust. As a consequence, all the possible combinations that can be considered is one order of magnitude smaller, near $1.2 \cdot 10^5$ taxi runs. Despite of this reduction in the number of cases, the computation time would still comprise up to several months, so this methodology for the statistical analysis of taxi loads is considered to be not affordable due to the time constraints that characterize the aerospace military industry.

Moreover, although the number of cases considered for each parameter of Table 4.1 yields a representative amount of taxi scenarios to be analyzed, the total number of possible taxi cases is in fact infinite, since any intermediate value of speed or ISA offset could also happen in a real operation. Besides, there would be infinite combinations of fuel and payload to cover the whole mass states envelope of the aircraft.

Hence, discarding the previous approach, a more efficient strategy to estimate an approximate probability of limit load occurrence during taxi operations would involve the definition of the EBH curves. The EBH curves computation process leads to the specification of a set of guarantee curves, in such a way that, if the operational limitations imposed for each roughness level are fulfilled, the aircraft structural integrity will always be preserved in any case. This guarantee statement does not imply that limit loads on the airframe will never be reached, but, according to the definiton of limit load itself, the probability of exceeding the structural capability of the aircraft will be at least equal or smaller to 10^{-5}. This probability threshold will later serve as basis for the validation of the statistical approach methodology presented later.

Therefore, thanks to the EBH method, the EBH curve of a given runway profile can be computed and compared to the EBH design curve of the roughness level corresponding to the mission that is to be carried out. Thus, for all those points at which, at a specific 1-cos bump wavelength, the runway EBH curve is tangent or lays below the design curve defining the maximum allowable bump height, the probability of limit load occurrence is equal or smaller to the aforementioned threshold of 10^{-5}. However, to estimate a roughly accurate probability of limit load exceedance when encountering those bumps whose height is greater than the one specified by the design curve, a procedure similar

to that proposed for the actual runway profile (Equation 4.1) should be considered. At each of these 1-cos bumps, defined by particular wavelength and height values, taxi runs should be performed considering all the possible combinations of parameters specific for the desired operations. Although in this case only one runway direction should be considered as a consequence of the bump profile symmetry, this approach to the problem is still unaffordable due to the long period of time necessary to complete all the numerical simulations considered, which aggravates to a greater extent if several bump heights must be considered.

As a consequence of the time span that this problem presents, a more elaborated methodology must be developed by combining a more complex probability theory concerning the definition of 2D probability maps and a more exhaustive engineering criteria to reduce the overall casuistry considered. With this two ingredients, the objective is to come up with a efficient statistical approach applicable to taxi operations in any runway. To introduce the procedure considered in the development of this statistical analysis methodology, a brief description of the sequence of steps accomplished is provided below.

1. Definition of the starting point from which the statistical analysis is performed. This step includes the selection of the roughness level to be studied and the corresponding bump characterization for the simulation of the taxi cases. Then, at such particular point of the EBH curves, the most critical taxi cases for the two magnitudes of interest studied are identified from the results of previous loads loops.

2. Supporting the criteria on the parameters defining the most critical taxi cases previously identified and on the experience from previous loads loops, the most relevant parameters that influence the taxi load magnitudes are analyzed. Then, the criteria for the association of these parameters to define the 2D probability maps included in the statistical analysis is worked out.

3. Based on the most relevant parameters previously determined, the casuistry to be included in the statistical analysis is defined, comprising a relevant number of taxi cases considered for numerical simulation. This step implies also the definition of the reference cases for the overall casuistry, which are based on the most critical cases already identified. Hence, for this reference cases, the different probability maps are defined in order to account for the effect of all the parameters selected to describe them.

4. The methodology for the definition of the iso-load curves included in each probability map is described. At this stage, the computation of taxi loads for the casuistry considered is carried out according to the numerical simulation presented in Chapter 3. Then, interpolation of the data in the whole envelope of each probability map is required for the definition of the iso-load curves. Hence, the procedure to accomplish both tasks with the corresponding MATLAB® functions is explained.

5. The statistical analysis concerning the operation in the design EBH curve of the roughness level selected is performed. For this purpose, the iso-load curves for the most representative cases are presented. Then, using the results for the 2D probability maps, the probability curves for the two magnitudes studied are computed at the maximum allowable height of the roughness level point subjected to study. Therefore, the probability calculation philosophy is previously developed, detailing all the maths involved in the computation of such curves.

6. The same procedure is followed to consider the operation in more severe runways. First, the iso-loads curves are defined to study the effect of increasing the bump height on the probability maps. Then, the final output of the present project is presented, concerning the definition of the probability curves at several bump height increments as a tool to assess the risk involved in the operation in unpaved runways, which are beyond the limitations defined by the aircraft EBH curves.

4.2. Starting point: AFM EBH curves

The starting point of the taxi loads statistical analysis developed in the present project consists of the A400M EBH curves already defined by the Structural Dynamics and Aeroelasticity Department of Airbus DS, since, as explained in Section 4.1, they serve as a first basis for the estimation of the probability of limit load exceedance. Due to the high complexity of the probability calculation task, the problem was reduced to the analysis of taxi cases at a unique bump wavelength as a matter of illustrative example for the application of this approach to any other roughness scenario.

In order to validate the statistical approach methodology according to the reference value of 10^{-5} imposed by the definition of limit load, one of the five roughness levels that define each of the A400M EBH design curves was selected.

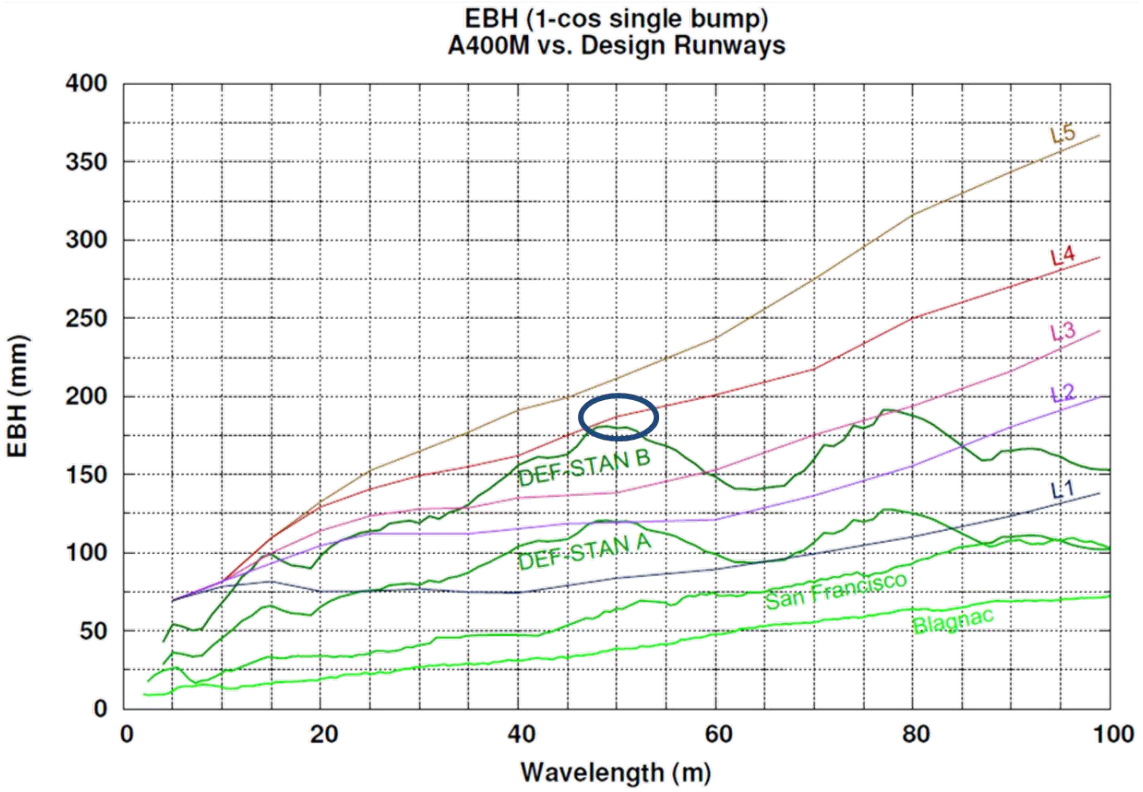

Fig. 4.1. A400M EBH curves and bump selected for analysis (blue ellipse)

Minimum Servicing Classes Allowed		Runway Roughness				
		R ≤ L1	R ≤ L2	R ≤ L3	R ≤ L4	R ≤ L5
A/C Weight [T]	Low Weight Tactical MLW = 107 MZFW = 109.6 MTOW = 115	A	C	C	C	D
	Tactical (TLL-1) MLW = 115 MZFW = 109.6 MTOW = 131	B	C	C	D	Not Allowed
	Logistic (LH-1) MLW = 123 MZFW = 117.1 MTOW = 141	C	C	D	Not Allowed	Not Allowed

TABLE 4.2. A400M MINIMUM SERVICING CLASSES ALLOWED

As presented in Figure 4.1, the roughness level tangent to the DEF-STAN B EBH curve was chosen, since this runway constitutes the most severe certification requirement demanded for the operation of the A400M in unpaved runways. This roughness level corresponds to the EBH curve denominated as L4, in which only Low Weight Tactical and

Tactical Missions operations are allowed. Among the previous two, the Tactical Mission, characterized by a $MTOW = 131\ T$ and a $MLW = 115\ T$, was selected as the specific aircraft configuration to carry out the statistical analysis since it is more severe in terms of aircraft total weight considerations and, thus, constitute the dimensioning cases of such EBH design curve. Besides, for the Tactical Mission operation in a runway profile equal or lower than the roughness level L4, the manoeuvre is limited to a Servicing Class D, i.e., the tyres must be overpressured. In addition to the tyre pressure values, the following limitations also apply for the specified mission weights and roughness profile:

- At Landing:
  - Fuel weight should be less or equal to 25T.
  - x_{CG} position should be greater than 25% MAC at altitudes higher than 9000 ft.
- At Take-Off:
  - Fuel weight should be less or equal to 43T.
- For the previous two manoeuvres, only tactical fuel filling sequence is allowed.

Apart from considering the operation in a more severe runway, the consideration of taxi cases with mass states and ambient conditions ranging outside of this restrictions will further complete the analysis of the taxi capabilities beyond the aircraft operational limits.

Moreover, among the set of bumps that define the roughness level L4, the bump selected as reference obstacle to perform the statistical analysis was the one closest to the point of tangency between the EBH curve of such roughness level and that of the DEF-STAN B profile. This point of tangency occurs at a wavelength of about 48 meters, but since in the previous loads loops just runs at bump wavelengths multiple of 5 meters are performed, the closest set of taxi cases already simulated were at a wavelength of 50 meters. Hence, at such specific wavelength, the corresponding maximum allowable bump height defining the L4 EBH design curve corresponds to 18 centimeters. As a summary, the two parameters defining the 1-cos bump used as a reference obstacle in the statistical analysis are gathered in Table 4.3.

WAVELENGTH [m]	HEIGHT [cm]
50	18

TABLE 4.3. 1-COS BUMP CHARACTERIZATION

In addition to the simplification by which the analysis is reduced to a single bump wavelength, other assumptions were also considered in order to streamline the problem for affordability purposes.

First, among all the possible monitoring stations defined for the aircraft FEM model, the statistical approach was focused on two different load magnitudes at two particular points of the aircraft structure. Following the guidelines of the sizing problem previously presented in Section 1.2.1, the two load magnitudes and corresponding monitoring stations studied are the following:

- **LWR - MX**.

  It corresponds to the down bending moment at the left wing root, considering the root as the intersection of the wing with the fuselage. Generally, the first wing down bending mode of the aircraft when taxiing over a 1-cos bump is symmetric and so are the loads in both wings, but in the case of the A400M, the centre of gravity position is slightly oriented to the port side of the aircraft due to its inherent design mass configuration. Therefore, the loads at the left wing are a bit more critical and that constitutes the reason that leads to choose that side of the wing as the limiting design case.

  Taxiing over unpaved runways corresponds to such limiting design case since the wing root has to withstand the down bending moment due to the wing structural weight and the fuel stored within the wing tanks. At the moment in which the aircraft passes the highest point of a bump profile and rolls over its negative slope, or the NLG lands back if it has lost contact with the ground, the inertia of these two spanwise distibuted masses bends the wing downwards creating high dynamic stresses at the wing root. This is further aggravated due to the absence of enough lift force at very low angles of attack to alleviate the loads at the root as a consequence of low taxiing speed or the application of propeller reverse thrust that practically destroys the aerodynamic performance of the lifting surfaces.

- **NLG - FZ**.

  It comprises the vertical force (positive downwards) at the wheel axle of the nose landing gear. In the same manner, by the time at which the aircraft encounters a bump, or during the impact of the NLG with the ground if this has remained in the air (usually less than one second) after crossing the obstacle, the inertia of the aircraft mass generates high compressive dynamic loads which are transmitted form the shock strut to the wheel axle. In addition, this compression is further enhanced by the pitch down moment induced by the braking action applied at the MLG wheels. Hence, the sizing of this NLG component is of extreme importance to avoid undercarriage collapse in this type on manoeuvres.

The second assumption concerned the consideration of just landing manoeuvres to develop the statistical analysis. Discarding the exceptional cases concerning rejected take-offs, the experience from previous loads loops concluded that, among landings and take-offs, the first type of manoeuvres are, in the vast majority of cases, the sizing scenario of the two aforementioned load magnitudes.

4.3. Definition of most critical cases

Once the starting point has been defined and the first assumptions for the statistical analysis have been considered, the next step involved the definition of the most critical taxi cases for each of the two load magnitudes studied. The objective at this stage is to find the aircraft configuration, operational parameters and runway ambient conditions in taxi operations that lead to the most critical loads for the two magnitudes of interest proposed for this statistical analysis.

For the definition of the A400M EBH curves, around 4.000 taxi cases were simulated to assess the problem and served as the source for this purpose. At each roughness level and bump wavelength, three different sets of taxi cases, one for each of the manoeuvres required for study (LD, TO and RTO), were simulated. Each set included taxi cases with different aircraft and operational parameters in order to find the limiting design case for that combination of roughness level and bump wavelength. The taxi case that, when increasing the bump height, first presents a monitoring station reaching limit loads corresponds to the design case. Also, the bump height at which that situations occurs corresponds to the Equivalent Bump Height defining the EBH curve. Therefore, taking advantage of the these taxi cases already simulated, among the landings considered for the roughness level L4 and bump wavelength of 50 meters, the most critical cases found for the two magnitudes studied are gathered in Table 4.4. Besides, the actual sizing case and its corresponding load magnitude (LWR - FZ) are also included.

MAGNITUDE	LWR - MX	NLG - FZ	LWR - FZ
TOTAL MASS [T]	115	115	115
FUEL MASS [T]	25	7.982	25
PAYLOAD [T]	7.201	25.511	7.201
PODS	ON	OFF	ON
ARMOURING	ON	ON	ON
x_{CG} [%MAC]	34.818	23.601	25.082
SPEED [KTAS]	100	75	120
THRUST	GROUND IDLE	MAX. REVERSE	GROUND IDLE
BRAKES	ON (ABrake)	ON (ABrake)	ON (ABrake)
FLAPS [°]	47	40	47
SPOILERS	IN	IN	IN
ALTITUDE [ft]	14600	9000	14600
ISA OFFSET [°C]	+24	+40	+24

TABLE 4.4. MOST CRITICAL CASES

As shown in the previous table, the sizing magnitude that defines the maximum allowable bump height for the specific combination of roughness level and bump wavelength is given by the vertical downward shear force near the left wing root, although the moni-

toring station is not completely coincident with that in which the study of the wing down bending is focused. The corresponding monitoring station to this sizing magnitude is a bit more outboard, close to the inboard engine, due to the effect that its excitation has on the vertical force around this region. Despite of the slightly different location of the monitoring station, the parameters defining the sizing taxi case are coincident with those of the wing down bending, except for the longitudinal position of the centre of gravity.

Considering the other two cases of interest in the statistical analysis, both occur at the MLW of the Tactical Mission defining the roughness level L4, which corresponds to 115 tones, and mounting the extra feature (pods or armouring) that makes these load magnitudes studied to be more critical.

In the particular case of the wing down bending at the left wing root, the most critical case is given by the presence of AAR pods (Figure 4.2), which gives the A400M the in-flight refueling capability through probe and drogue technique. They comprise two heavy underwing masses located near the wing tips that make the down bending at the wing root to be more critical and thus, the wing-to-fuselage attachment to be reinforced. Besides, apart from the mass increment as a consequence of the operation with pods, this most critical case takes place with the maximum fuel quantity allowed by the limitations imposed for the roughness level L4, expecting the addition of such distributed weight along the wing to aggravate the dynamic bending moment response due to the higher inertia involved. Moreover, due the arrangement of pods and fuel mass, critical cases for the wing down bending are characterized by a backward longitudinal position of the centre of gravity. In addition, the most critical scenario is given by the operation at the maximum altitude and temperature allowed by the engine performance map, since the high magnitudes of these two parameters imply lower lift force to alleviate the loads at any point of the aerodynamic surfaces.

Fig. 4.2. A400M fitted with AAR pods (wing outboard sections)

On the other hand, the most critical case for the vertical force at the NLG wheel axle occurs operating with armouring. The armouring is an optional defensive aid system that can be installed in the cockpit to protect pilot and co-pilot from impacts. It constitutes and additional weight at the aircraft nose that makes the forces acting on this NLG component to be greater. Also, a forward position of the centre of gravity due to a large amount of payload close to the cockpit, in addition to the pitching down moment created as a conse-

quence of the braking action, makes the load path to be concentrated in the front fuselage and, thus, such configuration to be critical for the sizing of the NLG wheel axle. Finally, in the same manner as for the wing down bending moment, this critical case takes place at the maximum allowed altitude imposed by the limitation for the roughness level considered and at the maximum possible temperature regarding the engine performance map. At this values of height and temperature, the air density presents the lowest possible value and so is the lift. This fact translates into a high apparent weight and hence, the wheel axle has to withstand higher loads due to the lack of alleviation by the lifting properties of the aircraft.

The characterization of the parameters of these critical cases will serve as basis to define other two similar cases for each magnitude of interest that will be the reference ones for the definition of the 2D probability maps. Therefore, the objective is, for each one of those four reference cases, to vary their parameters two-by-two in other to study the effect that each pair has on the taxi loads magnitude at the monitoring stations studied. Hence, the definition of this loads magnitude variation is the preceding step to study the contribution that each pair of parameters imply in the probability of limit load occurrence.

4.4. Identification of most relevant parameters

Since an exhaustive analysis of the problem leads to a number of taxi cases to be simulated that is unfeasible due to the computation speed limitations of the IT resources currently available, efforts must must focused on establishing an substantiated engineering criteria in order to reduce the total casuistry considered in the statistical analysis and subsequent definition of 2D probability maps.

Prior to define this criteria, first, an analysis of all the possible parameters that define a taxi case is must be elaborated.

- **MANOEUVRE**

  The three possible manoeuvres considered in taxi loads analysis are landings, take-offs and rejected take-offs. However, only landing manoeuvres are studied in this statistical analysis since they are usually the most critical scenarios for the parts which are sized by taxi manoeuvres. This election implies further restrictions on the other parameters that define a taxi case.

- **MASS STATE**

  The mass state envelope is different depending on the aircraft mission since it is defined by the parameters described below, which are in turn correlated by the following equation:

$$TM = OWE + FM + PL + W_{PODS} + W_{ARMOURING} \tag{4.2}$$

– **TOTAL MASS**

The maximum take-off, landing and zero fuel weights definitions are particular for each mission. Hence, for the Tactical Mission operation in the roughness level L4 and considering only landing manoeuvres, the total mass range is characterized by the following values:

OWE [T]	80.25
MLW [T]	115
MZFW [T]	109.6 (107 if $x_{CG} \leqslant 25\%$MAC)

TABLE 4.5. TACTICAL MISSION WEIGHTS DEFINITIONS

– **FUEL MASS**

The maximum amount of fuel mass that can be carried on board depends upon the maximum total mass considered in the mass states envelope. According to the limitations imposed for Tactical Mission landings in the roughness level L4, the fuel weight should be less or equal to 25 tones and tactical fuel filling sequence must be considered. However, although the fuel filling sequence was respected, the maximum fuel mass considered in this statistical analysis was the one required to reach MLW for zero payload, equal to 34.75T, to study the probability of wing root limit load exceedance if these restrictions are not met.

– **PAYLOAD**

The maximum payload weight that can be carried on board is defined by the MZFW and constitutes the main factor that influence the excursion of the centre of gravity positions. For the A400M Tactical Mission, the maximum amount of payload is equal to 29.35T, which is further restricted to 26.75T if the $x_{CG} \leqslant 25\%$MAC to avoid limit load occurrence on the front fuselage and landing gear components. In any case, the load density limitations imposed for the different regions of the cargo bay and rear ramp were always fulfilled in the definitions of the different mass states for the statistical analysis.

– **PODS**

The operation with pods is mainly focused for logistic operations. From the experience of previous loads loop, it was concluded that mass cases with AAR pods for tactical operations must be excluded from the global envelopes if they are critical and only used in separate studies. Despite of this recommendation, the operation with pods was considered in this statistical analysis to alleviate the conservatism implicit in the definition of the EBH curves.

– **ARMOURING**

The operation with armouring is mainly focused for tactical operations in warfare conditions, although the different customers demand also the possibility

to be installed on aircraft devoted to logistic operations if required. For the purpose of this project, since the operation in unpaved runways is mainly considered within the tactical capabilities of the aircraft, the operation with armouring was considered in the statistical analysis.

- **CG POSITION**

  The centre of gravity position is determined by the arrangement of the different components of Equation 4.2 and its envelope with respect to the total aircraft mass is also particular for each mission considered. Generally, the taxi cases considered do not imply a high degree of asymmetry, so among the three coordinates that define the centre of gravity position, only the longitudinal one (x_{CG}) is considered as the main factor contributing to the variation of the taxi loads magnitude in the aircraft structure. Therefore, for the Tactical Mission mass states considered in this statistical analysis, the maximum x_{CG} excursion varies between 21.24% and 37.47%. However, the extreme values of the maximum possible x_{CG} excursion depend on the aircraft configuration analyzed (operation with or without pods or operation with or without armouring).

- **ENGINE THRUST**

  The possible thrust settings, including MTOP, Flight Idle, Ground Idle and Max. Reverse, depend on the manoeuvre considered. For landing operations, just Flight Idle, Ground Idle and Max. Reverse taxi configurations are possible. Since landing manoeuvres performed with Flight Idle are limited to a very few number of cases at high velocities, this thrust setting was discarded from the statistical analysis. Moreover, the total thrust and propeller RPM for each setting vary according to the engine performance map, which is determined by speed, altitude and temperature (ISA offset) of operation.

- **SPEED**

  The maximum operation ground speed is limited by the maximum speed that the tire is able to withstand, which corresponds to 178 KTS for logistic misions. Furthermore, there is an additional limitation for operation on severe unpaved runways (DEF STAN B) for which the maximum speed at roughness level L4 is restricted to 152 KTS. In addition, the minimum speed value considered is 20 KTS, which corresponds to the one stipulated by the civil airworthiness taxi regulations as described in Section 1.3.1.

- **BRAKES**

  The application of brakes depends on the manoeuvre, being restricted to landings and rejected take-offs. The effect of an auto-braking system can be included, whose 'power' is also dependent on the manoeuvre, being 'hard' for RTO manoeuvres and 'medium' for landings. The value of the braking coefficient applied by the auto-braking system is the required one for the aircraft to experience a deceleration rate

of 3.5 m/s^2. If auto-braking effects are not included, the typical braking friction coefficient for unpaved runways corresponds to an average value of 0.3, although in this statistical analysis greater values are consider to study the impact of a more severe braking scenario in the probability of limit load exceedance. If no brakes are applied, a typical average value of 0.07 is considered as rolling friction coefficient for unpaved surfaces.

- **FLAPS SETTING**

  Flaps settings are also dependent on the manoeuvre. Deflections of 15°, 20°, 30° are exclusive for take-off and RTO manoeuvres. Regarding landings, discrete positions at 40° and 47° were considered for the purpose of this statistical approach, which are the only possible one for this manoeuvre.

- **SPOILERS SETTING**

  The spoilers deployment depends on the manoeuvre, engine thrust setting and speed of operation selected by the pilot. It is fully controlled by the FCS as a function of these other three possible parameters that define a taxi case.

- **ALTITUDE**

  The altitudes considered in the statistical analysis range from sea level up to the maximum ceiling altitude given by the aircraft flight envelope, which corresponds to 14600 ft. Besides, concerning the limitation applicable to the roughness level L4, by which the aircraft must operate in airfields at altitudes lower or equal to 9000 ft if the x_{CG} is below 25% MAC, is not considered in order to explore the aircraft taxi capabilities beyond its operational limits.

- **TEMPERATURE**

  The atmospheric conditions at which the aircraft can operate are established by the temperature limitations defined in the engine performance map. The temperature range considered in the A400M engine performance map varies from an ISA offset of -70° to +40°. Since the conditions of the runways at which the A400M is being currently operated do not reach such extreme low levels and the severity of the loads is not determinant at those temperature values, a symmetric ISA offset range from -40° to +40° was considered.

After analyzing all the possible parameters that define a taxi case, the most relevant ones must be selected. This relevancy implies selecting those cases for which the most critical loads are obtained and that also lead to a greater variation of their magnitudes for a good assessment of the probability of limit load occurrence. Besides, for the probability calculation to be valid, the parameters considered in the statistical analysis must fulfill an additional criteria. This criteria implies that all the parameters subjected to variation must be uncorrelated, i.e., none of them can be determined by a combination of other parameters selected. For example, including the pods or armouring as part of the OWE,

which is a constant, the payload could not be selected as a relevant parameter if the total mass and fuel mass are considered, since it is completely defined by the previous two according to Equation 4.2. By doing so, the contribution of each factor to the probability calculation is considered once and not repeated.

Considering the criteria of no correlation and the concluding guidelines from previous loads loops, the relevant parameters selected for analysis in the present statistical approach are the following: TOTAL MASS, FUEL MASS, OPERATION WITH PODS AND/OR ARMOURING, x_{CG}, THRUST, SPEED, BRAKES, FLAPS SETTING, ALTITUDE and ISA OFFSET.

The fuel mass and operation with pods are considered relevant parameters in the study of the wing down bending since their inertia has a direct effect on the structural dynamic response of the wing root components. On the other hand, total mass, operation with armouring, x_{CG}, thrust and brakes are considered relevant parameters in the analysis of nose landing gear loads due to the preferred load path affecting its components for a relevant initial pitch down attitude induced by all of them. Flaps setting, altitude and ISA offset are considered important due to their direct implication in the aerodynamics of the aircraft affecting the apparent weight. Likewise, the speed is considered crucial in the analysis as it is the main factor involved in the excitation of a particular mode frequency. As consequence, apart from the payload, the spoilers setting is the only parameter discarded for the analysis since it is correlated to the manoeuvre selected, engine thrust setting and operational speed. Besides, experience from previous loads loops concluded that the variation of the loads magnitude according to this parameter is very small and can be neglected. Although the reduction in the number of parameters considered seems to be insufficient, considering 11 of of 13 possible parameters leads to a more accurate evaluation of the probability of limit load exceedance on the airframe.

Once the most relevant parameters have been identified, the 2D probability maps were defined. For that, the parameters selected must be grouped in pairs to define the X and Y axis of the probability maps. Hence, each probability map reflects how the variation of each parameter affects the probability of limit load occurrence. As a consequence, four types of 2D probability maps were determined, considering the following association of parameters given in (Y-AXIS)-(X-AXIS) pattern:

- **TOTAL MASS (TM) [T] - FUEL MASS (FM) [T]**

  This two parameters define the overall mass configuration of the aircraft. Therefore, mass states with different combinations of payload and fuel mass were defined to cover the entire aircraft mass-fuel envelope, including extreme cases at the envelope corners such as OWE, MZFW, MLW with max. payload and MLW with max. amount of fuel. Intermediate total mass configurations were considered for fuel quantities ranging from zero amount of fuel to max. possible fuel, in order to consider discrete points that perfectly define the convex-hull of the mass states envelope required for data post-processing.

Doing a pre-analysis of the possible load magnitudes trend, critical scenarios for the wing root down bending are expected to occur in those cases in which the fuel mass is the maximum possible,i.e., at MLW. Likewise, those cases close to the zero fuel weight line in which the payload on board is maximum are thought to be the most critical scenarios for nose landing gear load magnitudes.

- **BRAKING COEFFICIENT (μ_{brk}) - x_{CG} [%MAC]**

  This probability map shows the variation of two factors that are closely related to the pitch attitude of the aircraft. Cases including braking coefficients ranging from no application of brakes to an unusual high value of 0.4 for severe braking scenarios were defined for forward, mid and backward longitudinal positions of the centre of gravity. Auto-braking effects were also included. Since both parameters directly affect the aircraft pitch attitude, the load magnitudes variation is thought to be more representative for the nose landing gear components. In these cases, loads are expected to be more critical when these two parameters induce the greatest pitching down moment from all the possible combinations, which should correspond to the lowest value of x_{CG} position and the highest braking coefficient considered. As a consequence, the graph is expected to show a diagonal increasing trend from backward x_{CG} position and no braking effects to forward x_{CG} position and high μ_{brk} values.

- **ALTITUDE (h) [ft] - SPEED (v) [KTAS]**

  Both parameters have a direct impact on the lifting capabilities of the aircraft, which affect its apparent weight during taxi manoeuvres, i.e., the 1G static loads. According to the typical definition of the lift force as given in Equation 4.3, the effect of the height is included by means of the density, as reflected in the ISA model. On the other hand, the effect of the speed is quadratic, so the rate of change of the 1G taxi loads magnitude is expected to be dominated by this factor.

$$L = \frac{1}{2}\rho V^2 S C_L \tag{4.3}$$

  Apart from its effect on the lifting properties, the effect of the speed is considered to be predominant in the excitation of the aircraft modes (incremental forces) at a particular frequency (f) when taxiing over a bump of specific wavelength (λ). At a particular aircraft speed and bump wavelength, the frequency is defined according to the following equation, which corresponds to the black lines of Figure 4.3.

$$f = \frac{V}{\lambda} \tag{4.4}$$

  Also, as depicted in Figure 4.3, if the frequency of excitation is coincident with that of the mode of an specific aircraft structural component, the dynamic response will be exacerbated to a greater extent and the load magnitudes will be more critical. Therefore, to investigate this effect, several combinations of altitude and speed

were analyzed to cover the complete runway altitude-ground speed envelope. Most critical scenarios are expected to be encountered at the particular speed that make the frequency of excitation to be coincident with that of the mode of the structural parts of interest. At that particular speed, taxi loads are expected to be more critical when increasing the runway altitude, since the density is lower and so is the lift force generated by the aerodynamic surfaces.

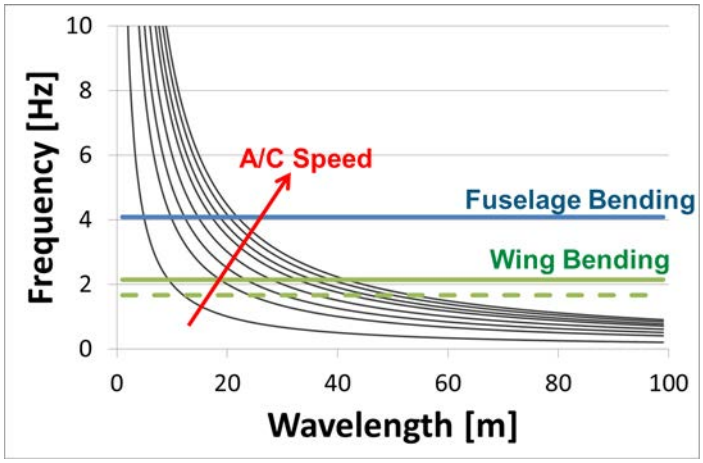

Fig. 4.3. Frequency excitation for different aircraft modes

- **ISA OFFSET (ΔT) [°C] - FLAPS DEFLECTION (δ_f) [°]**

  As in the previous probability map, the variation of these two parameters implies a variation on the lift force that alleviates the apparent weight during taxi manoeuvres. In the same manner as the altitude, the temperature offset has a direct effect on the density value according to the ISA model. On the other hand, the deflection of the flaps has a direct impact on the aerodynamic properties of the wings, modifying the overall lift coefficient considered in Equation 4.3. Hence, cases at different temperature conditions within the engine performance map were combined with the two possible flaps deflections concerning landings. As a consequence of the aforementioned effect on the aerodynamics of the aircraft, most critical values are expected to take place at the combination in which the lift force is the lowest, implying highest temperature and lowest flap deflection setting considered.

4.5. Casuistry

According the idea of finding the appropriate balance between computation time and accuracy for the present statistical analysis to succeed, a relevant number of cases was selected to perform the probability calculation of limit load occurrence for the two magnitudes of interest. Besides, in the definition of the 2D probability maps, only 8 out of the 11 parameters identified as relevant for the statistical were considered in the definition of the probability maps. Therefore, in order to include the effects of thrust and operation

with pods and/or armouring, improving the completeness of the statistical approach as much as possible, the following casuistry was considered:

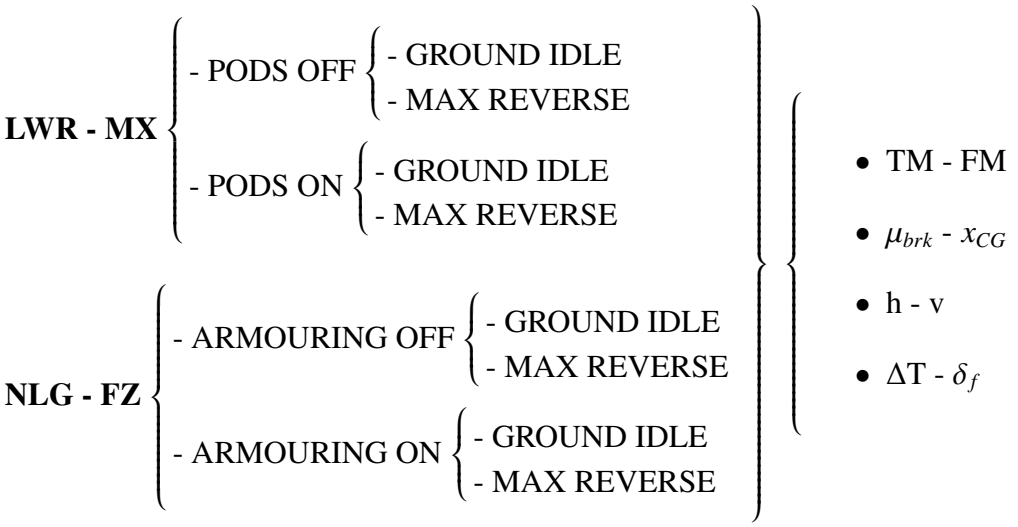

As illustrated in the previous schema, at the roughness level L4 design bump height for a 50 m wavelength and for each magnitude of interest, two reference taxi cases were defined to study the influence of the operation with that extra feature (PODS/ARMOURING) that makes the magnitude of the particular loads studied more critical. As a consequence, the operation with and without pods but no armouring is considered to study the probability of limit load exceedance for the down bending moment at the wing root. In the same manner, the operation with and without armouring but no pods is considered to study the probability of limit load exceedance for the downward vertical force at the NLG wheel axle. This criterion of including just the extra feature that induces a higher severity in the load magnitudes studied allows reducing the number of cases to be simulated, since, for instance, cases with pods and armouring do not have to be included. In fact, the difference of the load magnitudes achieved in comparison to the cases including just pods is insignificant in the study of the wing down bending at the wing root. The same reasoning would apply for the study of the NLG wheel axle vertical force. Also, this criterion reduces the conservatism implicit in the definition of the EBH curves, since the operation with pods or armouring is devoted for different types of aircraft missions and the installation of both components at the same time would be very unlikely.

Based on the parameters of the most critical cases identified in Table 4.4, the reference cases for each magnitude of interest correspond to:

- **LWR - MX**

MAGNITUDE	PODS OFF	PODS ON
TOTAL MASS [T]	115	115
FUEL MASS [T]	25	25
PAYLOAD [T]	9.750	8.458
ARMOURING	OFF	OFF
x_{CG} [%MAC]	34.830	34.962
SPEED [KTAS]	100	100
BRAKES	ON (ABrake)	ON (ABrake)
FLAPS [°]	47	47
SPOILERS	IN	IN
ALTITUDE [ft]	14600	14600
ISA OFFSET [°C]	+24	+24

TABLE 4.6. LWR - MX REFERENCE CASES

- **NLG - FZ**

MAGNITUDE	ARMOURING OFF	ARMOURING ON
TOTAL MASS [T]	115	115
FUEL MASS [T]	8	25
PAYLOAD [T]	26.750	25.511
PODS	OFF	OFF
x_{CG} [%MAC]	25.916	23.572
SPEED [KTAS]	75	75
BRAKES	ON (ABrake)	ON (ABrake)
FLAPS [°]	40	40
SPOILERS	IN	IN
ALTITUDE [ft]	9000	9000
ISA OFFSET [°C]	+40	+40

TABLE 4.7. NLG - FZ REFERENCE CASES

Moreover, the engine thrust is not included among the parameters defining each reference case since both settings applicable for landing manoeuvres are now considered. Thus, each reference was simulated with ground idle and maximum reverse to include the effect of the thrust in the probability calculation.

Then, for each reference case and thrust considered, the four probability maps are defined. Hence, the parameters of each reference case are varied in pairs according to the two factors considered in each probability map, and as a result, there is one taxi case, which is the reference one, that is repeated in the four different probability maps. For each magnitude of interest, the cases considered in each probability map are described below.

- **TOTAL MASS (TM) [T] - FUEL MASS (FM) [T]**

  Four different groups of mass states were defined to account for the operation with or without pods but no armouring in the study of the down bending moment at the wing root and, likewise, to consider the operation with or without armouring but no pods in the analysis of the NLG wheel axle vertical force. The payload of those mass states associated to a specific magnitude of interest varies in weight but not in position. Therefore, since the payload distribution is always located at the same grid points, the variation of total mass and fuel mass implies also a variation in the longitudinal position of the centre of gravity, which is a parameter considered in another probability map. However, the range of x_{CG} excursion with respect to the reference case is assumed to be not the relevant parameter determining the load magnitudes variation in this probability map, so that the statistical analysis is considered to be valid.

  - **LWR - MX**

    28 mass states were considered for both the operation with and without pods. Besides, the maximum associated x_{CG} excursion, given as %MAC, is of the order of [-2.445, +2.490] with respect to the reference case of the mass states without pods, and about [-2.078, +2.490] with respect to the reference case of the mass states with this extra feature installed.

PODS OFF		PODS ON	
TM [T]	FM [T]	TM [T]	FM [T]
115.000	5.400	115.000	5.400
115.000	10.000	115.000	10.000
115.000	15.000	115.000	15.000
115.000	20.000	115.000	20.000
115.000	25.000	115.000	25. 000
115.000	30.000	115.000	30.000
115.000	34.750	115.000	33.458
109.600	0.000	109.600	0.000
110.000	5.000	110.000	5.000
110.000	10.000	110.000	10.000
110.000	15.000	110.000	15.000
110.000	20.000	110.000	20.000
110.000	25.000	110.000	25.000
110.250	30.000	111.542	30.000
104.800	0.000	104.800	0.000
104.800	5.000	104.800	5.000
104.800	10.000	104.800	10.000
104.800	15.000	104.800	15.000
104.800	20.000	104.800	20.000
104.800	24.550	104.800	23.258
97.000	0.000	97.000	0.000
97.000	5.000	97.000	5.000
97.000	10.000	97.000	10.000
97.000	16.750	97.000	15.458
90.250	0.000	90.250	0.000
90.250	10.000	90.250	8.708
85.250	5.000	85.250	3.708
80.250	0.000	81.542	0.000

TABLE 4.8. TM - FM PROBABILITY MAP CASES FOR LWR - MX

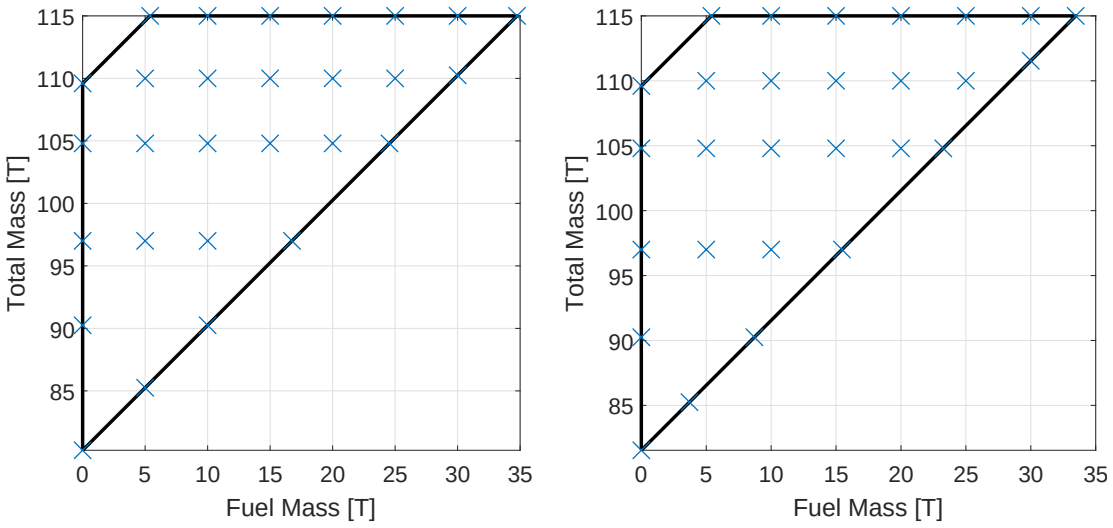

(a) PODS OFF (b) PODS ON

Fig. 4.4. TM - FM probability map cases for LWR - MX

– **NLG - FZ**

In the same manner, 26 mass states were considered for both the operation with and without armouring. Besides, the maximum associated x_{CG} excursion, given as %MAC, is of the order of [-2.163, +8.958] with respect to the reference case of the mass states without armouring, and about [-2.331, +7.852] with respect to the reference case of the mass states with this feature implemented. This greater aft excursion compared to the other two groups of mass states is due to the forward location of the payload which is far from the average CG position of the fuel mass. As a result, when the payload is reduced in favour of fuel mass, the differences in x_{CG} are greater.

ARMOURING OFF		ARMOURING ON	
TM [T]	FM [T]	TM [T]	FM [T]
115.000	8.000	115.000	7.982
115.000	15.000	115.000	15.000
115.000	20.000	115.000	20.000
115.000	25.000	115.000	25. 000
115.000	30.000	115.000	30.000
115.000	34.750	115.000	33.493
110.000	3.000	110.000	2.993
110.000	10.000	110.000	10.000
110.000	15.000	110.000	15.000
110.000	20.000	110.000	20.000
110.000	25.000	110.000	25.000
110.250	30.000	111.507	30.000
107.000	0.000	107.000	0.000
104.800	5.000	104.800	5.000
104.800	10.000	104.800	10.000
104.800	15.000	104.800	15.000
104.800	20.000	104.800	20.000
104.800	24.550	104.800	23.293
97.000	0.000	97.000	0.000
97.000	5.000	97.000	5.000
97.000	10.000	97.000	10.000
97.000	16.750	97.000	15.493
90.250	0.000	90.250	0.000
90.250	10.000	90.250	8.743
85.250	5.000	85.250	3.743
80.250	0.000	81.542	0.000

TABLE 4.9. TM - FM PROBABILITY MAP CASES FOR NLG - FZ

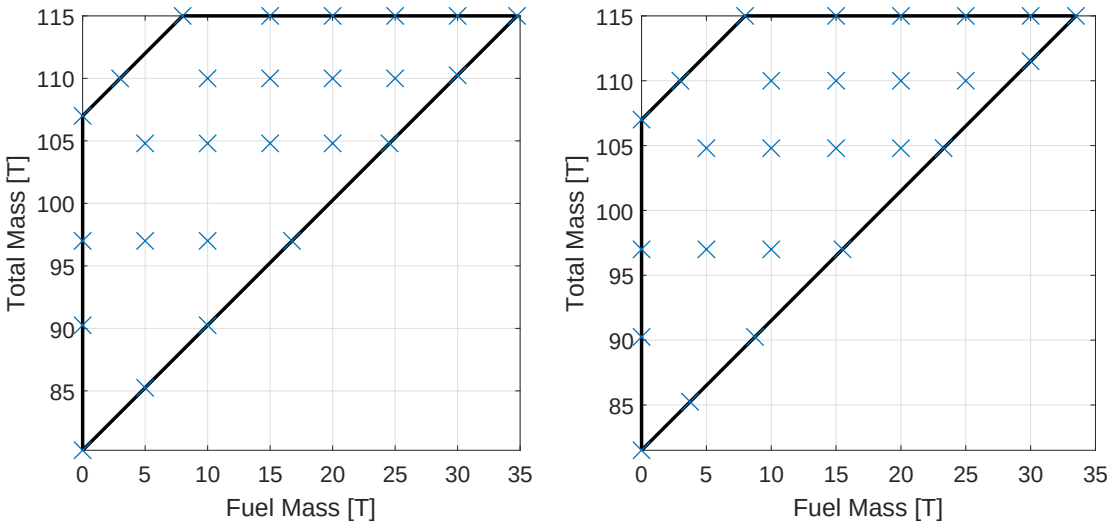

(a) ARMOURING OFF (b) ARMOURING ON

Fig. 4.5. TM - FM probability map cases for NLG - FZ

- **BRAKING COEFFICIENT (μ_{brk}) - x_{CG} [%MAC]**

  Regarding the the braking coefficient, the following values were considered: 0.07 (no brakes), 0.1, 0.2, 0.3, 0.4 and AUTO-BRAKING. The auto-braking value is dependent on the the particular mass state considered, due to the distribution of the loads at each undercarriage leg, and the thrust setting, as a consequence of the magnitude variation of the force pushing the aircraft backwards, which is in fact a function of the velocity, the altitude and the temperature ISA offset.

  To study the load magnitudes variation with respect to the x_{CG} position, two other additional mass states were defined for each reference case. The payload distribution was moved forward or backwards, depending on each reference case, to generate aircraft configurations with the corresponding two missing longitudinal CG positions considered in the analysis. The forward, mid and backward x_{CG} position variations are particular for each reference case and are gathered in Table 4.10.

REF. CASE			x_{CG} POSITION [%MAC]		
MAG.	PODS	ARMOURING	FWD	MID	BWD
LWR - MX	OFF	OFF	25.716	30.273	34.830
	ON	OFF	27.056	30.350	34.962
NLG - FZ	OFF	OFF	25.916	30.083	36.334
	OFF	ON	23.572	29.533	35.495

TABLE 4.10. VARIATION OF X_{CG} POSITION FOR EACH REFERENCE CASE IN μ_{BRK} - X_{CG} PROBABILITY MAPS

Note that since the A400M has swept wings and the pods are located close to the tips, the installation of this feature shifts the x_{CG} position of the aircraft backwards,

although the variation is not very significant since the pods are located close to the natural x_{CG} position of the aircraft structure. Likewise, since the armouring is located in the cockpit, the operation with this feature moves the x_{CG} position forward. Besides, since the location of the armouring is far to the front from the x_{CG} position of the aircraft OWE configuration, the shifts are greater when installing this feature, above all in forward x_{CG} configuration.

Moreover, the resulting 2D probability maps considering all the combination of x_{CG} positions and μ_{brk} values are displayed below.

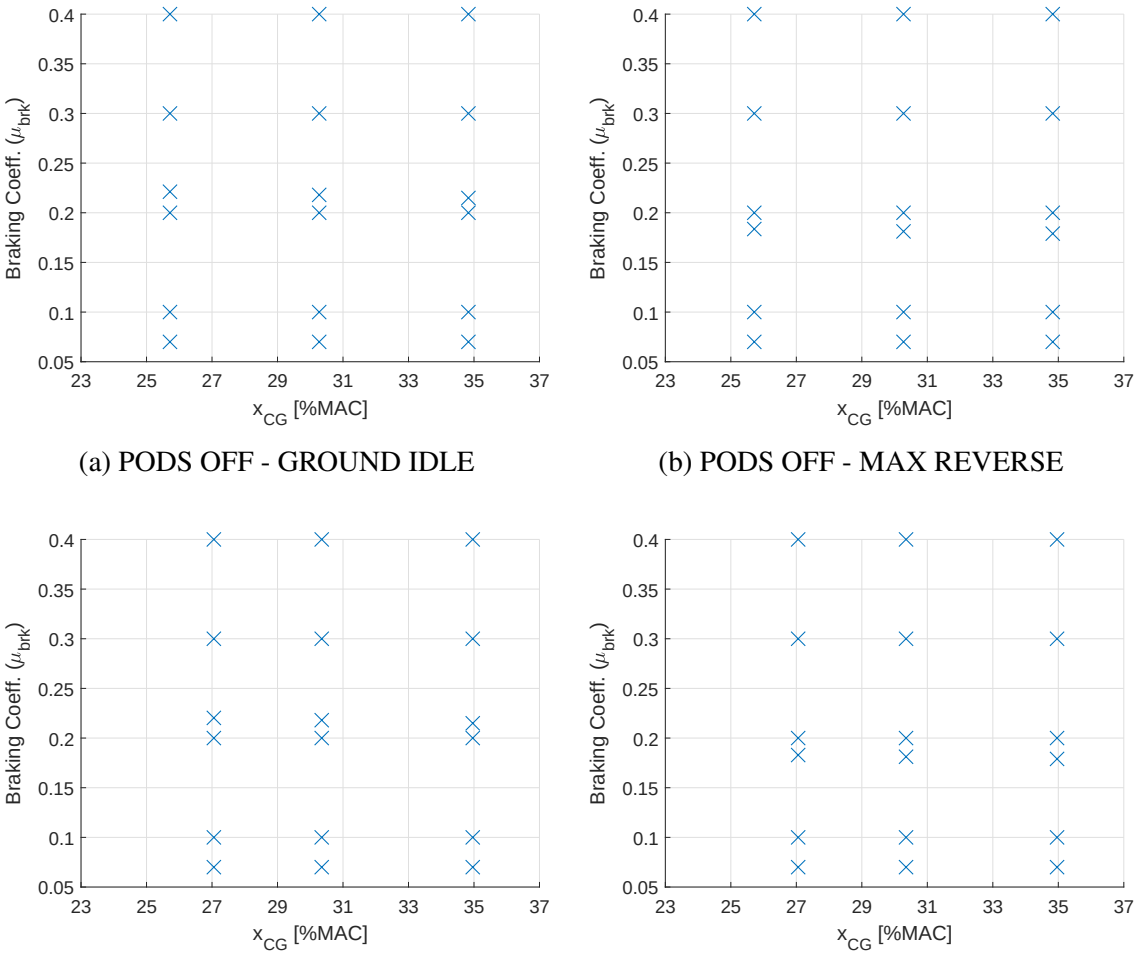

(a) PODS OFF - GROUND IDLE

(b) PODS OFF - MAX REVERSE

(c) PODS ON - GROUND IDLE

(d) PODS ON - MAX REVERSE

Fig. 4.6. μ_{brk} - x_{CG} probability maps for LWR - MX

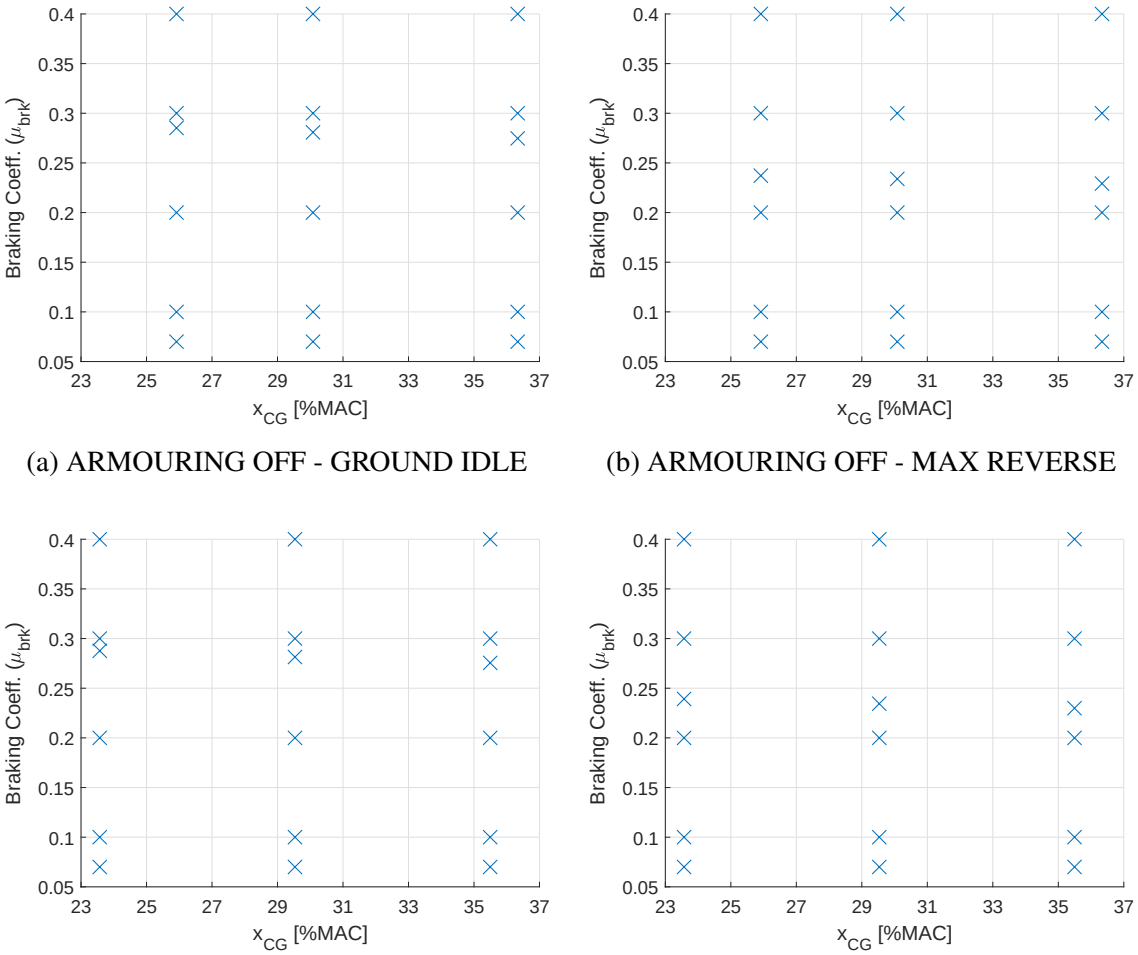

(a) ARMOURING OFF - GROUND IDLE

(b) ARMOURING OFF - MAX REVERSE

(c) ARMOURING ON - GROUND IDLE

(d) ARMOURING ON - MAX REVERSE

Fig. 4.7. μ_{brk} - x_{CG} probability maps for NLG - FZ

From the analysis of the previous figures, it can be concluded that for a given group of mass states and thrust, the auto-braking value is larger for forward positions of the centre of gravity since the normal force at the MLG legs (where the braking action occurs) is smaller and it must be compensated with a greater braking force. Moreover, analyzing the effect of the thrust settings at a given x_{CG} position, auto-braking values are lower for maximum reverse thrust since the force pushing the aircraft backwards is higher and it allows for the braking action to be alleviated.

- **ALTITUDE (h) [ft] - SPEED (v) [KTAS]**

  The variation of this two parameters is common for the four reference cases. The cases considered are a consequence of the combination of the following values of altitude and speed:

  - **ALTITUDE [ft]**: SL (0), 3000, 5000, 7000, 9000, 14600.
  - **SPEED [KTAS]**: 20, 50, 75, 80, 85, 90, 95, 100, 105, 110, 115, 120, 140, 152.

The refinement considered at medium velocities, between 75 KTAS and 120 KTAS, was aimed to more accurately find the velocity at which the loads were critical for the NLG wheel axle vertical force, i.e, the one that yielded a frequency of excitation similar to that of this component. In addition, the corresponding common probability map corresponds to Figure 4.8.

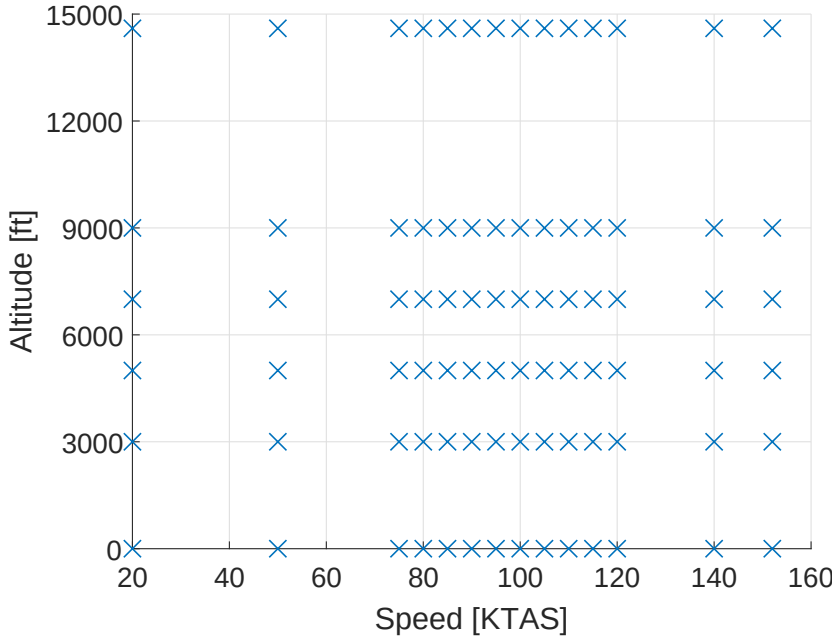

Fig. 4.8. h - v probability map

Also, note that for a given thrust setting at constant temperature, the net thrust force and corresponding propeller rotational speed are not constant for all the cases, since they depend at the same time on both the altitude, due to the variation of density, and the aircraft speed, as reflected in the engine performance map.

- **ISA OFFSET (ΔT) [°C] - FLAPS DEFLECTION (δ_f) [°]**

  The variation of parameters in the subsequent probability map is given by the combination of the following values considered:

  - **ISA OFFSET [°C]**: -40, -25, -15, 0, 15, 25, 40.
  - **FLAPS DEFLECTION [°]**: 40, 47.

  However, since the reference cases to study the wing down bending are characterized by an ISA offset of +24°C and a 47° flap setting, this discrete point was also included in the probability maps of this magnitude of interest to improve the accuracy of the interpolation.

  In an analogous way to the previous probability map type, for a given constant thrust setting, speed and altitude, the thrust force and propeller RPM are not constant among the cases considered due the temperature dependency of the density.

Moreover, the taxi cases constituting each probability map are summarized in Figure 4.9.

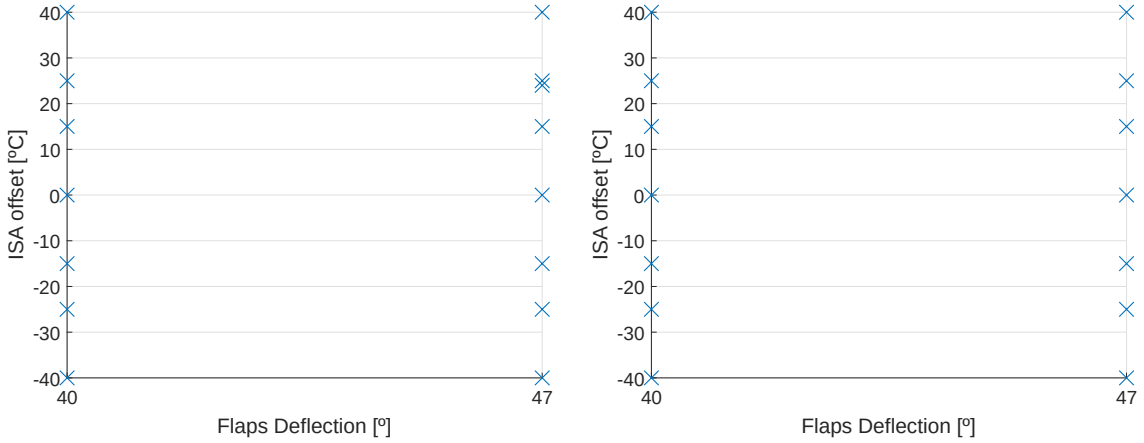

(a) LWR - MX (b) NLG - FZ

Fig. 4.9. ΔT - δ_f probability maps

Excluding the reference cases that are repeated among the probability maps, the definition of this four graphs for the four different reference cases and both thrust settings comprises a total number of 1124 taxi cases within 32 different probability maps for each bump height considered. Finally, the same casuistry was repeated for the design bump height and other four higher values to explore the taxi capabilities of the aircraft beyond the operational limits defined its EBH curves. As a consequence, the probability of limit load exceedance was calculated for the following 5 bump heights, given in centimeters: 18, 19, 20, 21 and 22. As a consequence of this bump height variation, the total number of taxi cases simulated to perform the statistical analysis amounts to 5620 different scenarios, shaping a total number of 160 probability maps.

4.6. Iso-load curves methodology: computation of taxi loads and interpolation.

The probability calculation of limit load occurrence requires the definition of the proportion of cases that exceed limit load magnitudes among all the possible ones considered within each probability map. This same methodology can be applied to compute the probability of exceeding any limit load percentage for the magnitudes of interest considered in the statistical analysis. Thus, for the assessment of this problem, iso-load curves for each probability map must be calculated. This iso-loads curves represent different load magnitude levels, i.e., encircle those cases in a probability map whose corresponding taxi loads for a specific magnitude of interest are equal or above a given percentage of their corresponding structural limit. The definition of the iso-loads curves concerns several stages, which are described in detail throughout this present section.

The first step in the definition of the iso-load curves implies the computation of the taxi loads of interest for the different cases constituting each probability map. For this purpose,

the numerical simulation of all the taxi cases considered was performed according to the process explained along Chapter 3. This procedure comprised in turn the definition of all the mass states considered in the statistical analysis, the preparation of the files for the static balance and the consideration of 1G loads for each case.

A total number of 116 mass states were considered for the definition of the probability maps. Therefore, for the definition of each mass configuration, files including the corresponding MSC.NASTRAN CONM2 entries were created to account for the OWE, extended landing gear mass, fuel mass, payload and optional installation of pods or armouring. Factorization of different sets of CONM2 entries from previously defined mass states was carried out to obtain the different combinations of fuel and payload.

Concerning the static balance, the different inputs gathered in Table 3.1 had to be defined for each taxi case. This step involved mainly the computation of the centre of gravity position for each mass state, air density value and equivalent air speed for each combination of runway altitude and temperature offset. Also, the computation of total net thrust, distinguishing between ground idle and maximum reverse and interpolating according to the engine performance map for specific velocities and temperature offsets if required.

Moreover, regarding the consideration of 1G loads, special attention must be devoted to the type of analysis performed for each magnitude of interest. Due to lack of time for the 1G loads of all the cases to be requested to the Static Loads Department, the analysis of the down bending moment at the wing root was performed using just incremental values of the dynamic response. As a consequence, the negligible variation of 1G loads among the cases devoted to study the wing down bending was assumed. This assumption can be considered of strong importance but still valid for methodological purposes. On the other hand, since the dynamic module of DYNTAXI directly outputs time histories of total forces at the interface points between movable and non-movable parts, the statistical analysis for the NLG wheel axle vertical force was carried out considering the corresponding total loads. Therefore, the corresponding 1G loads file used by DYNLOAD to calculate the total loads at the different monitoring stations were linked to a dummy file in which the static loads for the magnitudes of interest requested were considered to be zero.

MAGNITUDE OF INTEREST	TYPE OF ANALYSIS
LWR - MX	INCREMENTAL LOADS
NLG - FZ	TOTAL LOADS

TABLE 4.11. TYPE OF ANALYSIS FOR EACH MAGNITUDE OF INTEREST

Finally, from the time histories of the two magnitudes of interest, the most critical value for each taxi case is selected, as it is the one required for the probability calculation of limit load occurrence.

However, the resulting maximum taxi loads correspond to discrete points within the envelope of each probability map, but any point enclosed within the limits of such envelope is a possible taxi case that may occur in a real scenario. Therefore, the probability computation philosophy requires the definition of the corresponding taxi loads magnitudes at any point of the probability maps. Hence, since there is an infinite number of points defining each probability map and the numerical simulation of an exhaustive representative finite number of taxi cases would be unaffordable in time, interpolation is required. As a consequence, the load magnitudes of the different taxi cases considered in each probability map were interpolated for the whole envelope defined for each graph. For this purpose, the bulit-in MATLAB® *griddata* function was used. The particularity associated to this function lies on the fact that it only interpolates data for points that are within the convex-hull defined by the x and y coordinated of the scattered input data. Therefore, that is the reason why the casuistry considered for each probability map included at least the necessary discrete points to accurately define the envelope limits of each probability map.

For the interpolation to take place, MATLAB® *griddata* function requires the following inputs:

- Vectors of X and Y values of the two parameters considered in each probability map that define each discrete taxi case. This X and Y values correspond to the discrete taxi cases of the probability maps defined in Figures 4.4, 4.5, 4.6, 4.7, 4.8 and 4.9.

- Critical load magnitudes vector corresponding to the previous X and Y values describing each taxi case. This critical loads are obtained through the numerical simulation of the corresponding taxi cases according to the methodology explained in the previous first step of the iso-load curves definition procedure.

- Matrices defining the X and Y coordinates of the mesh points were the interpolation is requested. Due to the shape of the envelopes considered in each of the μ_{brk} - x_{CG}, h - v and ΔT - δ_f probability maps defined in Section 4.5, the meshes employed are rectangular and equispaced. However, in the case of the TM - FM probability map, a special algorithm is used to define a mesh that perfectly covers the convex hull of the mass states envelope, whose corners are particular for each reference case as illustrated in Figures 4.4 and 4.5. Besides, since the interpolation is only performed within the convex-hull of the scattered data, the mesh coordinates range from the minimum to maximum X and Y values considered in each probability map. In addition, the accuracy in the definition of the iso-load curves and further probability calculation will depend on the mesh utilized. Therefore, a sensitivity analysis to study the influence of the number of mesh points on the precision of the probability calculation was performed and is included in Appendix C. The final number of mesh points considered in each of the four types of probability maps are presented in Table 4.12.

PROBABILITY MAP TYPE		NUMBER OF MESH POINTS
TM - FM	PODS OFF	10,940,314
	PODS ON	11,076,305
	ARMOURING OFF	12,780,303
	ARMOURING ON	13,016,296
μ_{brk} - x_{CG}		4,000,000
h - v		4,000,000
ΔT - δ_f		1,000,000

TABLE 4.12. NUMBER OF MESH POINTS CONSIDERED IN EACH PROBABILITY MAP TYPE

Although the mesh introduced as input to perform the interpolation in TM-FM probability maps contains points that lie outside of the corresponding mass states envelope, MATLAB® *griddata* function discards those points which are out of its convex hull. Therefore, the value provided in Table 4.12 for this probability map type corresponds to the total number of mesh points enclosed within the associated mass states envelope. Moreover, the common number of mesh x-divisions discretizing the TM - FM probability maps of the four reference cases is equal to 4000. However, since the corners of their corresponding mass states envelope are defined by different TM - FM values, so are the number of mesh points for each reference case. A more detailed explanation of the particularities in the TM - FM probability maps mesh definition can also be found in Appendix C.

- Interpolation method. For the purpose of this statistical approach, a *cubic* method was implemented since it is the one that better yields the trend expected for the load magnitudes in the different probability maps types.

With all the previous inputs, MATLAB® *griddata* function outputs a matrix Z with the interpolated load magnitudes at the query points specified by the mesh.

After performing the preceding interpolation, the resulting loads of each probability map must be expressed as a fraction of the structural limit of the corresponding magnitude of interest studied in each one. This step is aimed to graphically depict the loads as a percentage of their corresponding sizing magnitude and then easily identify the taxi cases which are above or below a given load threshold for the probability calculation. Hence, the taxi loads of the casuistry devoted to the study of the down bending moment at the wing root must be non-dimensionalized by the corresponding limit load of such magnitude of interest. An analogous procedure must be carried out for the loads concerning the study of the NLG.

However, for the exemplifying purposes of this project, neither the down bending moment at the wing root nor the NLG wheel axle vertical force are the sizing magnitudes at the point of the roughness level L4 EBH curve subjected to study. As a consequence, a

criteria was elaborated to determine the sizing case for each magnitude of interest. Thus, since at a particular point of the design EBH curve the probability of limit load occurrence must exists due to the possibility of encountering the scenario that determines the maximum allowable bump height, one of the taxi cases considered for the study of each magnitude of interest must be assumed as the sizing scenario for each of the two structural components analyzed. Therefore, the sizing case assumed for each magnitude of interest corresponds to the one that yields the most critical load magnitude at the design bump height (h = 18 cm) among the four possible combinations of reference case (PODS OFF/ON or ARMOURING OFF/ON) and thrust (GROUND IDLE/MAX. REVERSE) considered for either LWR - MX or NLG - FZ respectively. As expected, the operation with the extra feature, pods or armouring, leads to more critical loads at the corresponding magnitudes of interest. Nevertheless, the effect of the thrust is not that obvious, although comparing the values associated to each setting, operation with ground idle yielded higher load magnitudes for the reference cases examined.

As a result of this assumption, the reference case including the operation with pods and ground idle was considered as the sizing case for the study of the wing down bending moment. In the same manner, the reference case including the operation with armouring and ground idle was considered as the sizing case for the study of the NLG wheel axle vertical force. By doing so, in the four probability maps considered for the previous two reference cases and associated engine thrust, there is at least one taxi case for each magnitude of interest that corresponds to the sizing scenario, and that leads to a probability of limit load exceedance at the design bump height very small but different from zero.

MAGNITUDE OF INTEREST	SIZING CASE FOR NON-DIMENSIONALIZATION
LWR - MX	PODS ON + GROUND IDLE
NLG - FZ	ARMOURING ON + GROUND IDLE

TABLE 4.13. SIZING CASES CONSIDERED FOR EACH MAGNITUDE OF INTEREST

Once the adimiensionalized data is available for each magnitude of interest, the iso-load curves can be defined for the different probability maps. The tool used to plot these curves was the built-in MATLAB® *contour* function. The required inputs for this function are the the matrices X and Y that define each probability map mesh and the corresponding matrix Z with the interpolated load magnitudes. Moreover, several iso-load levels were specified depending on the load magnitudes variation range of each probability map. Plotting several contour lines allows performing a sensitivity analysis of the different parameters defining a taxi case, analyzing the effect of each of them in the taxi loads magnitude. Also, it allows acquiring a better understanding of the magnitudes variation, trying to find a possible explanation for such trend. Besides, for better readability of the graphs, the contour lines follow a labeling code in which each iso-load level is associated to a specific colour, assigning dark blue and brown to the lower and higher ratios depicted, which

correspond to 0.1 and 1.05 respectively. In addition, the discrete taxi cases for which the numerical simulation was actually performed are included in their respective probability maps and are represented by means of a blue cross marker.

A more detailed documentation of MATLAB® *griddata* and *contour* functions can be found in [33] and [34] respectively.

4.7. Operation in design EBH curve

The statistical analysis is performed first at the design EBH curve selected for study in order to validate the methodology proposed in the present project. For this purpose, the results of operating at the weight limitations and maximum allowable bump height imposed by the roughness level L4 of the A400M EBH curves are presented. The set of results concerns first the definition of the iso-load curves for the probability maps considered to study the two magnitudes of interest. Then, the probability curve to assess the risk of limit load exceedance when operating at the design bump height of a given roughness level is computed for each magnitude of interest. Nevertheless, in order to illustrate the methodology that give rise to such probability curve, a deep explanation of the statistical and mathematical concepts that support the probability calculation philosophy is previously provided.

4.7.1. Definition of iso-load curves

Following the procedure described in Section 4.6, the iso-load curves of the 32 probability maps containing load magnitudes calculated at the design bump height (h = 18 cm) selected from the roughness level L4 can be defined. However, only a few of them are shown for illustrative purposes. Besides, a label containing the reference case, thrust setting and bump height is included prior to any set of four probability maps to easily identify the scenario depicted.

First, to study the load magnitude trend for both the down bending moment at the wing root and the NLG wheel axle vertical force, the four different probability map types are defined for each magnitude of interest. The reference cases selected as basis for the definition of the iso-load curves are those that do not include either the operation with pods or armouring combined with the thrust that leads to more critical loads for the sizing cases. Hence, these two cases correspond to PODS OFF + GROUND IDLE and ARMOURING OFF + GROUND IDLE respectively. Moreover, both are taken as a reference to perform a sensitivity study of the 8 parameters included in the four probability maps of each magnitude studied and compare the results with the ones expected, providing a possible explanation if discrepancies are found. Later, the effect of operating with the other engine thrust setting considered for landing is presented. Therefore, an analysis of the load magnitudes variation for the two previous reference cases due to the operation with maximum reverse is provided. Finally, the effect of operating with that extra feature that makes the

loads for each magnitude of interest to be more critical is assessed. As a consequence, the four probability maps for the two reference cases considered as the sizing ones for each magnitude studied (Table 4.13) are presented.

Apart from allowing to perform a sensitivity analysis of the different parameters defining a taxi case, the actual purpose of the definition of these iso-loads curves lies on the statistical approach itself. They constitute a prior step necessary for the probability calculation of limit load exceedance. This probability computation is based on the fact that each iso-load level graphically depicts the taxi cases, among all the possible ones given in each probability map, whose maximum resulting load for a particular magnitude of interest is above a given percentage of its structural limit. Therefore, the effect of each parameter results in an increase or reduction of the number of cases whose maximum load for a particular magnitude studied is above a given threshold value.

LWR - MX

REFERENCE CASE	THRUST	BUMP HEIGHT [cm]
PODS OFF	GROUND IDLE	18

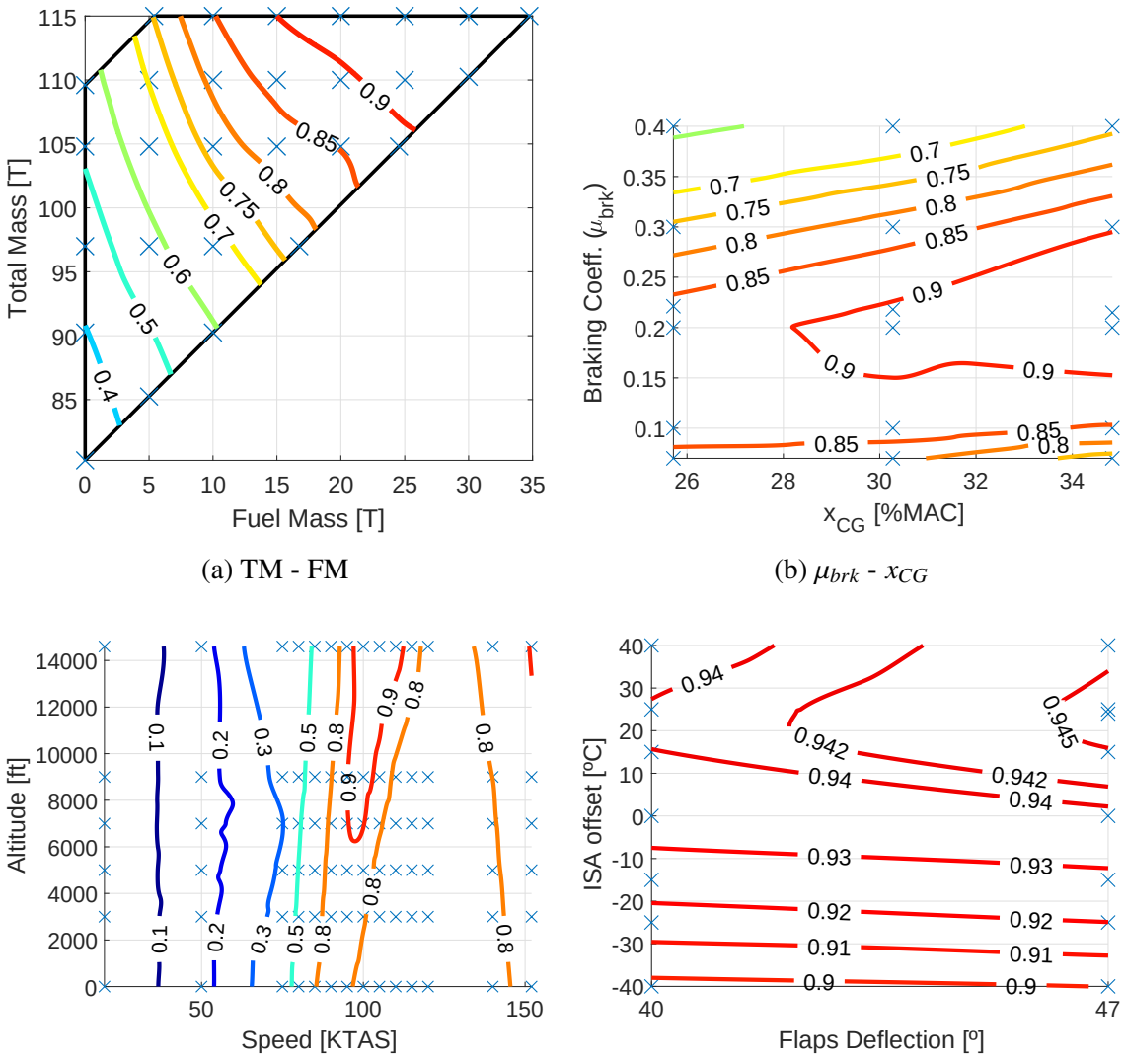

(a) TM - FM

(b) μ_{brk} - x_{CG}

(c) h - v

(d) ΔT - δ_f

Fig. 4.10. Iso-load curves for LWR - MX reference case

Concerning the sensitivity analysis for the TM - FM probability map, the behaviour of the loads magnitude variation is the one expected. For a constant total mass of the aircraft, the loads increase when the amount of fuel is increased, since a heavier distribution of mass allocated at the wing tanks increases the bending moment dynamic excitation, leading to higher loads at the wing root as a consequence of the higher inertia involved. The fuel mass that contributes to a higher amplification of the dynamic response of this structural component is that located at the outboard sections of the wing, since the moment arm contribution to the down bending at the wing root is larger, and hence, tactical fuel filling sequence for this roughness level must be considered. On the other hand, for a constant fuel mass, taxi loads increase when the total mass is increased. Increasing the overall mass of the aircraft while maintaining fixed the fuel mass means an increment in the payload carried on board. For low levels of fuel, the effect of adding payload in the severity of the loads is quite insignificant, since the iso-load curves are nearly vertical. This trend is a consequence of the payload being carried on the cargo hold, so its location does not affect

the dynamic response of the wing structure. However, the payload effect is aggravated when maximum fuel capacity is approached. As a result, the payload weight is smaller and then, the effect on the load magnitudes variation is again mainly due to the effect of the fuel carried on the wing tanks. Therefore, combining the previous effect of both parameters, the critical cases for the down bending moment at the wing root occur for maximum fuel and total mass.

The analysis of the braking coefficient and CG position effects is more complex, but the focus must be set of the influence of this two parameters on the overall pitch attitude of the aircraft. Therefore, from this probability map, it can be concluded that there is an intermediate pitch attitude of the aircraft that makes the loads at the wing root to be the most critical, which occurs for backward x_{CG} position and a coefficient of friction around 0.2. A backward longitudinal position of the centre of gravity pitches up the aircraft. Then, this attitude is lowered due to the pitching down moment generated by the braking forces at the wheels, giving rise to a specific position in which the transmission of ground forces from the MLG pintle points to the fuselage structure makes the magnitude of bending moment at the wing root to be considered a sizing problem. Note that, when the x_{CG} shifts forward, the braking action required to reach this critical attitude is lower, being the braking coefficient the main determinant factor for the wing down bending moment due to the low steepness of the iso-load curves.

Regarding the effect of the runway altitude in the h - v probability map, it is practically negligible for speeds which are not close to the one that produces a frequency of excitation similar to that of the wing bending mode. Nonetheless, when this critical speed is reached, greater load magnitudes are obtained during operations at higher altitudes, since a decrease in density leads to a detriment in the lifting capabilities of the aerodynamic surfaces. This effect on the net lift force reduces the alleviation of the loads at the wing root caused by the structural and fuel weights. On the other hand, when the altitude is fixed, the effect of the speed on the loads variation range is experience to a greater extent. This greater differences occur since the frequency at which one aircraft structural component is excited determines the amplitude of its dynamic response, and, as a consequence, the severity of the loads. Therefore, higher loads are encountered when the aircraft is taxiing at the speed that yields a frequency of excitation similar to the resonant frequency of the particular structural component being studied. Hence, as expected, the most critical cases occur at that particular velocity and the highest operational altitude considered, coinciding the speed with that identified in the most critical case for this particular magnitude studied (Table 4.4).

The ΔT - δ_f probability map concludes that the effect of this two parameters on the load magnitudes variation is small. For a constant flap deflection, the loads increase as so does the temperature, since the alleviation of the loads due to the lift force is aggravated as a consequence of the decrease in density according to the ISA model. The unexpected trend for which loads are more critical at a ISA offset of around 25°C may be due to the consideration of incremental forces for this magnitude of interest, since the alleviation due

to the 1G static loads may lead to more critical load magnitudes at higher temperatures. Moreover, a deeper analysis of the time history of that particular scenario may clarify the differences with the assumptions previously made. Likewise, for a fixed temperature, slightly greater load magnitudes are found for the largest flap deflection considered among the two. This trend is contrary to the behavior expected since, when the aircraft studied is operating with reverse thrust, the aerodynamic properties of the lifting surfaces with a 47° flap deflection setting are worse (generate less lift) compared to those at 40°.

NLG - FZ

REFERENCE CASE	THRUST	BUMP HEIGHT [cm]
ARMOURING OFF	GROUND IDLE	18

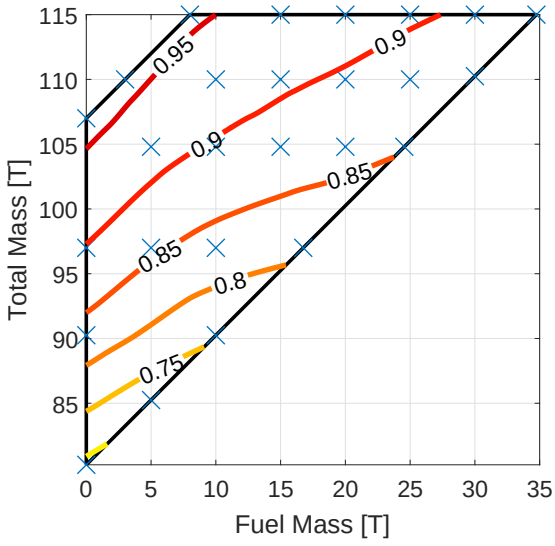

(a) TM - FM

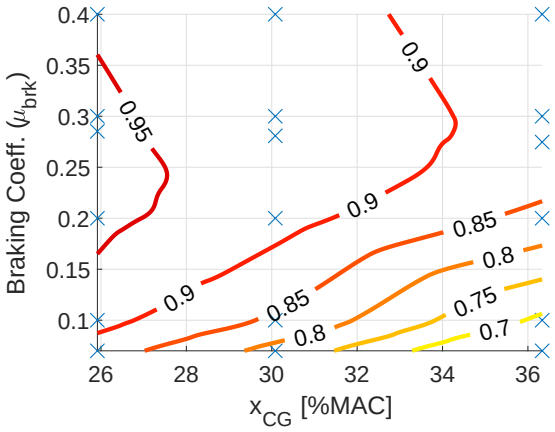

(b) μ_{brk} - x_{CG}

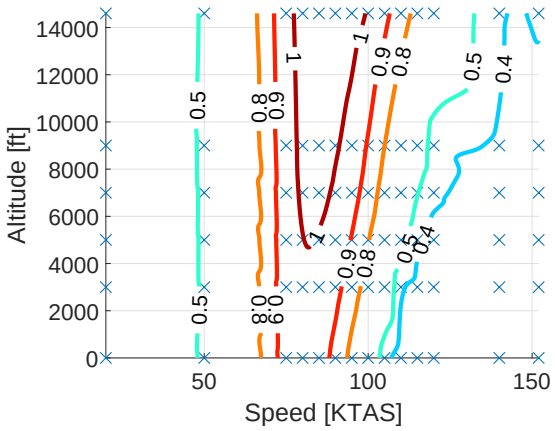

(c) h - v

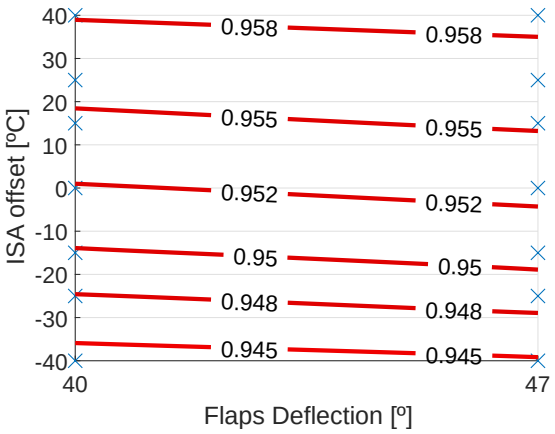

(d) ΔT - δ_f

Fig. 4.11. Iso-load curves for NLG - FZ reference case

In the same manner as for the wing down bending, a similar sensitivity analysis can be performed for the NLG wheel axle vertical force, finding some similarities among the probability maps of both magnitudes.

Referring to the TM - FM probability map, load magnitudes variation trend is also the expected one. On the one hand, for a constant fuel mass, increasing the total mass of the aircraft results in a greater amount of payload carried on board. As a result, the apparent weight increases and so are the loads that must be withstood by the undercarriage. Moreover, this effect is further aggravated for a forward x_{CG} configuration, which produces a nose down pitching moment and hence, the preferred load path for the transmission of the payload weight is focused on the nose landing gear structure. On the other hand, for a constant aircraft total mass, taxi load magnitudes decay when the fuel is increased. For a fixed total mass, an increase in fuel mass is compensated by a reduction in payload and thus, the weight contained in the fuselage, whose load path directly affects the undercarriage structure, is diminished. This trade-off between fuel and payload weights is translated into a backward shift of the x_{CG} position, alleviating the loads felt by the NLG. The combination of the previous two effects makes the slope of the iso-load curves to get more and more horizontal when the fuel is increased. This trend means that the NLG load magnitudes tends to be more and more independent of the fuel quantity, since its weight has a greater effect on the loads of the wing structure, specially at the root, rather than on the undercarriage.

Furthermore, the iso-load curves in the μ_{brk} - x_{CG} probability map follow also the expected trend. For a constant braking coefficient, the load increases when the x_{CG} position is shifted forward, since this configuration leads to a pitch down attitude of the aircraft that generates a higher compression on the NLG shock strut. Likewise, for a constant longitudinal position of the centre of gravity, the general behavior indicates that the load magnitudes increase when the braking action is stronger, due to the pitching down moment that this forces generates. However, for a forward x_{CG} configuration, the most critical loads are found for a braking coefficient around 0.24 instead of at the highest considered. This phenomenon occurs due to the nature of the aircraft dynamic response when rolling over the specific bump considered, which is further investigated in Appendix D.

Regarding the h - v probability map, the behaviour of the load magnitudes variation is similar to the trend found for the wing down bending. The detriment in the alleviation of the lift forces is negligible for speed below the the resonant one. However, at this particular speed and above, greater load magnitudes are found for higher speeds due to the decrease in density according to the ISA model. This effect is much more noticeable at higher speeds since the lift force is a quadratic function on this parameter,as reflected on Equation 4.3. On the contrary, operating in a runway at fixed altitude, more critical loads are found when the taxi speed leads to a frequency of excitation similar to the one of the particular aircraft component mode. However, in this particular case, which is not the sizing one for this magnitude of interest, a region in which loads greater than one is found. This fact is due to following two reasons:

- First, the altitude limitation for the roughness level L4 when operation with a x_{CG} configuration smaller than 25%MAC was not considered. Therefore, at altitudes higher than 9000 ft, limit loads are exceeded. This event only happens in the speed range near the resonant velocity, so the probability of limit load occurrence when the aircraft operates beyond this particular limitation is really low.

- Besides, the resonant speed for this particular structural component was found to be a bit higher than the one identified for the most critical case considered from previous loads loops, which corresponds to 75 KTAS as gathered in Table 4.4. Here lies the reason why a closer refinement of the number of cases considered in the speed range between 75 and 120 KTAS was performed. Then, for velocities close to the resonant speed, the resulting loads, even without considering the installation of armouring, are higher than the magnitude considered as the sizing case for this monitoring station. Therefore, when non-dimensionalizing the data, ratios higher than one at this particular speed range were found in all the h - v probability maps considered to study this magnitude of interest.

Finally, a similar trend to the wing down bending is found in the ΔT - δ_f probability map for this magnitude. The alleviation due to the lift force occurs to a greater extent for higher values of density, i.e., lower temperatures, reducing in such a way the apparent weight of the aircraft supported by the undercarriage. However, the effect of the temperature is much less noticeable than in the case of the wing down bending since the loads variation is of the order of 1%. Besides, greater loads are found at a 47°flap deflection setting due to the same reasons previously explained for the LWR - MX.

Effect of thrust

The general effect of considering the operation with maximum reverse thrust setting for both magnitudes of interest is the reduction of the area described by a number of taxi cases whose load magnitudes are above a given limit load percentage. Therefore, operating with this thrust setting leads to lower load magnitudes for the cases considered in each probability map. As the A400M is a high wing aircraft and the turboprop engines are attached to it, this reducing effect is a consequence of the greater nose up pitching moment generated by the maximum reverse in comparison to ground idle, since the net reverse thrust force generated with this setting is larger. In addition, the effect of this nose-up pitching moment is particular for each magnitude of interest:

- In the case of the down bending bending moment at the wing root, the greater nose-up pitching produced by maximum reverse sets the aircraft at an attitude which is far from that intermediate point in which the transfer of ground loads from the MLG to the fuselage through the pintle points is the most critical for this magnitude studied. However, as a consequence of this steeper nose up attitude of the aircraft, a larger

number of combinations of forward x_{CG} positions and higher braking coefficients provide the required nose-down pitching moment that leads to that intermediate balance in which the load magnitudes are more severe. As a consequence of this effect, the area enclosed by the 0.9 iso-load curve in the μ_{brk} - x_{CG} probability map concerning the operation with maximum reverse (Figure 4.12) is more extensive than that of the cases with ground idle (Figure 4.10)

- The explanation concerning the effect on the NLG wheel axle (Figure 4.13) is much more easier. Simply, the greater nose-up pitching moment resulting from the maximum reverse setting reduces the compression of the shock absorber and therefore, the loads at the NLG wheel axle are alleviated.

- **LWR - MX**

REFERENCE CASE	THRUST	BUMP HEIGHT [cm]
PODS OFF	MAX. REVERSE	18

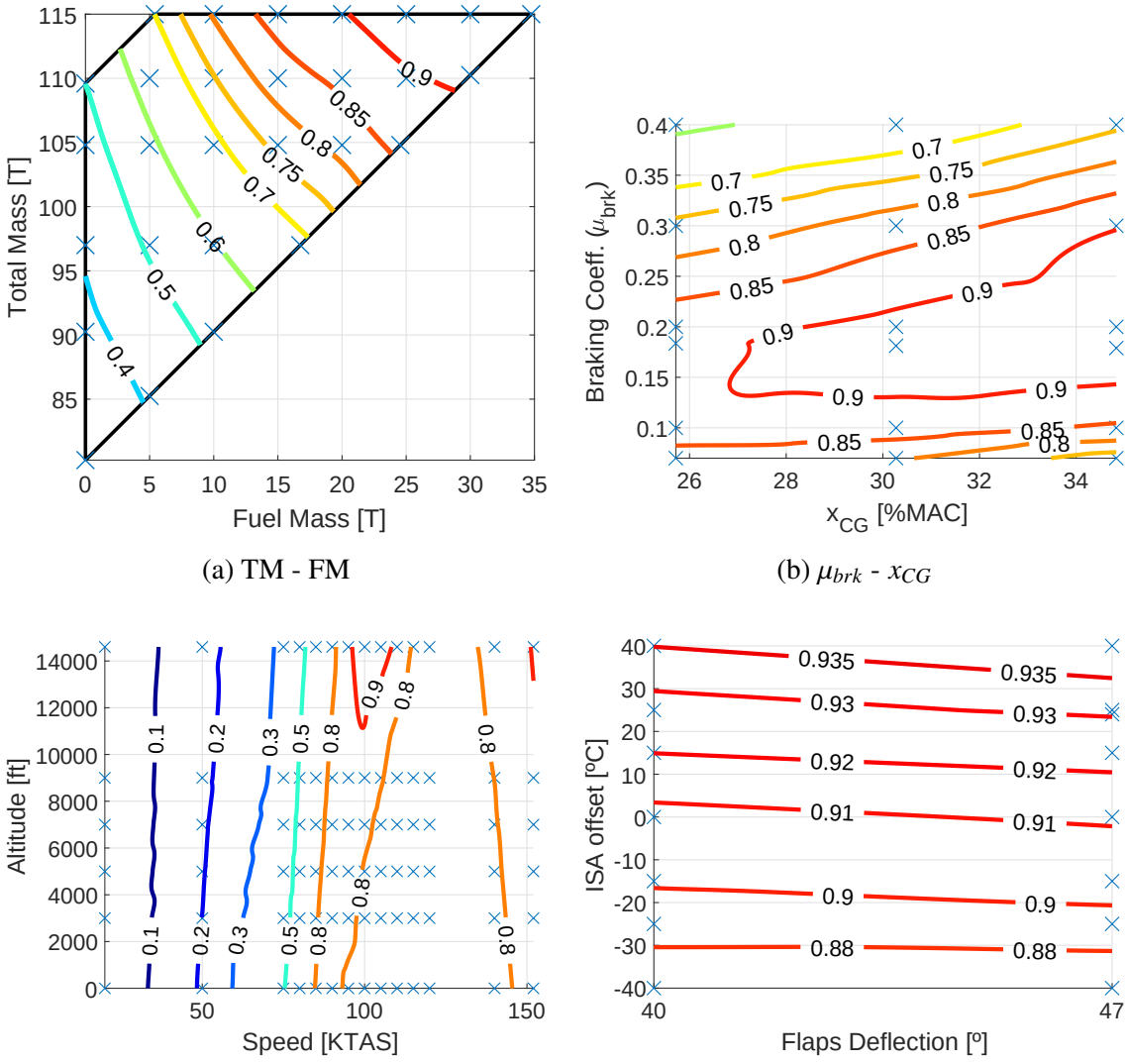

(a) TM - FM

(b) μ_{brk} - x_{CG}

(c) h - v

(d) ΔT - δ_f

Fig. 4.12. Effect of thrust on iso-load curves for LWR - MX

- **NLG - FZ**

REFERENCE CASE	THRUST	BUMP HEIGHT [cm]
ARMOURING OFF	MAX. REVERSE	18

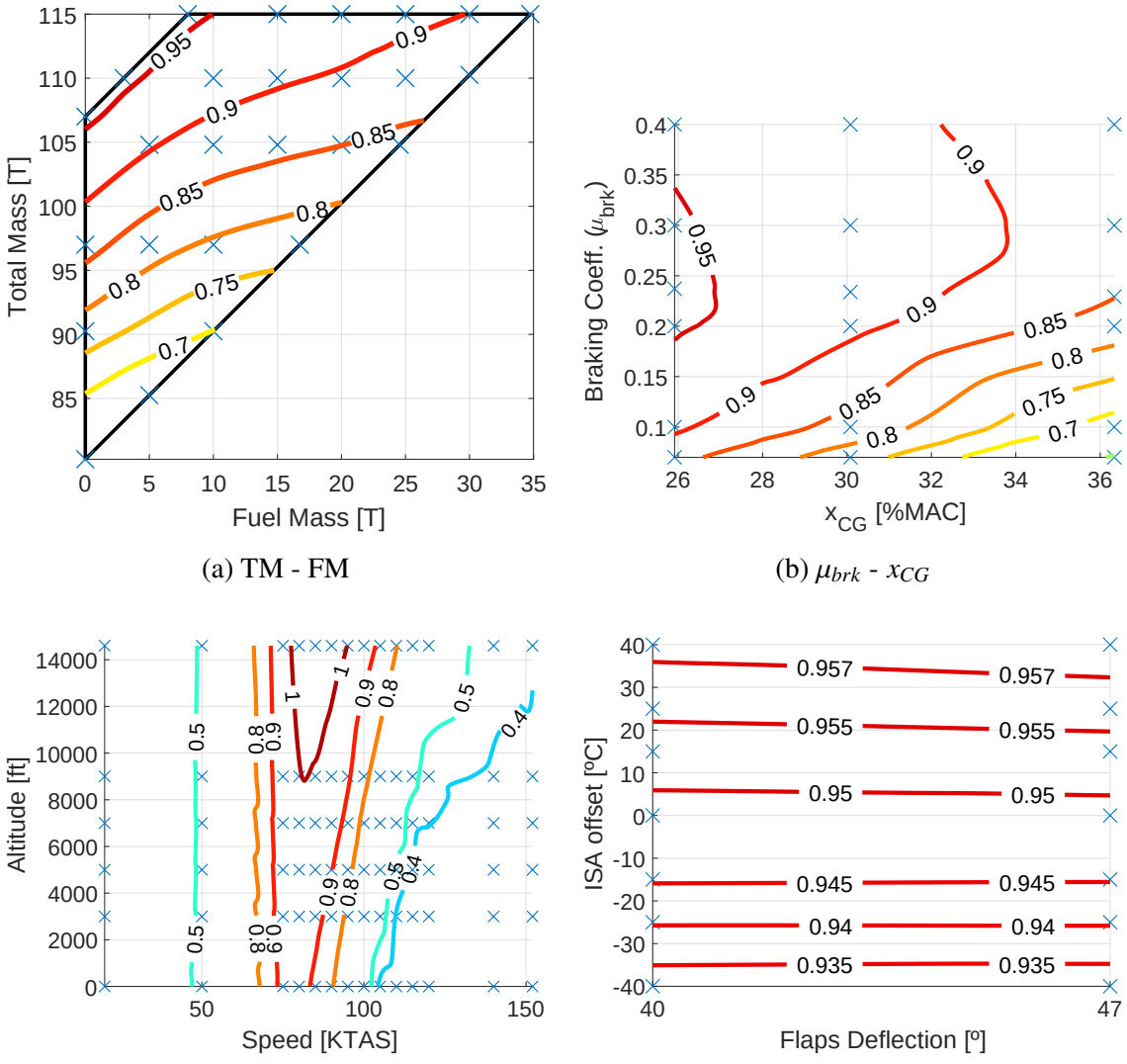

(a) TM - FM

(b) μ_{brk} - x_{CG}

(c) h - v

(d) ΔT - δ_f

Fig. 4.13. Effect of thrust on iso-load curves for NLG - FZ

Effect of operating with extra features

The operation with extra features, i.e., pods in the case of LWR - MX and armouring for NLG - FZ, has as a direct consequence the increase of the area determined by those cases whose resulting loads are above a specific limit load fraction. This increase in area is due to the fact that the installation of this extra features implies a higher degree of severity in the casuistry considered for each magnitude of interest, as a consequence of the reasons already explained in Section 4.3 when identifying the most critical cases from previous loads loops.

Moreover, the probability maps in Figures 4.14 and 4.15 correspond to the sizing cases considered for each magnitude of interest, whose resulting taxi load value was the one used for the non-dimensionalization of the data. Therefore, in each probability map, there is an iso-load curve of ratio equal to one (sometimes almost not noticeable in some prob-

ability maps) enclosing the combination of both parameters describing the sizing case. This small area corresponds to that for which the probability of limit load exceedance exists at the design EBH curve. However, far from this ideal scenario, the area of this iso-load curve referring to the occurrence of limit loads in some probability maps do not cover only a single discrete case and is larger than expected. These discrepancies are explained in the following sections corresponding to each magnitude of interest.

- **LWR - MX**

REFERENCE CASE	THRUST	BUMP HEIGHT [cm]
PODS ON	GROUND IDLE	18

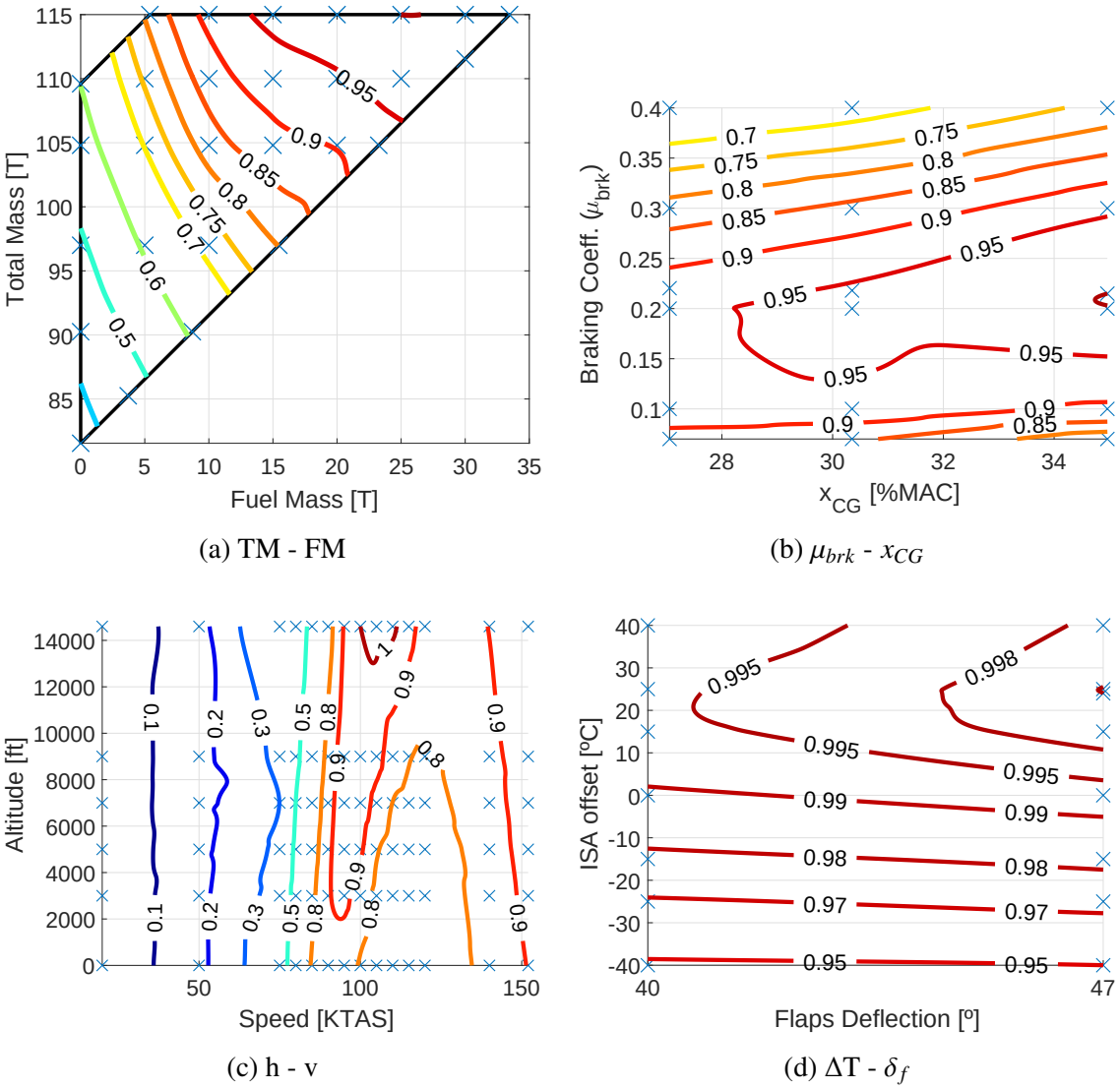

(a) TM - FM

(b) μ_{brk} - x_{CG}

(c) h - v

(d) ΔT - δ_f

Fig. 4.14. Effect of PODS operation on iso-load curves for LWR - MX

In the case of the TM - FM probability map, the most critical case is found at MLW (115T) and a fuel mass equal of 25T instead of at the top right corner of the mass states

envelope where the fuel is maximum. This discrepancy may be due to the fact that the analysis of the down bending moment at the wing root comprises incremental forces. Therefore, since according to the tactical fuel filling sequence, the last tank to be filled is the central one, which is located in the fuselage, a higher inertia closer to the wing root may alleviate the incremental dynamic response of the wing structure. Hence, the incremental loads are smaller for fuel weights greater than 25T. However, if total forces were considered in the analysis, the most critical case would be expected to occur at the aforementioned combination of maximum total and fuel mass.

Besides, concerning the h - v probability map, the limit load iso-load curve at the higher altitude considered extends over more than one discrete case since the resonant velocity found for the wing down bending mode is slightly higher than the one identified in the most critical case for this magnitude of interest (Table 4.4).

- **NLG - FZ**

REFERENCE CASE	THRUST	BUMP HEIGHT [cm]
ARMOURING ON	GROUND IDLE	18

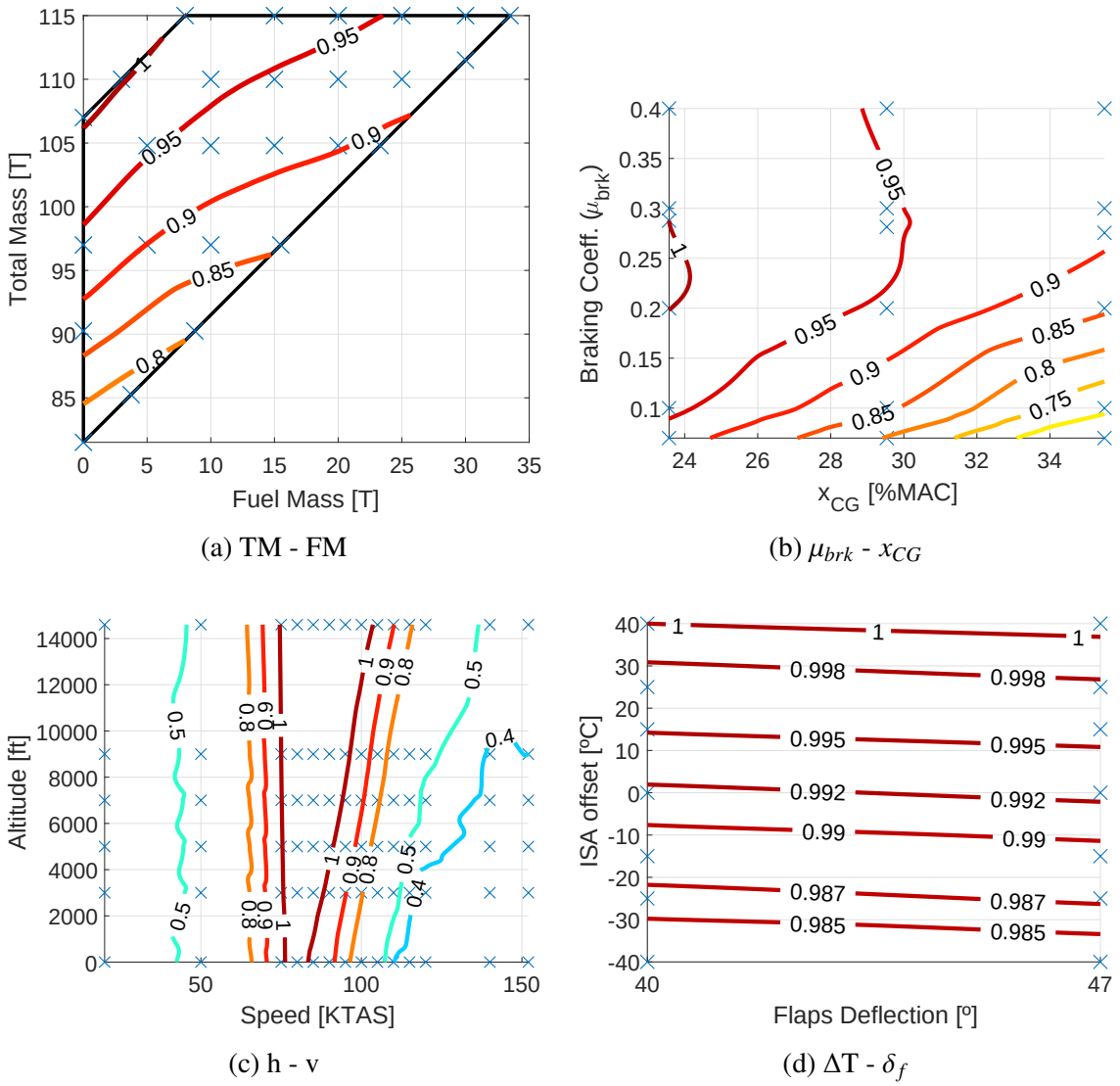

(a) TM - FM

(b) μ_{brk} - x_{CG}

(c) h - v

(d) ΔT - δ_f

Fig. 4.15. Effect of ARMOURING operation on iso-load curves for NLG - FZ

Regarding the analysis of the TM - FM probability map, the most critical case was found to occur at MZFW configuration instead of at the mass state identified as sizing case (115T and minimum possible fuel). Although the payload weight is the same for these two cases, this behaviour is explained since the operation without fuel shifts forward the x_{CG} position and thus, the compression at the NLG shock absorber is higher.

In the case of the ΔT - δ_f probability map for this magnitude of interest, the most critical case is found at the highest temperature considered and at a flap deflection of 47°, due to the detriment of the lifting capabilities of the wings at this flap setting when reverse thrust is considered. As a consequence, at an ISA offset of 40°C, both flaps cases are enclosed by the limit load iso-load curve since the reference cases considered for this magnitude of interest were simulated with a 40° flap deflection setting.

Moreover, the area enclosed by the limit load curve in the h - v probability map is larger than expected since the resonant velocity is also slightly larger that the one identified in the most critical case for this magnitude of interest. This phenomenon was previ-

ously explained in depth when analyzing the h - v probability map of Figure 4.11.

4.7.2. Probability calculation philosophy

In order to quantify the risk that the operation in a runway of a specific roughness profile involves, a methodology to assess the calculation of the probability of limit load exceedance demanded by the aircraft customers was developed. Once the casuistry for the statistical analysis was selected and the corresponding iso-load curves obtained, basic statistical concepts are applied in order to know how to compute the probability of limit load occurrence for a particular magnitude of interest from the corresponding probability maps, taking into account all the parameters identified as relevant for the present analysis.

But before dealing with the mathematics of the statistical analysis, the probability calculation philosophy is based on several assumptions in order to simplify this task with the results and post-processing tools currently available. These assumptions can be summarized in the following three points:

- The first assumption considered was the equiprobability of all the taxi cases considered for the statistical analysis. As explained at the beginning of Section 4.1, this assumption leads to the statement that all the discrete events subjected to study are assumed to be equally probable, i.e, they have the same likelihood to occur. However, this assumption was excluded for the taxi cases including pods in the study of the wing down bending. The operation with pods for air-to-air refuelling is mainly focused for logistic operations and carrying out this type of activities from unpaved runways, capability which is reserved for tactical missions, is very unusual, as it implies a high risk in the preservation of the structural integrity at the wing root. Nevertheless, including this possible scenario to reduce the conservatism of the probability calculation, the installation of pods was considered in only 10% of the operations in unpaved runways.

- Moreover, in a probability map, the behaviour of the load magnitudes variation as a consequence of all the possible combinations of the two corresponding parameters defining such graph is independent of the other common factors defining the taxi cases analyzed. The aim of this assumption is to reduce the casuistry considered in the statistical analysis due to the computation time constraints of the IT resources currently available. Therefore, although only a finite number of cases is considered in the statistical approach, the contribution of any possible taxi case to the probability calculation can be considered, since it can be described by the combination of the eight relevant parameters defining the four probability maps, which are in turn particular for a specific thrust setting. As a consequence, the trend of the iso-load curves is independent of the reference cases selected for study. However, the sizing case defining the maximum allowable bump height for a particular roughness level must be the reference case from which the analysis must be started. By doing so,

the probability maps in which this case is considered have load magnitudes ratios equal to one and the probability of limit load occurrence at the design EBH curve exists.

- Finally, for a magnitude of interest, the variation of the loads resulting from a bump height increase, follows the same trend as if it were the sizing magnitude for the particular point of the roughness level subjected to study. This assumption derives from the fact that neither the LWR-MX nor the NLG-FZ are the sizing magnitudes for the starting point considered in this statistical approach. It is reasonable to do so since the behaviour of a structural component differs when its limit load is being reached and plastic deformations may start having an important role on its dynamic response.

Once all the assumptions have been presented, the probability calculation procedure for a particular magnitude of interest, limit load percentage and bump height can be divided in the following 4 steps:

1. **PROBABILITY MAP (PM)**

   The probability of exceeding a specific limit load percentage as a consequence of the variation of two parameters defining a taxi case can be computed from its probability map. Therefore, applying Laplace's rule (Equation 4.1) in a probability map, the probability would be given by the ratio of the number of cases whose load magnitude is equal or above a given threshold value divided by the total number of cases considered in its corresponding envelope. Since any point in such envelope is a possible taxi case, there is an infinite number of cases enclosed within the iso-load curve of a given limit load percentage. Hence, as the addition of an infinite number of points yields an area, the likelihood resulting from any of the four types of probability maps is computed according to the following formula:

$$PM_{(Parameter\ 1)\bigcap(Parameter\ 2)} = \frac{AREA \geq LIMIT\ LOAD\ PERCENTAGE}{TOTAL\ AREA} \tag{4.5}$$

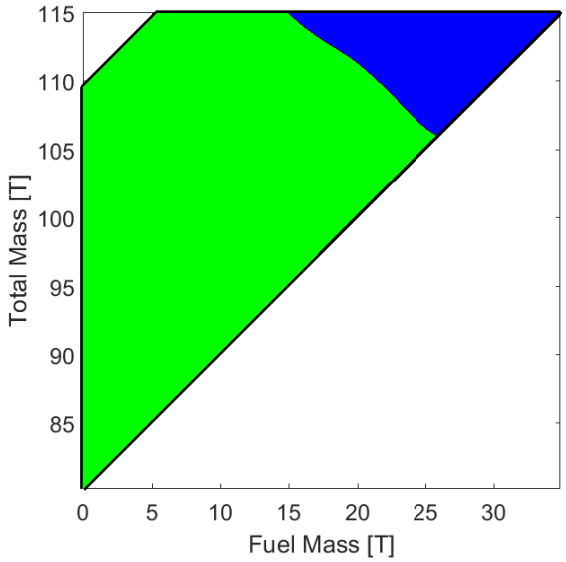

Fig. 4.16. Exemplification of $AREA \geq LIMIT\ LOAD\ PERCENTAGE$ (blue) and $TOTAL\ AREA$ (blue + green) in TM - FM probability map

Note that in ΔT - δ_f probability maps, the iso-load curves are defined at intermediate flap deflection values between 40° and 47°, settings which are not possible since the flap lever only have those two discrete positions. As a consequence, since only the vertical lines at those two flaps configurations are possible taxi cases, the likelihood in this type of probability maps would have to be calculated as the sum of the lengths of the segments defined by the taxi case whose loads are above a given limit load percentage divided by the addition of the total length of the two lines. However, since multiplying and dividing numerator and denominator with respect to the magnitude defined by the flap difference in the graphs, Equation 4.5 is also valid for this type of probability maps.

Finally, due to the lack of a software tool to quickly compute the area enclosed by a specific iso-load curve, the area of each graph was represented by a mesh of a specific number of points, considered as discrete taxi cases. Hence, Laplace's rule can now be applied and the likelihood for a given probability map was computed according to the following formula:

$$PM_{(Parameter\ 1)\bigcap(Parameter\ 2)} = \frac{number\ of\ taxi\ cases \geq limit\ load\ percentage}{total\ number\ of\ cases} \tag{4.6}$$

The accuracy in the probability computation depends on the size of the mesh considered in each probability map. Therefore, a sensitivity analysis included in Appendix C was carried out to study the effect of the number of mesh points considered for each probability map type on the convergence of its corresponding probability value for a given limit load percentage. The final number of mesh points considered for

each type of probability map is the same as the one employed in the definition of the iso-load curves, which is gathered in Table 4.12.

2. **REFERENCE CASE (RC) + THRUST (T)**

   In order to calculate the probability for a specific reference case (PODS ON/OFF or ARMOURING ON/OFF) and given thrust (GROUND IDLE/MAX. REVERSE) the contribution of the corresponding 4 probability maps must be considered. The combination of two parameters in a probability map to define a taxi case is an independent event. In other words, if such combination happens, it does not affect the probability of occurrence of any of the possible combinations resulting from the other three probability maps. This independence of events is due to the fact that the relevant parameters selected for the statistical analysis are uncorrelated.

   Hence, to include the effect of the 8 relevant parameters considered to define a taxi case with a predefined thrust, the formula describing the intersection of independent events must be used [35]:

$$P(A \cap B \cap C \cap D) = P(A) \cdot P(B) \cdot P(C) \cdot P(D) \tag{4.7}$$

   Applying this equation to the particular case of the combination of the four probability maps for a given reference case and thrust, the probability is computed according to the following expression:

$$P(RC \cap T) = PM_{(TM)\cap(FM)} \cdot PM_{(\mu_{brk})\cap(x_{CG})} \cdot PM_{(h)\cap(v)} \cdot PM_{(\Delta T)\cap(\delta_f)} \tag{4.8}$$

3. **REFERENCE CASE (RC)**

   The computation of the total probability for a particular reference case involves the consideration of both thrust settings considered in the statistical analysis. Hence, the formula for the union of events must be used [35]:

$$P(A \cup B) = P(A) + P(B) - P(A \cap B) \tag{4.9}$$

   Since the operation with one engine setting or the other comprises two mutually exclusive events, last term of 4.9 is dropped. Moreover, assuming that both configurations are equiprobable, i.e., both occur in the same proportion, the expression to calculate the probability for a given reference case is of the form:

$$P(RC) = \frac{1}{2}P(RC \cap GROUND\ IDLE) + \frac{1}{2}P(RC \cap MAX.\ REVERSE) \tag{4.10}$$

4. **MAGNITUDE (LWR - MX / NLG - FZ)**

   Finally, to compute the probability of limit load occurrence for a specific magnitude of interest, both the operation with and without the extra feature that determines the

corresponding sizing cases must be taken into account. These two events (operation with or without pods/armouring separately) are also mutually exclusive and the probability calculation also follows Equation 4.9. However, just for the NLG wheel axle vertical force the operation with or without armouring is considered to be equally probable. In the case of pods installation, as explained in the first assumption of the current section, the operation with this extra feature is assumed to take place in just 10% of the missions. Thus, the final probability of limit load exceedance for each magnitude of interest is computed according to Equations 4.11 and 4.12 respectively.

$$P(LWR-MX) = \frac{9}{10} \cdot P(PODS\ OFF) + \frac{1}{10} \cdot P(PODS\ ON) \tag{4.11}$$

$$P(NLG-FZ) = \frac{1}{2} \cdot P(ARMOURING\ OFF) + \frac{1}{2} \cdot P(ARMOURING\ ON) \tag{4.12}$$

The focus of this project was set in the probability of limit load exceedance. Nonetheless, the previous procedure was applied for several limit load percentages in order to study the trend followed by the probability of each magnitude of interest. The limit load percentages at which the probability was computed are the following: 70, 75, 80, 85, 90, 95, 98, 102, 105, 110, 115, 120, 125, 130, 135, 140, 145 and 150. Considering several threshold values allows the quantification of the risk for limit load percentages below 100% if the imposition of a safety factor is required for the structural integrity of an aircraft component. Also, percentages above the limit load threshold allows to study how much each magnitude of interest exceeds its limiting value when increasing the bump height and if any of them reaches ultimate loads (150%).

Moreover, all the probability computations were performed with a precision of 30 decimal figures, including the total probability for a particular magnitude of interest. Therefore, if a probability curve is not defined at one of the limit load percentages considered is because the likelihood of limit load occurrence is below 10^{-30}, and thus, considered non-existent for the average lifespan of an aircraft.

4.7.3. Definition of probability curve at design bump height

Following the probability calculation philosophy developed in Section 4.7.2, the probability curves for both magnitudes of interest were computed at the design bump height of the roughness level L4 considered for study in the present statistical analysis, which is equal to 18 cm.

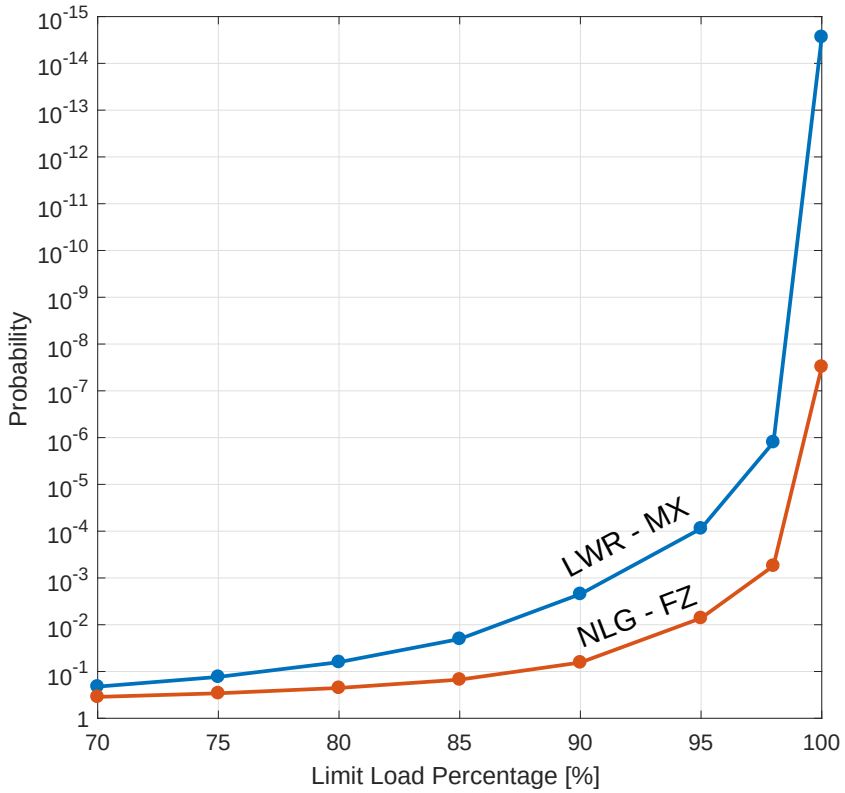

Fig. 4.17. Probability curves at design bump height (h = 18 cm) for LWR - MX (blue) and NLG - FZ (red)

According to Figure 4.17, the probability of both magnitudes studied follows an exponential increasing trend when the limit load percentage is approached. This behaviour occurs because, when the limit load percentage is increased, the area enclosed by the corresponding iso-loads becomes progressively smaller, since the number of taxi cases being critical for a particular magnitude of interest is reduced. Hence, for low limit load percentages, the area enclosed by the corresponding iso-load curves is close to the total area defined by the probability map envelope. As a consequence, the probability tends to one, since the resulting maximum loads of the taxi cases considered are above such threshold. On the contrary, for high limit load percentages, the probability is reduced several orders of magnitudes, since the area enclosed by the iso-loads tends to concentrate at a single point, the sizing case for each magnitude of interest.

For the sizing cases considered for each magnitude of interest in the statistical analysis, the probability of limit load occurrence for the down bending moment at the wing root is almost of the order of 10^{-15} whereas that of the NLG wheel axle vertical force approaches 10^{-8}. This difference is reasonable since the loads considered for the NLG - FZ, above all in TM - FM and h - v probability maps, tend to be closer to its limiting value than those concerning the study of the LWR - MX. The reason for this may lie in the fact the excitation of the NLG when rolling over a bump is of higher severity since it is the component directly in contact with the ground and the compression of the shock strut is critical in the magnitudes achieved. However, such a great divergence between the

probability values of each magnitude is further explained because the areas enclosed by the limit load iso-load curves of the NLG - FZ probability maps are larger, phenomenon which is due to two main reasons:

- In the TM - FM probability map for the sizing reference case, the most critical case does not coincide with the mass state considered as the limiting one. Therefore, there is a region of mass states for which the limit load ratio is greater than one and the area is not restricted to a single taxi case.

- Concerning the h - v probability maps, taxi cases beyond the limitation of 9000 ft for configurations with $x_{CG} \leq 25\%$MAC are considered. Thus, the resulting loads of taxi cases simulated in runways above this altitude are greater than the sizing magnitude considered. In addition, since the resonant speed is a bit higher than that of the reference case considered for this magnitude of interest, there is a range of velocities in which load magnitudes are above the limit load value considered. Therefore, the limit load iso-load curve appears not only in the h - v probability map of the sizing case, but also in the graphs for the reference case without armouring installation. As a consequence of this two facts, there is a large number of taxi cases considered for the study of the NLG - FZ exceeding the limit load value considered for this magnitude.

Note that, although the fuel limitation imposed for the roughness level L4 is not fulfilled, the areas enclosed by the limit load iso-load curves in the different probability maps of the sizing case considered for the study of the LWR - MX are not larger than expected. In the TM - FM probability map (Figure 4.14), the most severe incremental magnitude coincides with that considered for non-dimensionalization of the data. Therefore, the corresponding limit load area includes only one of the discrete taxi cases considered. Additionally, despite of the fact that the resonant speed is slightly higher than that of the reference cases, this effect is not so predominant in the h - v probability maps of this magnitude since the excitation transmitted through the pintle points is widely spread all along the fuselage and partially dissipated due to its greater damping characteristics.

To conclude, although the areas enclosed by the limit load iso-load curves are not restricted to just the sizing cases or cases beyond the the operational limitations of the aircraft, the probability of limit load occurrence for both magnitudes is smaller than 10^{-5}, maximum threshold value typically considered in the Airworthiness Regulations by which limit loads are expected to not be exceeded if taxi operations are carried out within the limitations imposed in the EBH curves. As a consequence, this scenario is the expected one for the validation of the methodology developed for the present statistical analysis.

4.8. Operation in a more severe runway

The same methodology followed for the operation in the design EBH curve (Section 4.7) can be applied to explore the taxi capabilities beyond the aircraft operational limits in terms of runway severity. According to the EBH method, the consideration of a more severe runway is translated into an increase in the maximum allowable bump height defined at a particular wavelength. The probability calculation philosophy can be applied to any bump height, implying that the corresponding probability maps for all the casuistry considered must be previously defined. Therefore, to study the effect of operating in more severe roughness profile on the behaviour of the iso-load curves and the definition of the probability curves, the same procedure was accomplished for four additional bumps considering height increments of 1 cm from the maximum allowable one.

4.8.1. Definition of iso-load curves

In order to illustrate the effect of operating in a more severe runway on the behavior of the iso-load curves, the probability maps for the reference cases anlyzed in Sections 4.7.1 and 4.7.1 are presented, but now considering a bump height of 20 cm. For exemplifying purposes, only the eight probability maps corresponding to Figures 4.18 and 4.19 are presented, since this effect is similar for the rest of bump heights, reference cases and thrust settings considered.

The overall effect of operating in a more severe runway comprises that, as long as the bump height is increased, the areas enclosed by the iso-load curves of a particular limit load ratio progressively increase. This behaviour of the iso-load curves occurs since an increase in the bump height is translated into a more severe excitation of the undercarriage and thus, the transmission of a more amplified dynamic response through the pintle points to the airframe.

In the case of the nose landing gear, the higher the bump height, the higher the compression suffered by the shock strut when the aircraft starts rolling over the bump. Also, if the compression of the shock strut and tyres is high enough, it is possible that, for some bump heights, the NLG loses contact with the ground, giving rise to a high impact when the wheel touches again the runway surface. In both scenarios, high compressive dynamic loads are transmitted from the shock strut to the wheel axle as a consequence of the high aircraft weight that must be withstood by this single component.

Regarding the excitation of the wing, the higher compression of the undercarriage is translated first into a more amplified up bending dynamic response of the structure when the aircraft rolls upwards up to the highest point of the bump. Then, when this point is crossed and the aircraft rolls over the negative slope of the bump, the wing structure tends to recover its static position due to its damping characteristics. Hence, the wing tips start moving downwards and all the inertia of the mass distributed along the wingspan generate high down bending loads at the wing root. This effect is further aggravated if the NLG

loses contact with the ground since the accelerations suffered by the structural elements of the wing outboard section are higher when the NLG falls back to the runway surface.

It is important to remark that, since the length of the bump is remained constant, increasing the bump height does not modify the frequency of the excitation experienced by the aircraft. Therefore, the most critical cases in the h - v probability maps are always encountered within the same speed range, near the resonant velocity, which remains unaffected. Moreover, not only in the h - v probability maps, but the trend of the iso-load curves in all the graphs also remains unchanged since the way each parameter affects the load magnitudes is independent of the bump height.

LWR - MX

REFERENCE CASE	THRUST	BUMP HEIGHT [cm]
PODS OFF	GROUND IDLE	20

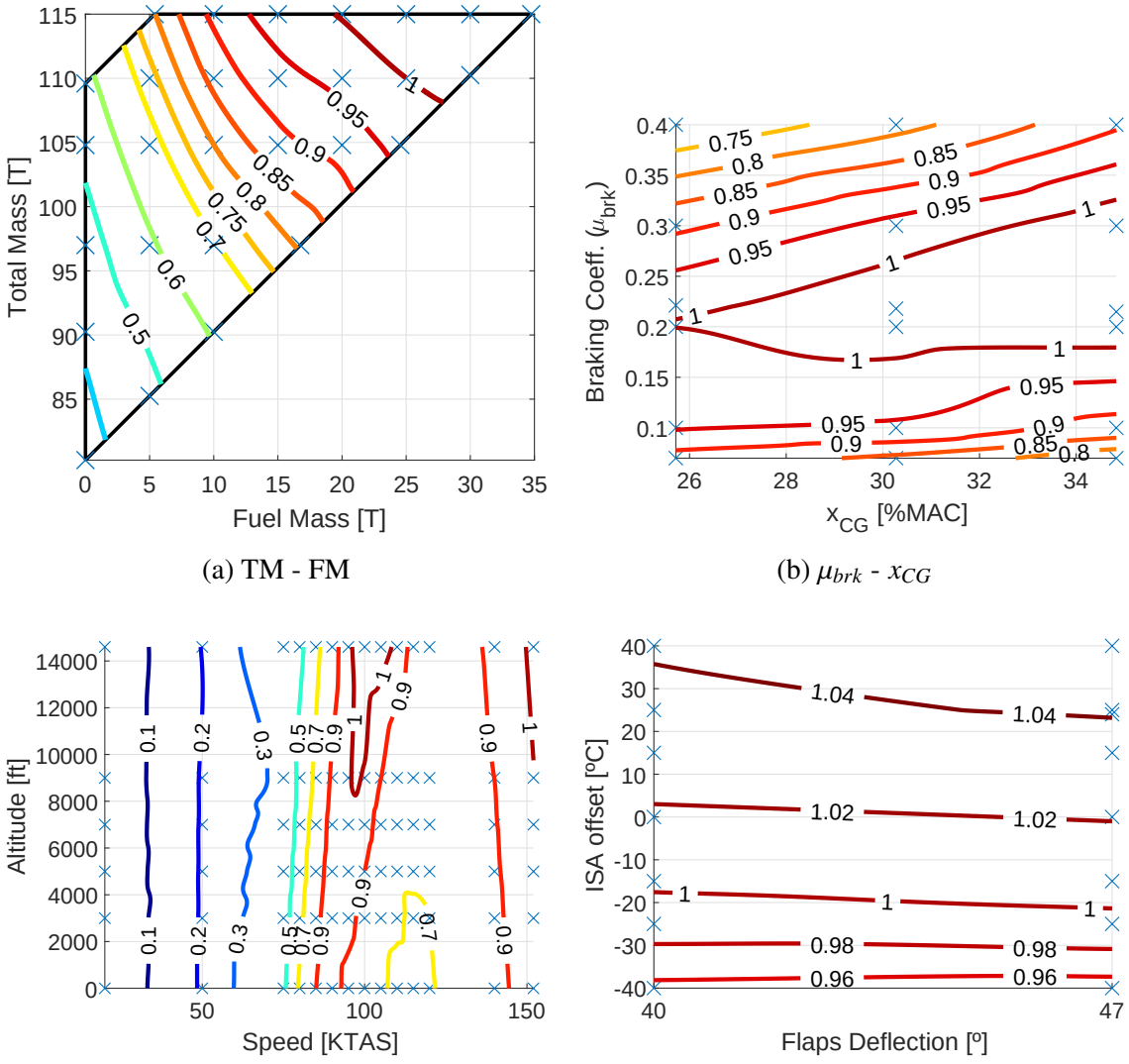

(a) TM - FM

(b) μ_{brk} - x_{CG}

(c) h - v

(d) ΔT - δ_f

Fig. 4.18. Effect of bump height on iso-load curves for LWR - MX

NLG - FZ

REFERENCE CASE	THRUST	BUMP HEIGHT [cm]
ARMOURING OFF	GROUND IDLE	20

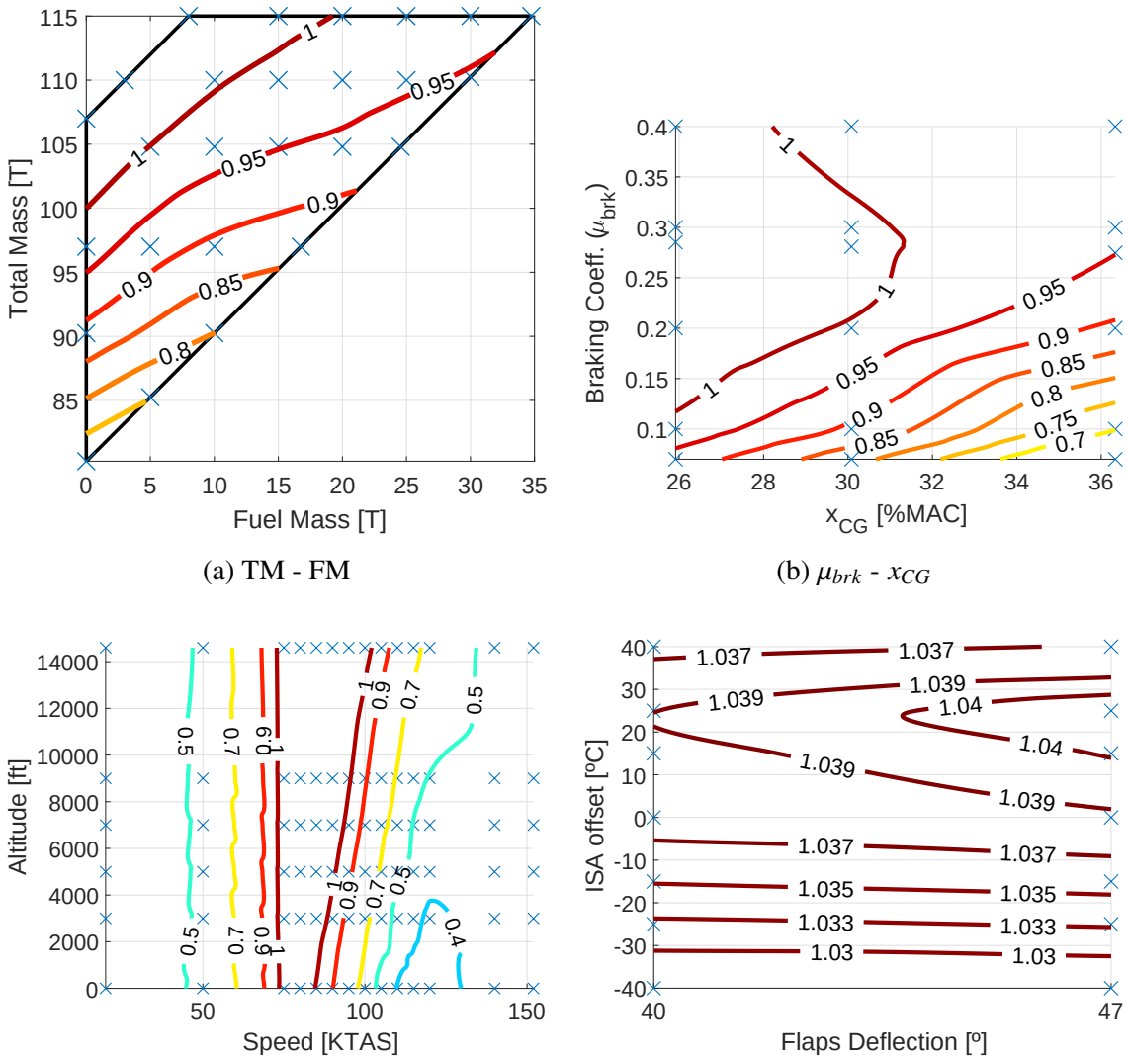

(a) TM - FM

(b) μ_{brk} - x_{CG}

(c) h - v

(d) ΔT - δ_f

Fig. 4.19. Effect of bump height on iso-load curves for NLG - FZ

4.8.2. Definition of probability curves

Following the same calculation philosophy as the one presented in Section 4.7.2, additional probability curves at bump heights of 19, 20, 21 and 22 cm were defined for both magnitudes of interest studied in the present statistical analysis. Also, the probability curve for the operation in the EBH design curve is included. The final results for the LWR - MX and NLG - FZ probability curves are presented in Figures 4.20 and 4.21 respectively.

- **LWR - MX**

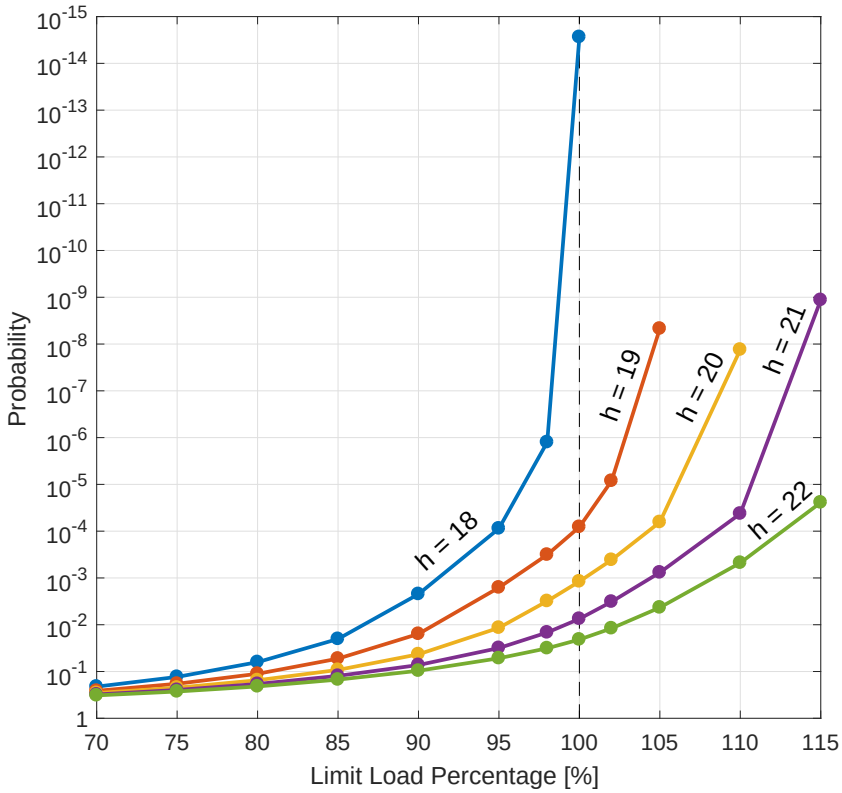

Fig. 4.20. Probability curves for LWR - MX at different bump heights

- **NLG - FZ**

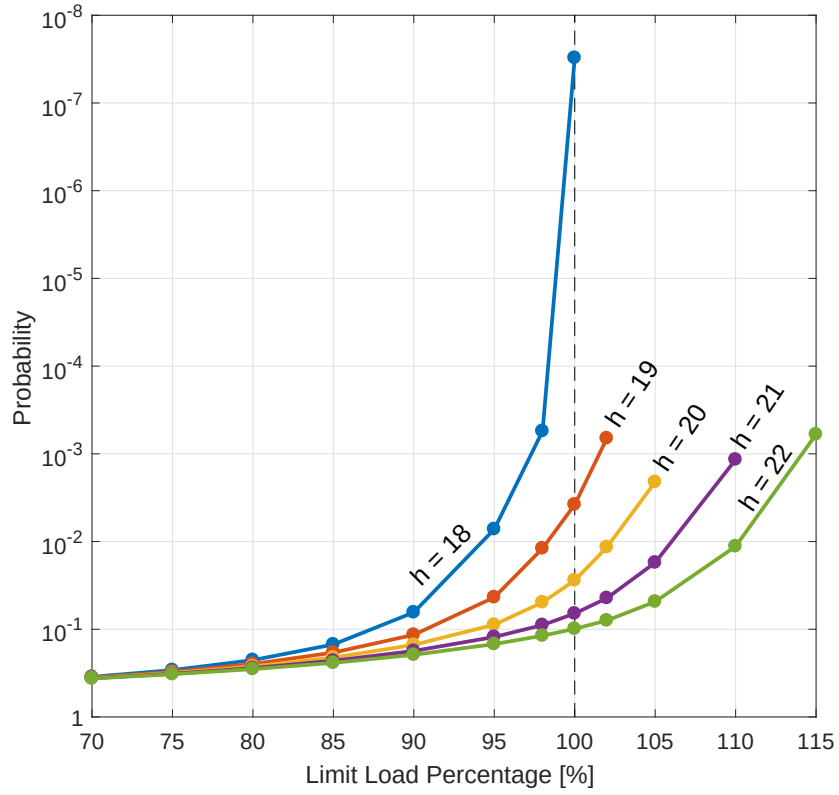

Fig. 4.21. Probability curves for NLG - FZ at different bump heights

For any of the particular magnitudes studied, the probability curves considered for more severe bump heights follow the same trend as the one computed for the EBH design curve. All of them approach a probability value equal to one for low limit load percentages and then exponentially increase when the limit loads percentage considered for the probability calculation are higher. The exponential behavior of the probability curves is relaxed when the bump height is increased. This trend means that the difference in the value of the areas enclosed by the iso-load curves corresponding to each limit load percentage is smaller. Or in other words, the iso-load curves are closer to one another when the operation is a more severe runway is considered. A possible explanation for this smaller excursion may lie in the asymptotic behavior of the resulting loads when the elastic deformation of a structural component is reaching its limiting value.

Also, note that the probability curves concerning the operation in the EBH design curve (h = 18 cm) are only defined up to the percentage that indicates limit load occurence. This is is due to the fact that, although limit loads are slightly exceeded in the cases considered which are beyond the operational limitations of the aircraft, the probability to achieve loads which are a 2% larger than is limiting value is smaller than 10^{-30}. The areas of the iso-load curves for limit load ratios greater than one are very small, so the probability can be considered neglegible. Concerning the other four probability curves representing more severe runways, the probability of limit load exceedance is significant, so they are defined for limit load percentages greater than 100%. In general, the higher the bump height, the larger the limit load percentage up to which the curves are defined, since the severity of the excitation is progressively increased. However, for the bump heights considered, ultimate loads are not achieved, so the components to which the magnitudes of interest refer will not bear the chance of fracture. In addition, the probability of limit load occurrence for bump heights larger than the design one is higher than 10^{-5} in both magnitudes of interest. If this were case, the definition of the EBH curves would have to be revisited, since the maximum bump height for which the probability is smaller than such threshold value should be the one defining the corresponding roughness level.

Therefore, summarizing the behavior of the set of probability curves for a particular magnitude, if the probability of limit load occurrence is held constant, the limit load percentage yielding such likelihood value increases as so does the bump height. This is because the area enclosed by the iso-load curves is more extensive as the bump height is increased and thus, higher limit load percentages are required to obtain the same probability value.

On the other hand, when the limit load percentage is fixed, the probability for loads of such threshold magnitude to occur is higher as the bump height considered increases. This phenomenon is also a consequence of the increment of the areas enclosed by the iso-load curves as a function of the bump height, as explained in Section 4.8.1. However, it is important to remark that the probability of limit load occurrence increases faster than expected. Since the sizing case considered for the non-dimensionalization of the LWR - MX is closer to the actual one, the expected behaviour for the probability curves would

be more similar to the one corresponding to this magnitude, in which the probability for more severe runway profiles increases about one order of magnitude per bump height increment of 1 cm. This large change in the likelihood values might be considered as disproportionate, but note that, for the typical weights of a military transport aircraft, although 1 cm seems to be a very small increment, such inertia magnitudes lead to a very high increase in the severity of the structural excitation.

In fact, probability curves of this type would be the ones presented to the different customers of the A400M. This final output of the project comprises the tool required to quantify the risk of performing taxi operations beyond the limitations imposed in the definition of the corresponding EBH curves. Hence, if the the aircraft is required to taxi in a more severe runway, clearance will be provided depending on the risk a customer is willing to take for such operation. For instance, in the hypothetical case in which the down bending moment would be sizing case (Figure 4.20), operating in a runway whose EBH curve is 2 cm above the maximum allowable bump height for a particular wavelength would imply a probability of limit load exceedance equal to 10^{-3}. This would mean that just one among a thousand taxi operations in that specific runway would lead to limit load ocurrence for this magnitude of interest. In addition, because of force majeure or other unusual circumstances that force the operation in such particular airfield, if the risk required to be assumed is higher, the probability to exceed greater limit load percentages is even smaller.

5. CONCLUSIONS AND FUTURE WORK

5.1. Conclusions

The analysis of taxi loads is a must for the proper design and certification of an aircraft since the taxi phase constitutes the sizing scenario for some particular aircraft structural components, especially the nose landing gear and the wing-to-fuselage attachment due to the down bending moment at the root of the lifting surfaces. The analysis of this sizing problem is further motivated if the specimen subjected to study comprises a new state of the art military transport aircraft, such as the A400M, with the capability to perform tactical operations in unpaved airstrips, characterized by a higher severity of the excitation induced by its roughness profile and the subsequent amplification of the dynamic response of the structure. Once the design of the aircraft has been completed, so its structural capability has been fixed, the definition of the EBH curves is a good starting point to define the taxi operational limitations of an aircraft in order to preserve its airframe integrity. However, in order to go one step further in the analysis of taxi loads, the development of an statistical approach would constitute the perfect tool to explore the taxi capabilities of an aircraft beyond its operational limitations. This new statistical analysis is aimed to complement the definition of the EBH curves and reduce the conservatism inherent in their computation procedure by introducing the concept of probability in the assessment of the taxi loads problem.

The main contribution of this Bachelor Thesis is the development of a methodology whose main goal comprises the quantification of the risk involved in taxi manoeuvres on unpaved runways, providing a solution to the demand of the A400M customers currently performing worldwide operation in airfields of very diverse characteristics. The quantification of such risk implies the determination of the probability of limit load exceedance at any point of the aircraft structure, with the main objective of providing clearance for the operation in more severe runways than that for which the aircraft is designed. In fact, this methodology is not only applicable to tactical airlifters operating in unpaved runways, but also to any type of aircraft performing taxi operations over surfaces characterized by any roughness profile. Moreover, due to the overall complexity of the problem as a consequence of the large number of taxi scenarios that might be encountered, one of the main achievements of the present project is the development of a statistical analysis which is feasible in time, overcoming the speed computational limitations of the technological resources that are available nowadays in the aerospace industry.

In addition, as a result of the different assumptions made, the methodology involves simple statistical concepts, although the probability distributions considered could be of higher complexity for further refinement of the approach. Hence, basic mathematics make easier the development of the tools required for the assessment of the problem and help

speed up the procedure followed to complete the statistical analysis. Despite of this simplicity, from the probability curves obtained for both magnitudes studied, positive conclusions can be drawn for the validity of the methodology proposed. Since the limit load occurrence probability for both magnitudes of interest is below the 10^{-5} threshold value at the design EBH curve analyzed (Figure 4.17), this simplified calculation philosophy can be considered to be a good preliminary approach for the statistical analysis of taxi loads, as it constitutes a statistical model that perfectly combines accuracy of the results and computation time. In addition, this statement is reaffirmed with the fact that the probability of limit load occurrence for the curves representing more severe runways is above such threshold value, concluding that the definition of the EBH curves was properly done. However, two main lessons were learnt to succeed in the application of this particular methodology.

Firstly, for the definition of the probability maps, the identification of the most critical cases for each magnitude studied is a crucial step to accomplish this task. Each point of an EBH curve is defined by a taxi case at which one load magnitude at a particular monitoring station of the aircraft reaches its limit load value. Hence, to properly determine the areas enclosed by the iso-load curves, such sizing case must be included in the casuistry considered to perform the statistical analysis at the corresponding particular point of the EBH curve. By doing so, in the probability maps including the sizing case and devoted to study the probability of limit load occurrence at the design bump height, the area of the limit load iso-load curves would just enclose such limiting case and also those cases, if any, outside of the limitations imposed for the roughness level being studied. As a consequence, a first preliminary definition of the probability maps could be performed in order to investigate if the most critical case found in the probability maps coincides with the sizing case identified during the EBH curves computation process. If great differences are discovered, this initial step would fix any possible discrepancy with the results from previous loads loops. In addition, the final load magnitudes in a probability map strongly depends on the interpolation method, so the one that better fits the expected behavior of the data should be used. Hence, to improve the accuracy in the interpolation, it is also of great importance to choose a relevant number of taxi cases in order to cover the most critical scenarios that can be found in the envelope of each probability map, supporting the decision criteria on the experience acquired from previous loads loops. Finally, time histories as the one presented in Appendix D should be analyzed in order to fully understand the dynamics of the most critical cases if they do not coincide with the ones expected.

Secondly, in the definition of the probability curves, the probability values for each limit load percentage strongly depend on the calculation philosophy considered. Therefore, further adjustment of the pondering for the probability contribution of each parameter defining the different taxi cases could be carried out by means of more complex probability distributions, in order to improve the accuracy of the statistical analysis. Therefore, the definition of the probability curves at the design bump height is indispensable for the validation of the final computation methodology.

5.2. Future work

Taking as a basis the methodology presented in the present project, further activities would be required to fully complete the taxi loads statistical analysis of the A400M, which are also applicable to any other aircraft.

For affordability purposes, the methodology proposed was illustrated with results that comprised the analysis of the down bending moment at the wing root and the NLG wheel axle vertical force. However, none of these magnitudes was the sizing one for the particular point of the roughness level subjected to study. In a real loads loop, the statistical analysis should be performed to the actual sizing magnitude that determines the maximum allowable bump height for a particular wavelength in the definition of an EBH curve. Apart from being the sizing magnitude at the design EBH curve, it is prone to be the most critical one when analyzing the operation in more severe runways. Nonetheless, the statistical analysis should be carried out for the load magnitudes that are about to reach its limiting value, since they might reach a higher limit load percentage when increasing the bump height in the numerical simulations. Therefore, taking into account the chance that any of those magnitudes may reach its limiting value (Equation 4.9), the total probability of limit load occurrence at each bump height (h) considered for a particular wavelength (λ) would be calculated according to the following expression:

$$P\left(h+\lambda\right) = \sum_{i=1}^{N} P\left(MAG_i\right) + O(P) \tag{5.1}$$

where N includes all the magnitudes whose limit load percentage at the design bump height is above a threshold value close to 100% (95%, for instance). Moreover, $P\left(MAG_i\right)$ represents the probability of limit load exceedance of one of those magnitudes considered. Finally, $O(P)$ corresponds to the probability of the rest of magnitudes at the different monitoring stations of the aircraft, which are not taken into account for analysis since its probability of limit load exceedance is expected to be null or a few orders of magnitude smaller, so it can be considered negligible in the computation of the total probability.

In order to further simplify the expression given by Equation 5.1, just the magnitude, among all the ones considered, leading to the highest probability of limit load exceedance could be considered at each particular bump height and wavelength combination. In addition, the analysis at a particular wavelength and roughness level should be performed up to the bump height at which one of the magnitudes studied reaches ultimate loads, in order to study the probability of failure for the corresponding component.

Moreover, in order to perform a realistic statistical analysis, the magnitudes considered in the probability maps should be total loads. As a consequence, the 1G loads to be included in the numerical simulation should be requested in advance to the Static Loads Department once the overall casuistry for the statistical analysis has been defined. Note that the magnitude used for non-dimensionalization of the data in the iso-loads definition

process is the limit load value for each magnitude analyzed. Hence, no criteria should be elaborated to determine a mock sizing magnitude for this purpose.

Furthermore, each sizing magnitude for which the statistical analysis must be performed is associated to a taxi characterized by a specific a manoeuvre type. Nevertheless, the statistical analysis could also be carried out for the two other remaining manoeuvres (take-off and rejected take-off in the case of the present analysis) in the order to compare the probability order of magnitude of such scenarios. In addition, just for exemplifying purposes, the methodology of the statistical approach was particularized for a single point of one of the roughness levels defined in the EBH computation process. However, for the sake of completeness in the assessment of the problem, the statistical analysis should be performed for all the different wavelengths at which an EBH curve is defined. Then, the statistical analysis should be carried for every roughness level considered in the definition of the EBH curves.

Besides, in order to reduce the time to accomplish the statistical analysis, a future approach would concern the reduction of the total number of taxi cases that must be simulated. According to the experience from previous statistical loads loops and guidelines from uncertainty control theory, just a quarter of the total casuistry is expected to be needed. For each probability map, the aim is to simply consider those cases closer to the iso-load curve defined by the limit load ratio subjected to study, which in most of the cases will be one. Therefore, the simulation of the rest of cases would not be required to achieve the same level of accuracy in the calculation of the total probability.

Finally, one of the most important milestones to achieve concerns the no assumption of equiprobability of the events considered in the statistical analysis, since not each possible configuration of the aircraft studied is operated in the same proportion. For that, Airbus has requested actual statistical data of the A400M operations to the different customers currently operating the aircraft. The objective is to develop more realistic probability distributions that better model the likelihood of the different configurations in which the aircraft is operated. Having this data available, the probability maps could be divided in several regions, each being multiplied by a different influence coefficient depending on the likelihood of the combination of parameters enclosed by a particular area portion. Also, the pondering weights associated to each thrust setting or operation with extra feature can be further refined depending on the percentage of times in which each event occurs. As a result, a more accurate probability calculation philosophy for the assessment of the problem would arise from this statistical data request.

BIBLIOGRAPHY

[1] J. R. Wright and J. E. Cooper, *Introduction to Aircraft Aeroelasticity and Loads*, 2nd ed., ser. Aerospace Series. John Wiley & Sons, 2014.

[2] T. L. Lomax, *Structural Loads Analysis for Commercial Transport Aircraft: Theory and Practice*, ser. AIAA Education Series. American Institute of Aeronautics and Astronautics, 1996.

[3] G. Pastor and H. Climent, "Stress Taxi Loads Task Description and Calculation Philosophy", Airbus Military, Tech. Rep. IF-T-AA0-10007-B, 2016.

[4] F. M. Hoblit, "Notes on the Prediction of Dynamic Taxi Loads", Lockheed, Tech. Rep. 8854, 1956.

[5] R. Ortasse, "Evaluation of a Method to Determine Airplane Taxi Loads Using a Generated Random Profile", AIAA, Tech. Rep. 66-469, 1966.

[6] A. G. Gerardi and A. K. Lohwasser, "Computer Program for the Prediction of Aircraft Response to Runway Roughness", Air Force Weapons Laboratory, Tech. Rep. AFWL-TR-73-109, 1973.

[7] L. D. Hokanson, "Analysis of Dynamic Aircraft Response to Bomb Damage Repair", Air Force Weapons Laboratory, Tech. Rep. AFWL-TR-75-138, 1975.

[8] A. G. Gerardi, "Collection of Commercial Aircraft Characteristics for Study of Runway Roughness", FAA, Tech. Rep. FAA-RD-76-64, 1977.

[9] A. Krauss, O. Bartsh, and G. Kempf, "Influence of Mathematical Modelling of Undercarriages on the Prediction of Aircraft Loads due to Damaged and Repaired Runways", in *Aircraft Dynamic Response to Damaged and Repaired Runways*, Brussels, Apr. 1982.

[10] C. Maderuelo and H. Climent, "Validación de un Método Analítico para el Cálculo de Cargas de Rodadura", CASA, Tech. Rep. CASA DT-5-ADD-99011, 1990.

[11] G. Pastor, M. Oliver, and H. Climent, "A400M Taxi Loads Analyses for Runway EBH Curves Computation", Airbus Military, Tech. Rep. ME-A4-NT-130755, 2014.

[12] NTSB, *NTSB Identification: MIA64A0041*, Sep. 1963. [Online]. Available: `https://www.ntsb.gov/investigations/%7B%5C_%7Dlayouts/ntsb.aviation/brief.aspx?ev%7B%5C_%7Did=130%7B%5C&%7Dkey=0` (visited on 04/12/2018).

[13] CIAA, "Informe Final CIAA-Accidente-013-2015, Peruvian Air Line S.A.C., Boeing B-737-3K2, OB-2040-P", Comisión Investigadora de Accidentes de Aviación, Cuzco, Perú, Tech. Rep., Oct. 2017. [Online]. Available: `https://reports.aviation-safety.net/2015/20151023-0%7B%5C_%7DB733%7B%5C_%7DOB-2040-P.pdf` (visited on 04/12/2018).

[14] NTSB, *NTSB Identification: WPR15LA184*, Jun. 2015. [Online]. Available: https://www.ntsb.gov/%7B%5C_%7Dlayouts/ntsb.aviation/brief2.aspx?ev%7B%5C_%7Did=20150615X00136%7B%5C&%7Dntsbno=WPR15LA184%7B%5C&%7Dakey=1 (visited on 04/12/2018).

[15] ASN, *Aircraft accident Lockheed EC-121T Super Constellation 55-0121 Reykjavík-Naval Air Station Keflavík (KEF)*, Mar. 1978. [Online]. Available: https://aviation-safety.net/database/record.php?id=19780315-0 (visited on 04/12/2018).

[16] ——, *ASN Aircraft accident Lockheed C-130 Hercules registration unknown Minneapolis-St. Paul International Airport, MN (MSP)*, Apr. 2004. [Online]. Available: https://aviation-safety.net/database/record.php?id=20040429-0 (visited on 04/12/2018).

[17] CFEAA, "Rapport final de la Comission fédérale d'enquête sur les accidents d'aviation concernant l'accident de l'avion Fokker 28-0100, PH-KLC du 5 mars 1989 à l'aéroport de Genève-Cointrin", Département fédéral des transports, des communications et de l'énergie, Tech. Rep., 1989. [Online]. Available: https://reports.aviation-safety.net/1989/19890305-0%7B%5C_%7DF100%7B%5C_%7DPH-KLC.pdf (visited on 04/12/2018).

[18] NTSB, "Aviation Accident Final Report - FTW01FA127", National Transportation Safety Board, Tech. Rep., Nov. 2003. [Online]. Available: https://reports.aviation-safety.net/2001/20010523-0%7B%5C_%7DF100%7B%5C_%7DN1419D.pdf (visited on 04/12/2018).

[19] BEA, "Rapport d'enquête etabli suite a l'accident survenu a Bruxelles National le 29 Août 1998 a l'avion Airbus A340 immatriculé OO-SCW", Bureau d'Enquêtes et d'Analyses, Tech. Rep., 1998. [Online]. Available: https://aviation-safety.net/database/record.php?id=19980829-1 (visited on 04/12/2018).

[20] EASA, *Certification Specifications for Large Aeroplanes CS-25*, Dec. 2007. [Online]. Available: https://www.easa.europa.eu/sites/default/files/dfu/CS-25%7B%5C_%7DAmdt4.pdf (visited on 03/12/2018).

[21] U. D. Standardization, *Leaflet 49: Design of Undercarriages - Operation from Surfaces other than Smooth Hard Runways. Specification of Continuous Ground Unevenness*, Dec. 1999. [Online]. Available: ftp://ftp.iks-jena.de/mitarb/lutz/standards/dstan/00/970/01040249.pdf (visited on 03/12/2018).

[22] D. Howe, *Aircraft Loading and Structural Layout*, ser. Aerospace Series. Professional Engineering Publishing, 2004.

[23] J. L. Pérez-Galán, L. Benítez, M. Oliver, and H. Climent, "Survey of Aircraft Structural Dynamics Non-Linear Problems and Some Recent Solutions", in *European Air & Space Conference*, Manchester, Oct. 2009.

[24] J. L. Pérez-Galán, J. A. Portas, J. M. Chorro, J. L. López-Arévalo, and H. Climent, "Aircraft Taxi Loads Full Scale Tests and Correlation with Numerical Simulations", EADS-CASA, Tech. Rep. IFASD-2001-080, 2001.

[25] C. Maderuelo, J. L. Pérez-Galán, S. Claverías, H. Climent, and B. Rendueles, "Flight Test Validation of a Fully Coupled Flexible Landing Gear and Flexible Aircraft Models", EADS-CASA, Tech. Rep. IFASD 2005, Paper 21, 2005.

[26] G. Pastor *et al.*, "A400M Tests used for Dynamic Loads Model Validation", Airbus Military, Tech. Rep. IFASD-2011-166, 2011.

[27] J. L. Pérez-Galán and H. Climent, "C295M Military Operation. Dynamic Taxi Loads Analysis on Unpaved Runways", CASA, Tech. Rep. DT-5-ADD-99011, 2000.

[28] BAe, "BAe Equivalent Bump Height Method", British Aerospace, Tech. Rep. B63/A321/962486, Dec. 1996.

[29] EASA, *Type-Certificate Data Sheet for Airbus A400M*, Dec. 2015. [Online]. Available: https://www.easa.europa.eu/sites/default/files/dfu/TCDS%7B%5C_%7DEASA%20A%20169%7B%5C_%7D%20Airbus%7B%5C_%7DA400M%7B%5C_%7D%20Iss%7B%5C_%7D06.pdf (visited on 04/03/2018).

[30] R. J. GUYAN, "Reduction of Stiffness and Mass Matrices", *AIAA Journal*, vol. 3, no. 2, Feb. 1965. DOI: 10.2514/3.2874. [Online]. Available: https://arc.aiaa.org/doi/10.2514/3.2874%20http://arc.aiaa.org/doi/10.2514/3.2874.

[31] L. González, "Aircraft Taxi Loads in Unpaved Surfaces", PhD thesis, Bioengineering and Aerospace Engineering, Universidad Carlos III de Madrid, Madrid, Spain, 2017.

[32] H. Schwarzlander, *Probability Concepts and Theory for Engineers*. John Wiley & Sons, 2011.

[33] MathWorks, *Interpolate 2-D or 3-D scattered data - MATLAB griddata*, 2006. [Online]. Available: https://es.mathworks.com/help/matlab/ref/griddata.html (visited on 02/21/2018).

[34] ——, *Contour plot of matrix - MATLAB contour*, 2006. [Online]. Available: https://es.mathworks.com/help/matlab/ref/contour.html (visited on 02/21/2018).

[35] A. J. Hayter, *Probability and Statistics for Engineers and Scientists*. Cengage Learning, 2012.

[36] SIPA Únete, *Tabla de Salarios por Puesto Tipo y Banda*. [Online]. Available: http://www.sipa.es/files/calendarios/SIPA%7B%5C_%7DCubo%7B%5C_%7D2018%7B%5C_%7DGetafe.pdf (visited on 05/29/2018).

[37] A. Tributaria, *Tabla de Coeficientes de Amortización Lineal*. [Online]. Available: https://www.agenciatributaria.es/AEAT.internet/Inicio/%7B%5C_%7DSegmentos%7B%5C_%7D/Empresas%7B%5C_%7Dy%7B%5C_%7Dprofesionales/Empresas/Impuesto%7B%5C_%7Dsobre%7B%5C_%7DSociedades/Periodos%7B%5C_%7Dimpositivos%7B%5C_%7Da%7B%5C_%7Dpartir%7B%5C_%7Dde%7B%5C_%7D1%7B%5C_%7D1%7B%5C_%7D2015/Base%7B%5C_%7Dimponible/Amortizacion/Tabla%7B%5C_%7Dde%7B%5C_%7Dcoeficientes%7B%5C_%7Dde%7B%5C_%7Damortizacion%7B%5C_%7Dlineal%7B%5C_%7D.shtml (visited on 05/29/2018).

A. LIST OF SYMBOLS

α	Angle of attack
B	Bulk modulus
b	Wing span
C_L	Lift coefficient
C_{L_0}	Zero lift coefficient
$C_{L\alpha}$	Angle of attack lift curve slope coefficient
$C_{L\delta_e}$	Elevator deflection lift curve slope coefficient
C_{Lih}	HTP trim setting angle lift curve slope coefficient
$C_{L_{tail}}$	HTP lift coefficient
$C_{L_{wing}}$	Wing lift coefficient
C_l	Rolling moment coefficient
$C_{l\delta_a}$	Aileron deflection contribution to rolling moment coefficient
$C_{l\phi}$	Bank angle contribution to rolling moment coefficient
C_M	Pitching moment coefficient
C_{M_0}	Zero pitching moment coefficient
$C_{M\alpha}$	Angle of attack pitching moment curve slope coefficient
$C_{M\delta_e}$	Elevator deflection lift pitching moment slope coefficient
C_{Mih}	HTP trim setting angle pitching moment curve slope coefficient
$C_{M_{tail}}$	HTP pitching moment coefficient
$C_{M_{wing}}$	Wing pitching moment coefficient
C_T	Total net thrust coefficient
c	Viscous damping coefficient
$\bar{c}$	Mean aerodynamic chord
ΔC_L	Lift coefficient offset due to asymmetries
ΔC_M	pitching moment coefficient offset due to asymmetries
ΔT	Temperature ISA offset
δ_a	Shock absorber deflection (Equation 2.2)
δ_a	Aileron deflection angle (Equation 3.3)
δ_e	Elevator deflection angle
δ_f	Flap deflection angle
δ_r	Tyre deflection
D	Drag force
ϵ	Thrust force angle with respect to horizontal reference plane
$\vec{F}$	Damping force
$\{F_0\}$	External forces
$\{F_a\}$	Shock absorber forces
$\{F_{a/t}\}$	Aircraft to landing gear interaction forces
$[F_c]$	Nonlinear terms

F_g	Gas force
F_R, $\{F_r\}$	Tyre force(s)
$\{F_{t/a}\}$	Landing gear to aircraft interaction forces
$F_{z_{CG}}$	Total vertical force at centre of gravity
f	Frequency of excitation
γ	Polytropic gas constant
$[GM]$	Aircraft generalized mass matrix
$[GS]$	Aircraft generalized stiffness matrix
h	Runway altitude
h	Bump height (Equation 5.1)
$h(x)$	Runway profile vertical coordinate
ih	Elevator trim setting angle
K_{r1}	Tyre ressure dependent constant
K_{r2}	Rubber plasticity dependent constant
λ	Bump wavelength
L	Lift force
μ	Friction coefficient
μ_{brk}	Braking friction coefficient
μ_{roll}	Rolling friction coefficient
$M_{x_{CG}}$	Total rolling moment at centre of gravity
$M_{y_{CG}}$	Total pitching moment at centre of gravity
m	Mass
N	Tyre pressure dependent constant (Equation 2.1)
N	Normal force (Equation 3.2)
ω_0	Critical damping frequency
ϕ	Bank angle
P	Probability
P_0	Initial gas pressure
$\{q\}$	Landing gear geometric coordinates
ρ	Air density
S	Piston area (Equation 2.2)
S	Wing surface (Equations 3.1, 3.2, 3.3)
T	Total net thrust force
$[TM]$	Landing gear generalized mass matrix
V, $\vec{v}$	Aircraft speed/velocity
V_0	Initial gas volume
V_1	Initial liquid volume
$[V_a]$	Shock absorber forces geometric transformation matrix
V_{L_2}	Touchdown forward speed during landing (CS 25.479 Level landing conditions)
V_R	Rotation speed during take-off (CS 25.107 Take-off speeds)
$[V_r]$	Tyre forces geometric transformation matrix
W	Aircraft weight

$W_{ARMOURING}$	Armouring weight
W_{PODS}	Pods weight
$\{x\}$	Modal generalized coordinates
x_{CG}	centre of gravity x-coordinate
x_{CP}	centre of pressure x-coordinate
x_T	x-coordinate of thrust application point
y_{CG}	centre of gravity y-coordinate
y_{CP}	centre of pressure y-coordinate
y_T	y-coordinate of thrust application point
z_{CG}	centre of gravity z-coordinate
z_{CP}	centre of pressure z-coordinate
z_T	z-coordinate of thrust application point
$[\emptyset]$	Modal matrix
$\cap$	Intersection of events
$\cup$	Union of events

B. LIST OF ABBREVIATIONS

AAR	Air-to-Air Refuelling
ABrake	Auto-Brake
A/C	Aircraft
AFM	Aircraft Flight Manual
AGARD	Advisory Group for Aerospace Research and Development
AMC	Acceptable Means of Compliance
BAE	British Aerospace
CASA	Construcciones Aeronáuticas S.A.
CBR	California Bearing Ratio
CG	centre of Gravity
CRI	Certification Review Item
CS	Certification Specifications
DEF-STAN	Defence Standards
DS	Defence and Space
EASA	European Aviation Safety Agency
EBH	Equivalent Bump Height
EMS	Engine Mounting System
EPI	EuroProp International
FCS	Flight Control System
FEM	Finite Element Method
FM	Fuel Mass
GI	Ground Idle
GVT	Ground Vibration Test
HDU	Hose Drum Unit
HTP	Horizontal Tail Plane
ISA	International Standard Atmosphere
IT	Information Technology
KEAS	Knots Equivalent Air Speed
KTAS	Knots True Air Speed
LG	Landing Gear
LH	Logistic Heavy
LN	Logistic Normal
LND	Landing
LWR - MX	Down Bending Moment at Left Wing Root
LWR - FZ	vertical Force at Left Wing Root
MAC	Mean Aerodynamic Chord
MCRI	Military Certification Review Item
MFW	Maximum Fuel Weight

MLG	Main Landing Gear
MLW	Maximum Landing Weight
MPL	Maximum Payload
MTOP	Maximum Take-Off Power
MTOW	Maximum Take-Off Weight
MZFW	Maximum Zero Fuel Weight
NLG	Nose Landing Gear
NLG - FZ	Nose Landing Gear Wheel Axle vertical Force
OCCAR	Organisation Conjointe de Coopération en matière d'Armement
OWE	Operational Weight Empty
PL	Payload
PM	Probability of Probability Map
PSD	Power Spectral Density
RC	Reference Case
RPM	Revolutions Per Minute
RTO	Rejected Take-Off
STOL	Short Take-Off and Landing
TLL	Tactical
TM	Total Mass
TO	Take-Off
UK	United Kingdom
VTP	Vertical Tail Plane
2D	Two-dimensional

C. PROBABILITY MAPS MESH SENSITIVITY ANALYSIS

The shape of the areas enclosed by the iso-load curves depend on the probability map considered and the limit load ratio for which they are computed. Hence, the lack of a program to automate the computation of such areas made unfeasible the computation of the likelihood given by a probability map according to Equation 4.5. As a consequence, in order to solve this issue, the total area of the probability maps envelope was discretized using a mesh of points. By doing so, the probability could be calculated using the expression given in Equation 4.6. This method, based on Laplace's rule, is easier to code and much faster in the probability computation. However, the accuracy of the results obtained with this procedure depends on the mesh employed for such task. The higher number of mesh points, the more precise the probability computation will be. Not only the number of points is important, but other aspects must also be taken into account to define a suitable mesh.

For a proper probability calculation, the density of points in the mesh must be constant, so the ratio of areas is analogous to the ratio of events, since all the regions of a probability map envelope have the same likelihood to include such points. In more simple words, there would not be more points in a specific region of the envelope, which may coincide with the area enclosed by the iso-load curve of interest, leading to an unrealistic result.

As a result of this consideration, the meshes for the μ_{brk} - x_{CG}, h - v and ΔT - δ_f probability maps are rectangular to easily fit the shape of its envelope. Moreover, the meshes extend from the minimum to the maximum values of the X and Y sets of data, so the MATLAB® *griddata* function does not discard any of the points defined in the mesh. Moreover, the range of both X and Y data is split in the same number of equispaced divisions to preserve a constant density of mesh points over the envelope.

For the particular case of the TM - FM probability maps, first a squared mesh is considered to cover region from the OWE to the MZFW in the y-axis and from zero fuel to the maximum possible fuel mass at the MZFW. Both X and Y data sets within the aforementioned range are split into the same number of divisions, so the density of mesh points within this first region considered is constant. Then another second mesh is considered to cover the region from the MZFW to the MLW. To preserve the constant density of points, the same discretization step of the first mesh was considered to split such total mass data range. However, if the last total mass value of such vector does not coincide with the MLW, it was replaced by the corresponding value of the MLW to perfectly cover the upper limit of the mass states envelope. Then, at each total mass value of such vector, the same number of divisions considered for the first mesh was used to discretize the corresponding fuel mass data from the minimum fuel to maximum fuel parallel lines. Hence, the number of x-divisions of the second mesh is the same as for the

first one, but the number of y-divisions will depend on the total mass difference between the MLW and MZFW, which is particular for each reference case. Finally, both meshes are combined to yield a total mesh that present points which lie outside of the convex hull of the corresponding mass states envelope discretized. This points correspond to the cases considered in the first mesh which lie below the maximum fuel line and are discarded by the MATLAB® *griddata* function when performing the interpolation.

Once the methodology for the definition of the meshes is fixed, a sensitivity analysis is performed to study the accuracy in the probability calculation and its computation time as a function of the number of mesh points in each probability map type. The sensitivity analysis was solely performed to the four probability maps of the reference case gathered in Table C.1 considering a limit load ratio of 0.9, assuming that the same number of mesh points would yield the same precision in all the probability maps of one of the four kinds.

The computation of the exact probability was specifically coded in MATLAB® by calculating the area enclosed by the 0.9 iso-load curve and the total area of the envelope for each of the four probability maps.

The number of divisions considered for the discretization of the X and Y data of each probability map are 10, 25, 50, 75, 100, 500, 1000, 2000, 3000, 4000, 5000 and 10000. In the case of the TM - FM probability maps, this values corresponds to the number of division for the squared part of the mesh. Then, each number of divisions yields a final number of mesh points in each probability map type, which are the ones included in Table C.2.

The percentage error between the probability calculated with its corresponding mesh and the exact one is computed according to the following expression:

$$\%_{error} = \left| \frac{Numerical\ Probability - Exact\ Probability}{Exact\ Probability} \right| \cdot 100 \tag{C.1}$$

Furthermore, the computation time is calculated with MATLAB® *tic* and *toc* functions and it is mainly due to the interpolation of the data. The selection of a mesh leading to a short computation time is crucial in the statistical analysis since, for a single magnitude of interest, the definition of its corresponding probability curve at a given bump height may take an average of 18 minutes to be completed.

REFERENCE CASE	THRUST	BUMP HEIGHT [cm]
PODS OFF	GROUND IDLE	18

TABLE C.1. REFERENCE CASE FOR MESH SENSITIVITY ANALYSIS

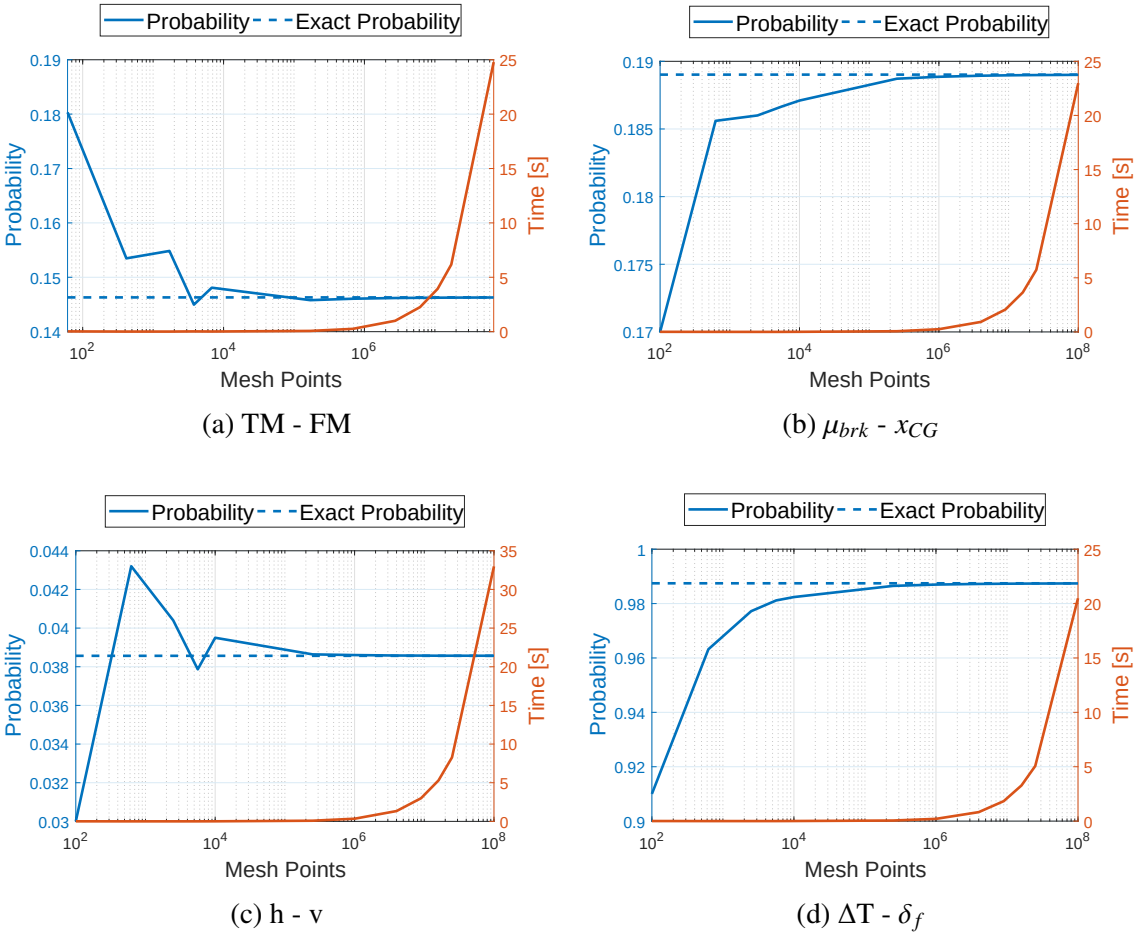

(a) TM - FM

(b) μ_{brk} - x_{CG}

(c) h - v

(d) ΔT - δ_f

Fig. C.1. Probability and computation time dependency on the number of mesh point for each type of probability map

Mesh Points	**Error** [%]	**Time** [s]
61	23.2608	0.0234
417	4.9074	0.0074
1,705	5.8380	0.0075
3,794	0.9105	0.0232
6,807	1.2201	0.0133
170,538	0.3461	0.0663
683,072	0.1671	0.2567
2,734,158	0.0766	0.9998
6,153,240	0.0515	2.2549
10,940,314	0.0371	3.9360
17,095,392	0.0273	6.1690
68,390,789	0.0101	24.7844

(a) TM - FM

Mesh Points	**Error** [%]	**Time** [s]
100	10.0610	0.0092
625	1.8078	0.0054
2,500	1.5962	0.0034
5,625	1.2435	0.0040
10,000	1.0142	0.0106
250,000	0.1592	0.0640
1,000,000	0.0841	0.2512
4,000,000	0.0425	0.9239
9,000,000	0.0285	2.0698
16,000,000	0.0214	3.6509
25,000,000	0.0171	5.7397
100,000,000	0.0085	22.9870

(b) μ_{BRK} - X_{CG}

Mesh Points	**Error** [%]	**Time** [s]
100	22.2102	0.0076
625	12.0174	0.0035
2,500	4.7570	0.0041
5,625	1.8119	0.0050
10,000	2.4233	0.0100
250,000	0.1933	0.0854
1,000,000	0.1000	0.3441
4,000,000	0.0397	1.3347
9,000,000	0.0288	2.9979
16,000,000	0.0139	5.2949
25,000,000	0.0155	8.2742
100,000,000	0.0102	32.9782

(c) H - V

Mesh Points	**Error** [%]	**Time** [s]
100	7.8442	0.0068
625	2.4566	0.0028
2,500	1.0389	0.0029
5,625	0.6383	0.0034
10,000	0.5123	0.0088
250,000	0.0962	0.0530
1,000,000	0.0475	0.2068
4,000,000	0.0237	0.8251
9,000,000	0.0158	1.8371
16,000,000	0.0118	3.2781
25,000,000	0.0095	5.0673
100,000,000	0.0047	20.4885

(d) ΔT - δ_F

TABLE C.2. RESULTS OF MESH SENSITIVITY ANALYSIS

Finally, the criterion followed to select the final number of points to discretize the areas of the probability maps was to choose the number of divisions leading to a percentage error smaller that 0.05. In such a way, the best trade-off between accuracy and computation time is reached, since the latter is not longer than four seconds for such convergence threshold value. The final number of mesh elements for each probability map type is previously included in Table 4.12.

D. EFFECT OF μ_{BRK} ON NLG - FZ

Among all the cases included in the μ_{brk} - x_{CG} probability maps, the most critical scenario was expected to happen at a forward x_{CG} configuration and at the highest braking coefficient considered (0.4). From the static point of view, such x_{CG} position induces a higher nose-down pitch attitude, so a greater fraction of the aircraft total mass is supported by the nose landing gear. In addition, the larger the force applied by the brakes, the higher the pitching down moment that contributes to such nose-down pitch attitude of the aircraft. However, in reality, larger load magnitudes occur at lower μ_{brk} values, between 0.2 and 0.3, close to the one given by the auto-braking system.

Therefore, to give an explanation for such discrepancy, the time histories of the taxi cases corresponding to the two aforementioned braking coefficient values were studied. The effect of both thrust settings, ground idle and maximum reverse, was considered to explain further differences. Moreover, due to confidentiality reasons, the NLG - FZ load magnitudes were non-dimensionalized with respect to the maximum shear force value among the four cases. Such most critical taxi case is characterized by ground idle and auto-braking configuration, since the pitching up moment with this thrust setting is smaller, and so is the load alleviation at the nose landing gear.

REFERENCE CASE	THRUST	BUMP HEIGHT [cm]
ARMOURING OFF	GROUND IDLE	18

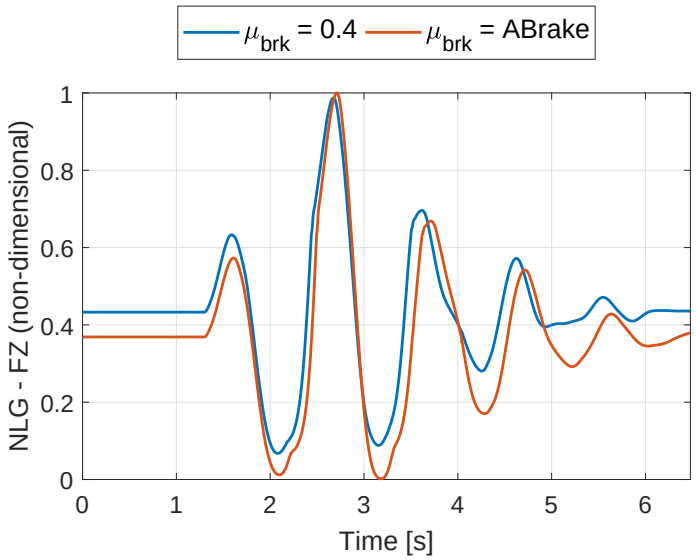

Fig. D.1. Time histories of NLG - FZ with Ground Idle thrust setting

As illustrated in Figure D.1, the first straight segments of both time histories correspond to the 1G static load magnitudes of the NLG wheel axle vertical force, which is

positive downwards. This segments correspond to the time period in which the aircraft rolls at constant velocity over the portion of flat runway prior to encountering the bump. Thus, the NLG-FZ corresponding to a braking coefficient of 0.4 (blue line) is larger that that yielded by the auto-braking setting, as a consequence of the static reasoning previously explained. Then, when the aircraft start rolling over the first half of the bump, the NLG shock absorber is compressed and the force magnitudes increases. For both cases, the increment of the force is equal, but a larger peak magnitude is reached for a braking coefficient of 0.4 since the static compression is greater. At about 2 seconds, the aircraft crosses the highest point of the bump and the load magnitudes reduce almost to zero, since the shock absorber is uncompressed due to the inertia previously gained by the aircraft when moving up along the bump. Half a second later, when the aircraft has totally passed through the bump, the aircraft tends to restore its equilibrium position, so the large inertia of the aircraft moving down compresses again the shock strut and, as a consequence, the peak load magnitude is reached. Therefore, since the decompression of the auto-braking scenario occurs to a greater extent, the kinetic energy gained in the upward movement is larger and such inertia produces a higher peak load for such taxi case. Finally, after reaching peak loads, both magnitudes decay to their corresponding static value due to the damping properties of the shock strut.

REFERENCE CASE	THRUST	BUMP HEIGHT [cm]
ARMOURING OFF	MAX. REVERSE	18

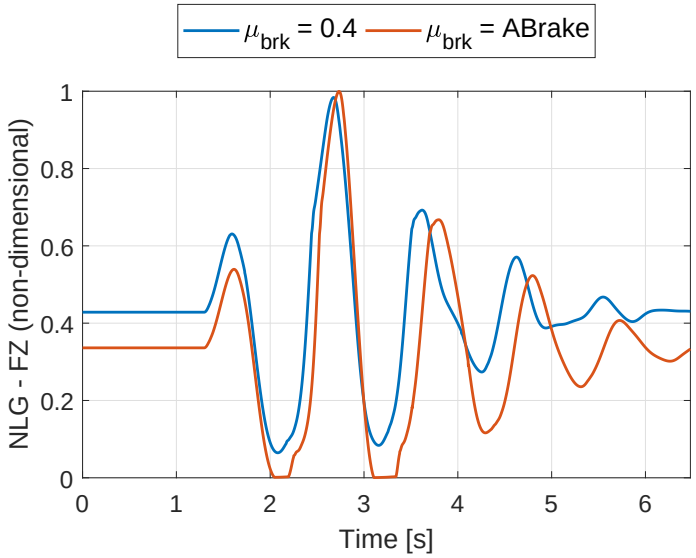

Fig. D.2. Time histories of NLG - FZ with Max. Reverse thrust setting

There is a greater difference in the peak load magnitudes when maximum reverse setting is considered, as depicted in Figure D.2. Considering the auto-braking scenario, the pitch-up attitude produced by the positive slope of the first half is further increased by the greater pitching up moment produced by the maximum reverse thrust. Hence,

the aircraft loses contact with the ground and the shock absorber is fully uncompressed, reason by which the load magnitudes are zero for a really short instant. Finally, when the NLG wheels lands again on the runway, higher peak loads are reached, although smaller than those obtained with ground idle due to the larger alleviation of the maximum reverse at the structural component under consideration.

E. DEFINITION OF LIMIT AND ULTIMATE LOADS (EASA CS 25.301/25.303/25.305)

E.1. CS 25.301: Loads

a) Strength requirements are specified in terms of limit loads (the maximum loads to be expected in service) and ultimate loads (limit loads multiplied by prescribed factors of safety). Unless otherwise provided, prescribed loads are limit loads.

b) Unless otherwise provided the specified air, ground, and water loads must be placed in equilibrium with inertia forces, considering each item of mass in the aeroplane. These loads must be distributed to conservatively approximate or closely represent actual conditions. (See AMC No. 1 to CS 25.301(b)). Methods used to determine load intensities and distribution must be validated by flight load measurement unless the methods used for determining those loading conditions are shown to be reliable. (See AMC No. 2 to CS 25.301(b)).

c) If deflections under load would significantly change the distribution of external or internal loads, this redistribution must be taken into account.

[Amdt. No.:25/1]

E.2. CS 25.303: Factor of safety

Unless otherwise specified, a factor of safety of 1·5 must be applied to the prescribed limit load which are considered external loads on the structure. When loading condition is prescribed in terms of ultimate loads, a factor of safety need not be applied unless otherwise specified.

E.3. CS 25.305: Strength and deformation

a) The structure must be able to support limit loads without detrimental permanent deformation. At any load up to limit loads, the deformation may not interfere with safe operation.

b) The structure must be able to support ultimate loads without failure for at least 3 seconds. However, when proof of strength is shown by dynamic tests simulating actual load conditions, the 3-second limit does not apply. Static tests conducted to ultimate load must include the ultimate deflections and ultimate deformation induced by the

loading. When analytical methods are used to show compliance with the ultimate load strength requirements, it must be shown that -

(1) The effects of deformation are not significant;

(2) The deformations involved are fully accounted for in the analysis; or

(3) The methods and assumptions used are sufficient to cover the effects of these deformations.

c) Where structural flexibility is such that any rate of load application likely to occur in the operating conditions might produce transient stresses appreciably higher than those corresponding to static loads, the effects of this rate of application must be considered.

d) *Reserved*

e) The aeroplane must be designed to withstand any vibration and buffeting that might occur in any likely operating condition up to VD/MD, including stall and probable inadvertent excursions beyond the boundaries of the buffet onset envelope. This must be shown by analysis, flight tests, or other tests found necessary by the Agency.

f) Unless shown to be extremely improbable, the aeroplane must be designed to withstand any forced structural vibration resulting from any failure, malfunction or adverse condition in the flight control system. These loads must be treated in accordance with the requirements of CS 25.302.

[Amdt. No.:25/1]

F. EASA CS 25.491/AMC 25.491

F.1. CS 25.491: Taxi, takeoff and landing roll

Within the range of appropriate ground speeds and approved weights, the aeroplane structure and landing gear are assumed to be subjected to loads not less than those obtained when the aircraft is operating over the roughest ground that may reasonably be expected in normal operation. (See AMC 25.491).

F.2. AMC 25.491: Taxi, take-off and landing roll

F.2.1. Purpose

This AMC sets forth acceptable methods of compliance with the provisions of CS-25 dealing with the certification requirements for taxy, take-off and landing roll design loads. Guidance information is provided for showing compliance with CS 25.491, relating to structural design for aeroplane operation on paved runways and taxy-ways normally used in commercial operations. Other methods of compliance with the requirements may be acceptable.

F.2.2. Related Certification Specifications

The contents of this AMC are considered by the Agency in determining compliance with CS 25.491. Related paragraphs are CS 25.305(c) and CS 25.235.

F.2.3. Background

a) All paved runways and taxi-ways have an inherent degree of surface unevenness, or roughness. This is the result of the normal tolerances of engineering standards required for construction, as well as the result of events such as uneven settlement and frost heave. In addition, repair of surfaces on an active runway or taxi-way can result in temporary ramped surfaces. Many countries have developed criteria for runway surface roughness. The Inter-national Civil Aviation Organization (ICAO) standards are published in ICAO Annex 14.

b) In the late 1940's, as aeroplanes became larger, more flexible, and operated at higher ground speeds, consideration of dynamic loads during taxi, landing rollout, and take-off became important in aeroplane design. CS 25.235, CS 25.491 and CS 25.305(c) apply.

c) Several approaches had been taken by different manufacturers in complying with the noted regulations. If dynamic effects due to rigid body modes or airframe flexibility during taxi were not considered critical, some manufacturers used a simplified static analysis where a static inertia force was applied to the aeroplane using a load factor of 2.0 for single axle gears or 1.7 for multiple axle gears. The lower 1.7 factor was justified based on an assumption that there was a load alleviating effect resulting from rotation of the beam, on which the forward and aft axles are attached, about the central pivot point on the strut. The static load factor approach was believed to encompass any dynamic effects and it had the benefit of a relatively simple analysis.

d) As computers became more powerful and dynamic analysis methods became more sophisticated, it was found that dynamic effects sometimes resulted in loads greater than those which were predicted by the static criterion. Some manufacturers performed calculations using a series of harmonic bumps to represent a runway surface, tuning the bumps to excite various portions of the structure at a given speed. U.S. Military Standard 8862 defines amplitude and wavelengths of 1-cosine bumps intended to excite low speed plunge, pitch and wing first bending modes.

e) Some manufacturers used actual runway profile data to calculate loads. The runway profiles of the San Francisco Runway 28R or Anchorage Runway 24, which were known to cause high loads on aeroplanes and were the subject of pilot complaints until resurfaced, have been used in a series of bi-directional constant speed analytical runs to determine loads. In some cases, accelerated runs have been used, starting from several points along the runway. The profiles of those runways are described in NASA Reports CR-119 and TN D-5703. Such deterministic dynamic analyses have in general proved to be satisfactory.

f) Some manufacturers have used a statistical power spectral density (PSD) approach, especially to calculate fatigue loads. Extensive PSD runway roughness data exist for numerous world runways. The PSD approach is not considered practical for calculation of limit loads.

g) Because the various methods described above produce different results, the guidance information given in paragraphs 4, 5, and 6 of this AMC should be used when demonstrating compliance with CS 25.491.

F.2.4. Runway Profile Condition

a) Consideration of airframe flexibility and landing gear dynamic characteristics is necessary in most cases. A deterministic dynamic analysis, based on the San Francisco Runway 28R (before it was resurfaced), described in Table 1 of this AMC, is an acceptable method for compliance. As an alternative means of compliance, the San Francisco Runway 28R (before it was resurfaced) may be used with the severe bump from 1530 to 1538 feet modified per Table 2. The modifications to the bump reflect

the maximum slope change permitted in ICAO Annex 14 for temporary ramps used to transition asphalt overlays to existing pavement. The points affected by this modification are outlined in Table 1.

b) Aeroplane design loads should be developed for the most critical conditions arising from taxy, take-off, and landing run. The aeroplane analysis model should include significant aeroplane rigid body and flexible modes, and the appropriate landing gear and tyre characteristics. Unless the aeroplane has design features that would result in significant asymmetric loads, only the symmetric cases need be investigated.

c) Aeroplane steady aerodynamic effects should normally be included. However, they may be ignored if their deletion is shown to produce conservative loads. Unsteady aerodynamic effects on dynamic response may be neglected.

d) Conditions should be run at the maximum take-off weight and the maximum landing weight with critical combinations of wing fuel, payload, and extremes of center of gravity (c.g.) range. For aeroplanes with trimable stabilizers, the stabilizer should be set at the appropriate setting for take-off cases and at the recommended final approach setting for landing cases. The elevator should be assumed faired relative to the stabilizer throughout the take-off or landing run, unless other normal procedures are specified in the flight manual.

e) **A series of constant speed runs should be made in both directions from 37 km/h (20 knots) up to the maximum ground speeds expected in normal operation (V_R defined at maximum altitude and temperature for take-off conditions, 1.25 V_{L2} for landing conditions). Sufficiently small speed increments should be evaluated to assure that maximum loads are achieved. Constant speed runs should be made because using accelerated runs may not define the speed/roughness points which could produce peak dynamic loads. For maximum take-off weight cases, the analysis should account for normal take-off flap and control settings and consider both zero and maximum thrust. For maximum landing weight cases, the analysis should account for normal flap and spoiler positions following landing, and steady pitching moments equivalent to those produced by braking with a coefficient of friction of 0.3 with and without reverse thrust. The effects of automatic braking systems that reduce braking in the presence of reverse thrust may be taken into account.**

F.2.5. Discrete Load Condition

One of the following discrete limit load conditions should be evaluated:

a) With all landing gears in contact with the ground, the condition of a vertical load equal to 1.7 times the static ground reaction should be investigated under the most adverse

aeroplane loading distribution at maximum take-off weight, with and without thrust from the engines.

b) As an alternative to paragraph 5.a. above, it would be acceptable to undertake dynamic analyses under the same conditions considered in paragraph 4 of this AMC considering the aircraft response to each of the following pairs of identical and contiguous 1-cosine upwards bumps on an otherwise smooth runway:

i) Bump wavelengths equal to the mean longitudinal distance between nose and main landing gears, or between the main and tail landing gears, as appropriate; and separately.

ii) Bump wavelengths equal to twice this distance.

The bump height in each case should be defined as:

$$H = A + B\sqrt{L}$$

Where:

H = the bump height

L = the bump wavelength

A = 1.2, B = 0.023 if H and L are expressed in inches

A = 30.5, B = 0.116 if H and L are expressed in millimetres

F.2.6. Combined Load Condition

A condition of combined vertical, sideDiscrete Load Condition and drag loads should be investigated for the main landing gear. In the absence of a more rational analysis a vertical load equal to 90% of the ground reaction from paragraph 5 above should be combined with a drag load of 20% of the vertical load and a side load of 20% of the vertical load. Side loads acting either direction should be considered.

F.2.7. Tyre Conditions

The calculation of maximum gear loads in accordance with paragraphs 4, 5, and 6, may be performed using fully inflated tyres. For multiple wheel units, the maximum gear loads should be distributed between the wheels in accordance with the criteria of CS 25.511.

[Amdt. No.:25/2]

G. DEF-STAN 00-970 LEAFLET 49: DESIGN OF UNDERCARRIAGES - OPERATION FROM SURFACES OTHER THAN SMOOTH HARD RUNWAYS. SPECIFICATION OF CONTINUOUS GROUND UNEVENNESS

G.1. Introduction

1.1. This leaflet is concerned with the specification of ground unevenness of a continuous nature, as distinct from discrete obstacles such as steps, bumps and hollows. It was previously issued as Leaflet 305/2. The background to such a specification is discussed and a procedure which will usually be satisfactory in relation to the requirements of Clause 4.13 is given.

G.2. Background to specification

2.1. The quantitative specification of continuous ground unevenness is necessary:

(i) to set a level for design which will ensure that the aeroplane can fulfil its projected roles,

(ii) to assess unevenness of ground which may be used for proving or clearance trials, and

(iii) to establish the relationship between the levels used for design or met in trials and that of a potential operating surface.

2.2. The unevenness of ground is determined by the variation of height (h) with the position (x, y) of a point on a reference plane. Most current descriptions of unevenness concentrate on the profile of height along a straight line, which may be represented by a function h(x). The requirements of Clause 4.13 necessitate the definition only of such a profile.

2.3. Quantifiable properties of the function h(x) are required to gauge the unevenness of the surface. The properties in current use relate either to the average level of unevenness (as, for example, does the spectral density) or to the identification of individual features, therefore caution is needed in their use. The specifications of the following section have been derived from a comparison of the spectral densities of measured profiles, with emphasis on wavelengths between 20 and 40 m. They are aimed at the establishment, for a particular class of runway, of a profile the use of which for design purposes will permit an aeroplane to operate on most runways of that class.

G.3. Determination of runway profile

3.1. The following procedure for the determination of a runway profile will usually be acceptable.

3.2. The profile function h(x) is obtained by multiplying each of the vertical co-ordinates of a standard profile shape by a factor dependent on the class of runway specified. See paragraph 3.4. The co-ordinates of the profile shape (mm height at intervals of 1 m) are given in Table 1. The factor to be employed will be specified by the Aeroplane Project Director: the following para gives guidance on values appropriate to various types of runway.

3.3. Runways may be divided into 4 classes as regards their likely levels of unevenness:

A Paved runways laid on a stable base and regularly maintained.

B Poor quality paved runways and unpaved runways which have been fully graded.

C Unpaved runways which have been partially graded.

D Unpaved runways on virgin ground.

3.4. Appropriate factors for the vertical coordinates for these classes are:

Class	Factor
A	1.0
B	1.5
C	2.5
D	4.0

3.5. The following points should be noted:

(i) The standard profile shape has been derived from an actual runway profile, in order to obtain a representative distribution of height variations.

(ii) In deriving the standard profile shape the unevenness of the actual profile has been attenuated at wavelengths greater that 120 m. Therefore the standard profile shape will be unsatisfactory if significant aeroplane response would be caused by unevenness at those wavelengths; in such a case the designer should consult the Aeroplane Project Director.

(iii) If a runway of length greater than 1499 m (1639 yds) is required the standard profile shape should be extended by reflection of both co-ordinates, i.e.:

$h(x) = - h(2999 - x); 1499 < x \leq 2999$

$h(x) = - h(3280 - x); 1639 < x \leq 3280$

H. SOCIOECONOMIC BACKGROUND

The main purpose of the present Bachelor Thesis comprises the developement of a methodology for the statistical analysis of taxi loads in unpaved runways, in order to quantify the risk that the operation on this type of airfields involves in terms of probability of limit load exceedance. To accomplish this task, the numerical simulation of the casuistry considered in the statistical analysis and the corresponding post-processing of the data is required for the definition of 2D probability maps and subsequent probability curves, which serve as the two basic tools for the assessment of the problem.

Since all the work was performed in a real industry environment to cover a current customers need, the different activities performed would incur in costs that must be covered and translated into revenues for the overall profit of the company. Commonly in military industry, the different programmes carried out to develop new warfare technology are mainly financed by the different governments that, in the end, will be the final customers of such products. Hence, the present project would be included in the A400M programme currently managed by OCCAR, which is an European intergovernmental organization that joints the collaboration of Belgium, France, Germany, Italy, Spain, and the United Kingdom, and from which Airbus company receives the vast majority of the funds for the development of such aircraft. Therefore, an approximate cost estimate is outlined for the application of the statistical analysis as presented in the scope of this project, although future activities for the completeness of the statistical taxi loads loop may lead to larger expenditures. In addition, it is important to remark that the costs associated to the definition of the EBH curves, which serve as starting point for the statistical analysis, are not included, since this task was completed by the Structural Dynamics and Aeroelasticity Department of Airbus DS at the beginning of 2014.

Due to time constraints in the development of the methodology, a planification was first laid out to succeed in the accomplishment of the present project. The time span for its completion ranged from January 29th to June 1st 2018 and comprised the following stages:

1. Introduction to the taxi loads problem in unpaved runways from the industry perspective: importance in the design of tactical airlifters, applicable airworthiness regulations, analysis of the numerical model of the specimen studied, stress taxi loads calculation philosophy, EBH method and EBH curves computation procedure.

2. Familiarization with Airbus computer resources and in-house software implemented for the numerical simulation of dynamic taxi loads.

3. Analysis of EBH curves taxi loads loop: starting point selection, identification of

most critical cases for the magnitudes of interest studied and identification of the most relevant parameters to be included in the statistical analysis.

4. Elaboration of the probability calculation philosophy: fundamentals of set theory, conceptualization of 2D probability maps and definition of casuistry

5. Definition of 2D probability maps: iso-load curves methodology, which includes the computation of taxi loads, interpolation of results and definition of contour lines.

6. Computation of probability curves: mesh sensitivity analysis.

7. Digestion of results and wrap-up: sensitivity analysis of the different parameters defining a taxi case (analysis of time histories), effect of the pondering weights of each parameter in the probability calculation, conclusions and future activities suggestion.

8. Project documentation.

The period of time particularly devoted to each of the aforementioned phases is defined in the Gantt chart depicted in Figure H.1.

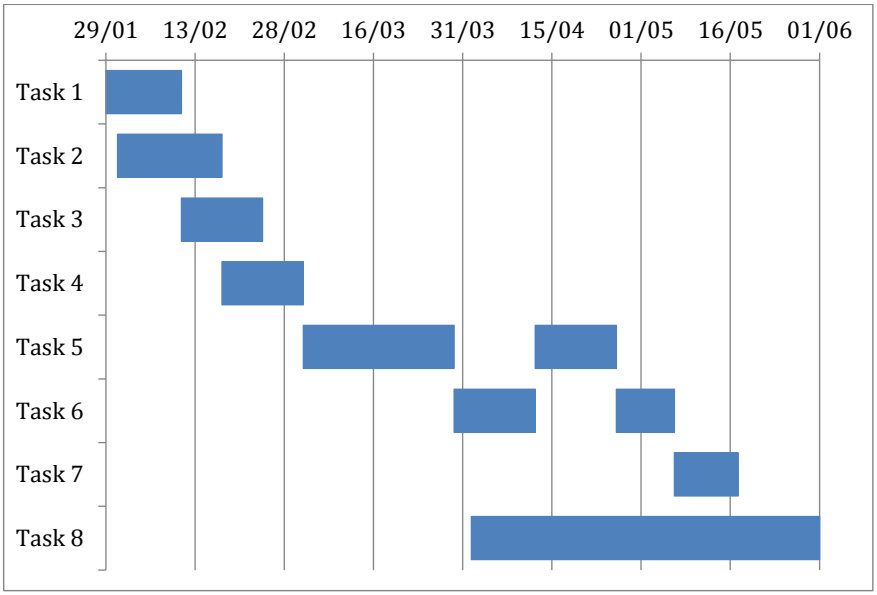

Fig. H.1. Project Gantt chart

Moreover, the planification extends up to 18 weeks, which comprise in turn a total number of 78 labour days during this period at Airbus factory located in Getafe. Estimating an average number of 8 hours a day, the schedule sums up to a total number of 624 working hours. In addition, the hours shared with the mentor to support the completion of the project must be included, which account for a rough estimation of one third of the total working time, i.e., 208 hours.

According to the basic accounting principles, an accurate cost estimate includes both direct and indirect costs. On the one hand, direct costs mainly involve salaries of employees and the depreciation of software licenses and computing equipment. On the other hand, the main concepts that can be included as indirect costs are electricity, heating and internet connection. Since the quantification of the latter is very imprecise, a good practice to estimate indirect costs is to consider them as a specific percentage of the direct ones, assuming such percentage to be of the order of 7% for the present cost analysis.

To estimate the labour costs, an amount of 14.33€/h [36] is estimated as the average wage received by an intern in 2018. Likewise, the average salary of an experienced senior employee of the same profession raises up to 34.31€/h [36]. Hence, the expenses related to the work force add up to 16,078.40€.

Employee	**Working Time** [h]	**Salary** [€/h]	**Total** [€]
Intern	624	14.33	8,941.92
Senior	208	34.31	7,136.48
			16,078.40

TABLE H.1. LABOR COSTS

To account for the depreciation of software licenses and computing equipment during the 4-month duration period of the project, a simple linear depreciation is considered. For simplicity, assuming maximum annual linear depreciation coefficients for 2018 in Spain [37], the total quarterly depreciation amounts to 5,203.63€. The contribution of each item included is gathered in Table H.2.

Item	**Original Cost** [€]	**Annual Depreciation** [%]	**Total** [€]
Computer	918.39	25	76.53
FORTRAN compiler for UNIX	571.00	33	62.81
MSC.NASTRAN	25,000.00	33	2,750.00
Dynamic taxi loads numerical simulation software	20,000.00	33	2,200.00
MATLAB® academic license	500.00	33	55.00
Microsoft® Office Professional Plus 2016	539.00	33	59.29
			5,203.63

TABLE H.2. SOFTWARE LICENSES AND COMPUTING EQUIPMENT QUARTERLY DEPRECIATION

Combining the results from Tables H.1 and H.2, the total direct costs are equal to 21,282.03€. Considering that the indirect costs are estimated as 7% of the direct ones, the total project cost estimate yields 22,771.77€.

Costs Type	**Total** [€]
Direct costs	21,282.03
Indirect costs	1,489.74
	22,771.77

TABLE H.3. TOTAL PROJECT COST